Loma Linda University

TheScholarsRepository@LLU: Digital Archive of Research, Scholarship & Creative Works

Loma Linda University Electronic Theses, Dissertations & Projects

6-2017

PAS Signaling Mechanisms in Aer and Aer2

Darysbel Garcia

Follow this and additional works at: http://scholarsrepository.llu.edu/etd

Part of the Bacteriology Commons, Genetic Processes Commons, Medical Microbiology Commons, and the Pathogenic Microbiology Commons

LOMA LINDA UNIVERSITY
School of Medicine
in conjunction with the
Faculty of Graduate Studies

_____

PAS Signaling Mechanisms in Aer and Aer2

by

Darysbel Garcia

_____

A Dissertation submitted in partial satisfaction of
the requirements for the degree
Doctor of Philosophy in Microbiology and Molecular Genetics

_____

June, 2017

Each person whose signature appears below certifies that this dissertation in his/her opinion is adequate, in scope and quality, as a dissertation for the degree Doctor of Philosophy.

_____ , Co-Chairperson
Barry L. Taylor, Emeritus Professor of Basic Sciences

_____ , Co-Chairperson
Kylie J. Watts, Assistant Professor of Basic Sciences

_____
Penelope Duerksen-Hughes, Professor of Basic Sciences

_____
Paul Herrmann, Professor of Pathology and Human Anatomy and Associate Professor for Clinical Laboratory Science

_____
Mark S. Johnson, Associate Professor of Basic Sciences

_____
Subburaman Mohan, Research Professor Medicine

ACKNOWLEDGEMENTS

CONTENTS

FIGURES

TABLES

ABBREVIATIONS

Aer	aerotaxis and energy taxis receptor
AS	amphipathic sequence
ATP	adenosine triphosphate
β-Me	β-mercaptoethanol
CAM	chloramphenicol
CCW	counterclockwise
CuPhe	copper phenanthroline
Cys-less	cysteine-less
CW	clockwise
dNTP	deoxyribonucleotide triphosphates
ETS	electron transport system
FAD	flavin adenine dinucleotide
FADH	semiquinone form of FAD
$FADH_2$	hydroquinone form of FAD
FMN	flavin mononucleotide
HAMP	histidine kinases, adenylate cyclases, methyl accepting proteins, phosphatases
Hb	hemoglobin
HbN	homodimeric hemoglobin
hERG	human ether-a-go-go related gene
HIF	hypoxia inducible factor
IPTG	isopropyl β-D-thiogalacto-pyranoside

LB	Luria-Bertani medium
LOV	light, oxygen, voltage
Mb	myoglobin protein
MCP	methyl-accepting chemoreceptor
MmoS	methane monooxydase S
N-cap	N-terminal cap
NifL	nitrogen fixation protein L
Nik1	nuclear shuttle protein-interacting kinase 1
PAS	period clock protein, aryl hydrocarbon receptor, single minded protein
PEG-mal	methoxypolyethylene glycol-maleimide 5000
PIR	protein interaction region
PMF	proton motive force
PYP	photoactive yellow protein
SAM	S-adenosyl methionine
SDS-PAGE	sodium dodecyl sulfate-polyacrylamide gel electrophoresis
SMART	simple, modular, architecture, research, tool
Tap	transmembrane peptide receptor
Tar	transmembrane aspartate receptor
TB	tryptone broth
TBST	tris buffered saline tween 20
TEMED	*N,N,N',N'*-tetramethylethylenediamine

TM	transmemebrane
Trg	transmembrane ribose and galactose receptor
Tsr	transmembrane serine receptor

ABSTRACT OF THE DISSERTATION

PAS Signaling Mechanisms in Aer and Aer2

by

Darysbel Garcia

Doctor of Philosophy, Graduate Program in Microbiology and Molecular Genetics
Loma Linda University, California USA, June 2017
Dr. Barry L Taylor and Dr. Kylie J. Watts, Co-Chairpersons

PAS domains are widespread signal sensors that share a conserved three-dimensional αβ fold that consists of a central β-sheet flanked by several α-helices. The aerotaxis receptor Aer from *Escherichia coli* and the Aer2 chemoreceptor from *Pseudomonas aeruginosa* both contain PAS domains. Aer senses oxygen (O_2) indirectly via an FAD cofactor bound to its PAS domain, while Aer2 directly binds O_2 to its PAS b-type heme cofactor. The Aer and Aer2 PAS domains both interact with a signal transduction domain known as a HAMP domain. The PAS-HAMP arrangement differs between Aer and Aer2, with Aer-PAS residing adjacent to its HAMP domain, and Aer2-PAS being sandwiched linearly between three N-terminal and two C-terminal HAMP domains. The differences between these PAS-HAMP architectures raise the possibility of two different PAS-HAMP signaling mechanisms: a lateral PAS-HAMP signaling mechanism for Aer, and a linear PAS-HAMP signaling mechanism for Aer2. This dissertation focuses on uncovering the PAS-HAMP transduction mechanisms and clarifying the signaling of conserved residues in Aer and Aer2 PAS. In Aer, I determined that a region on the PAS β-scaffold was sequestered by direct interaction with the HAMP domain. These data support a novel lateral PAS-

HAMP arrangement that is crucial for Aer signaling. In Aer2, I demonstrated that unique PAS domain residues are involved in heme-binding, oxygen-binding and PAS signal initiation. My data provide the first functional corroboration of the Aer2 PAS signaling mechanism previously proposed from structure.

The work presented in this dissertation demonstrates two variations of PAS-HAMP signaling mechanisms, both involving a global conformational change of the PAS domain that is transmitted from the PAS β-scaffold to the HAMP domain. My Aer and Aer2 studies provide the first direct evidence that HAMP domains can be activated by either linear or lateral interaction with a sensor module. Studying PAS-HAMP signaling mechanisms will help in understanding how sensing domains activate chemosensory systems that are involved in the survival of both commensal and pathogenic bacteria.

CHAPTER ONE

INTRODUCTION

Bacterial Chemosensory Systems

Bacterial chemosensory systems are found in 58% of prokaryotes (Wuichet *et al.*, 2010) and grant bacteria the ability to sense and respond to both external and internal signals. The best understood chemosensory system is the chemotaxis system of *Escherichia coli* whose main purpose is to navigate cells towards an optimal nutritional environment. Contrary to the simplicity of the *E. coli* chemotaxis system, *Pseudomonas aeruginosa* contains four chemosensory systems, and each system has a different function (Kato *et al.*, 2008, Wuichet *et al.*, 2010). Chemosensory systems consist of chemoreceptors and effector proteins. Chemoreceptors are capable of detecting chemoeffectors (e.g., environmental pH and temperature) or ligands (e.g., sugars, amino acids, and O_2), while effector proteins help translate sensory signals into cellular behaviors such as biofilm formation, directed motility, and gene modification (Bi *et al.*, 2015). The research described in this dissertation investigates the signaling mechanisms of both Aer-directed aerotaxis in *E. coli* and Aer2-directed excitation signaling in *P. aeruginosa*. These comparatively simple behavioral systems occur in a single cell and can be dissected by biochemical and genetic techniques.

Chemoreceptors

There are two main classes of chemoreceptors: membrane-bound and soluble cytoplasmic chemoreceptors (Collins *et al.*, 2014) (Fig. 1). In Gram-

1

negative bacteria like *E. coli* and *P. aeruginosa*, membrane-bound chemoreceptors are anchored to the inner membrane of cells by a transmembrane (TM) domain. Membrane-bound chemoreceptors are the most abundant and most studied type of chemoreceptor, accounting for 86% of bacterial chemoreceptors (Collins *et al.*, 2014). Membrane-bound chemoreceptors usually bind their ligands in the periplasmic space, allowing them to transmit information from the environment into the cell interior (Fig. 1). However, some membrane-bound receptors like Aer have an intracellular sensing domain that monitors the internal state.

The recent discovery of soluble cytoplasmic chemoreceptors has expanded the field of signal recognition and transduction. Sequenced genomes in the SMART database (http://smart.embl-heidelberg.de) revealed that out of 8,384 chemoreceptors, 14% (1,129 chemoreceptors) were cytoplasmic chemoreceptors (Collins *et al.*, 2014). Little is known about the function of cytoplasmic chemoreceptors, but the cytoplasmic chemoreceptors in *Rhodobacter sphaeroides* and *Sinorhizobium meliloti* have been speculated to monitor internal stimuli and modulate chemotactic responses (Alexandre *et al.*, 2001, Porter *et al.*, 2008, Armitage *et al.*, 1997). Although the functions of most soluble cytoplasmic chemoreceptors remain to be elucidated, cytoplasmic and membrane-bound chemoreceptors share similarities in their structural composition, making it easier to study their signal transduction mechanisms. Both cytoplasmic and membrane-bound chemoreceptors consist of a signal sensor domain, a signal transduction domain, and an output domain, which

allows the receptor to elicit a response by interacting with cytoplasmic proteins

(Fig. 1).
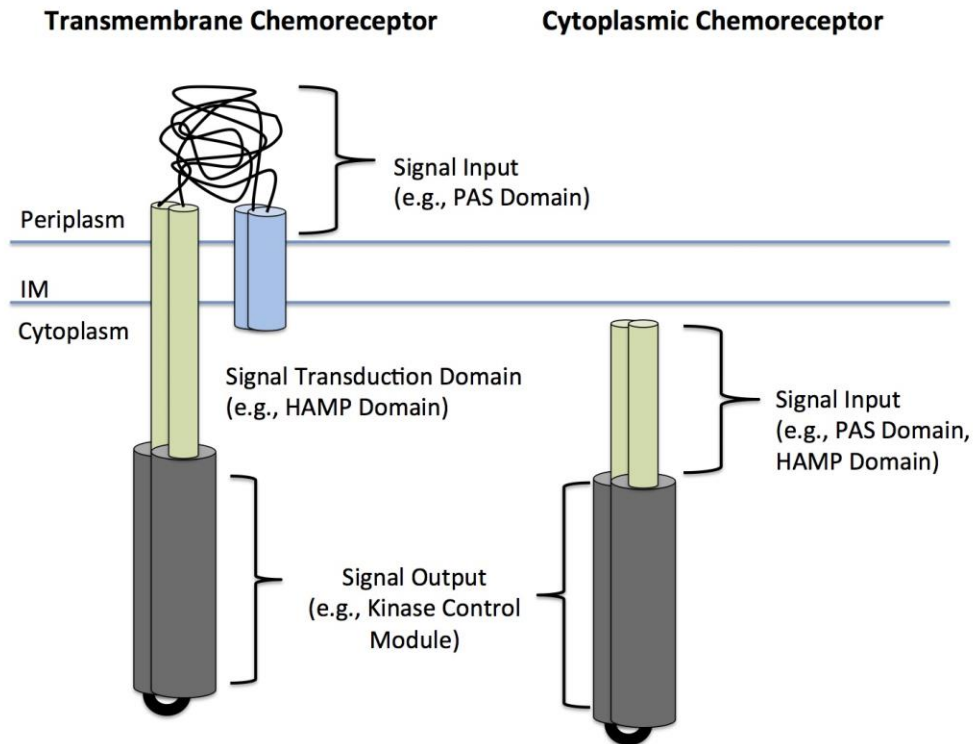
Figure 1. Comparison of transmembrane and cytoplasmic chemoreceptors. Transmembrane and cytoplasmic chemoreceptors are composed of a signal input domain such as a PAS domain, a signal transducer domain such as a HAMP domain, and a signal output domain or kinase control module. Abbreviation: IM, inner membrane.

Chemosensory Arrays

Higher-order structures of chemoreceptors, called chemosensory arrays, are critical in receptor function (Ames *et al.*, 2002). Both membrane-bound and cytoplasmic receptor chemosensory arrays consist of chemoreceptor

homodimers, clustered into trimers-of-dimers (Ames *et al.*, 2002, Studdert *et al.*, 2005) and stabilized by the chemotaxis proteins CheA and CheW (Studdert *et al.*, 2005). Transmembrane and cytoplasmic chemoreceptors both form 12-nm hexagonal arrays (Briegel *et al.*, 2009). However, some cytoplasmic receptors have a sandwiched architecture consisting of two CheA and CheW baseplates sandwiched between two opposing receptor arrays (Briegel *et al.*, 2014). In addition, chemosensory arrays are found at cell poles and at sites of future cell division known as lateral patches (Maddock *et al.*, 1993, Kentner *et al.*, 2006). Polar patches move along the curvature of the cell pole while lateral patches remained fixed (Kentner *et al.*, 2006).

Chemotaxis

Bacteria respond to changes in chemical gradients in their surrounding environment (Adler, 1966). For both *E. coli* and *P. aeruginosa,* chemotaxis involves modulation of their swimming patterns. *E. coli* has a peritrichous flagellar arrangement, whereas *P. aeruginosa* has a single polar flagellum. Bacterial swimming patterns result from the direction in which the individual flagella rotate, which itself is dependent on the stimuli the bacteria sense. In an isotropic environment, *E. coli*'s swimming pattern is known as a "random walk" in which cells swim smoothly and then tumble for ~0.1 sec (Berg *et al.*, 1972). If the concentration of an attractant increases, bacteria swim smoothly by suppressing tumbling. When a repellent stimulus is encountered, bacteria tumble frequently to change swimming direction in search of a more favorable environment (Berg,

2003). In monotrichous bacteria such as *P. aeruginosa*, there is a brief reversal in direction instead of tumbling (Taylor *et al.*, 1974). The ability of *E. coli* and *P. aeruginosa* to change swimming direction is due to the interaction of chemotaxis proteins with the flagellar motor/s of the cell.

Chemotaxis Proteins

The output domain in all chemoreceptors is known as the kinase control module (Fig. 2) (Alexander *et al.*, 2007). The kinase control module is highly conserved in sequence and protein structure, consisting of two monomers with antiparallel helices and a hairpin tip or "U-turn" that forms a supercoiled, four helix bundle (Fig. 2). The kinase control module can be divided into three regions: i) the adaptation region, which contains four to six glutamine or glutamic acid residues that are methylation sites for adaptational modification in methyl-accepting chemoreceptors (Terwilliger *et al.*, 1983, Terwilliger *et al.*, 1984), ii) the flexible region that contains a glycine hinge (Alexander *et al.*, 2007), and iii) the protein interaction region where the kinase control module interacts with downstream chemotaxis proteins (Fig. 2). Chemotaxis proteins CheA (histidine kinase), CheW (docking protein), CheB and CheD (methylesterase and deamidase), and CheR (methyltransferase) all interact with the kinase control module (Hazelbauer *et al.*, 2008).

Structurally, CheA is a homodimer with each dimer consisting of five structural subunits (P1, P2, P3, P4, and P5) that have different functions (Jahreis *et al.*, 2004, Morrison *et al.*, 1994, Swanson *et al.*, 1993).

Kinase Control Module
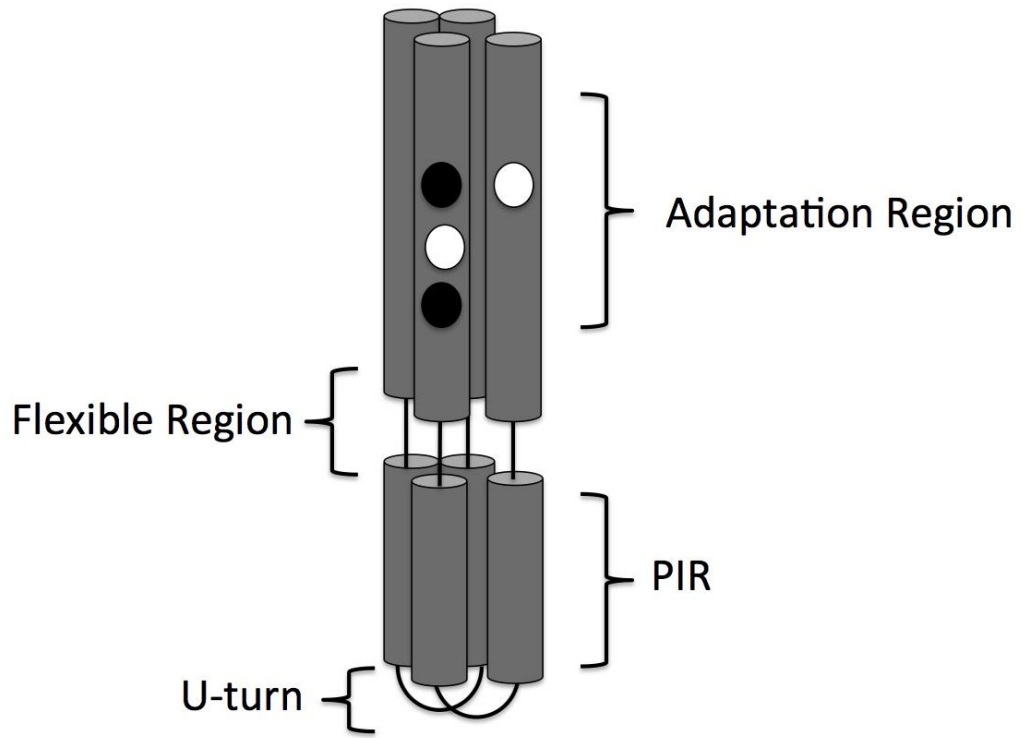
Figure 2. Subregions of the kinase control module. The kinase control module consists of i) an adaptation region containing methylation sites, ii) a flexible region, and iii) a protein interaction region (PIR). The circles in the adaptation region represent glutamine (black circles) and glutamic acid residues (white circles). Glutamine residues must be deaminated before they can be methylated. The black lines in the flexible region represent the glycine hinge. The U-turn allows the kinase control module to form a supercoiled four-helix bundle. Refer to Fig. 1 for the location of the kinase control region in the context of a complete chemoreceptor.

The P1 subunit has autokinase activity. The P2 subunit binds either CheB or the response regulator CheY and transfers phosphoryl groups from the P1 subunit to specific aspartate residues in CheB and CheY (McEvoy *et al.*, 1996, Stewart *et al.*, 2000, Jahreis *et al.*, 2004). Dimerization of CheA occurs at the P3 subunit (Park *et al.*, 2004), and the P4 subunit catalyzes the transfer of phosphate from adenosine triphosphate (ATP) to a histidine residue on the P1 subunit (His48 in *E. coli* CheA) (Garzon *et al.*, 1996, Bilwes *et al.*, 2001). Together, the P3 and P4 subunits provide sites for contact with chemoreceptors (Miller *et al.*, 2006). The fifth subunit, P5, binds to both CheW and chemoreceptors, and is necessary for CheA activation by receptors (Bourret *et al.*, 1993, Zhao *et al.*, 2006b, Zhao *et al.*, 2006a). Although the exact docking mechanism of CheW remains to be elucidated, it is crucial for CheA activation (Fig. 3). Chemoreceptor signaling activates CheA autophosphorylation, with subsequent transfer of the phosphate to CheY (Fig. 3). The phosphorylation site on *E. coli* CheY is Asp57, and this triggers a conformational change in CheY that promotes binding to the flagellar motor protein FliM (Formaneck *et al.*, 2006, Stock *et al.*, 2006). When phosphorylated CheY (CheY-P) binds to FliM, this changes the direction of flagellar rotation from counterclockwise (CCW; the default direction) to clockwise (CW), causing the cell to tumble (Fig. 3) (Formaneck *et al.*, 2006, Stock *et al.*, 2006). In order to stop the cell tumbling, the CheZ phosphatase rapidly moves from the membrane to the cytoplasm to dephosphorylate CheY (Zhao *et al.*, 2002) (Fig. 3).
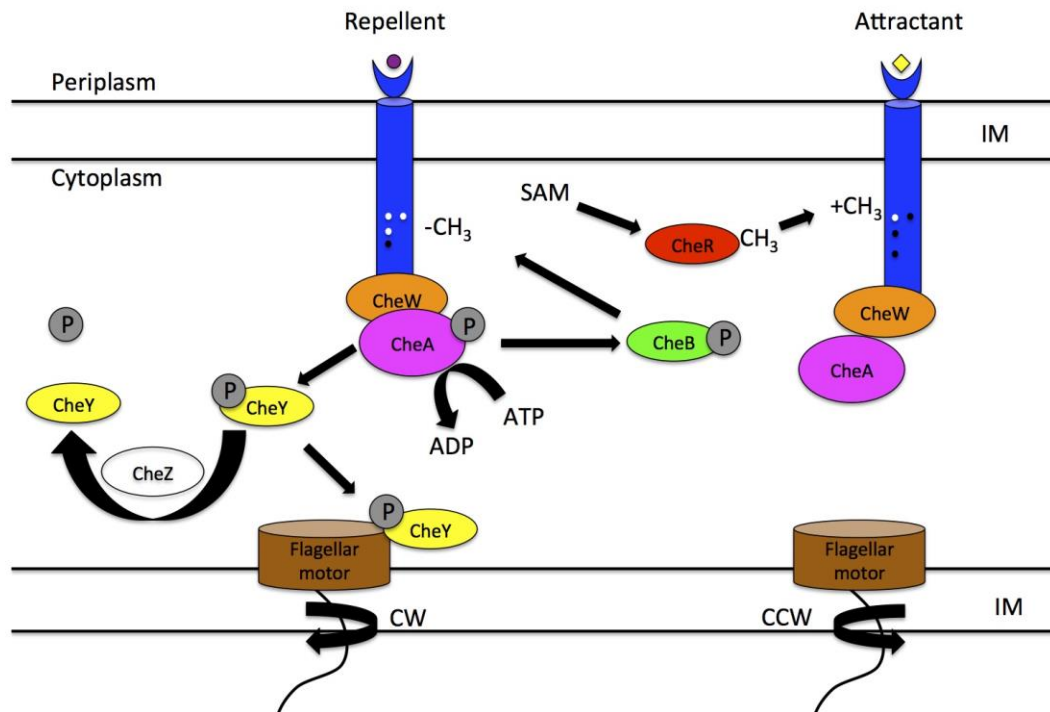
Figure 3. Chemotaxis sensing and protein phosphorylation cascade as observed in *E. coli* and *P. aeruginosa* chemotaxis. When a receptor encounters a repellent, it activates CheA (magenta), which autophosphorylates by catalyzing phosphate transfer from ATP. Phosphorylated CheA transfers a phosphate group to CheY (yellow). Phosphorylated CheY binds to the flagellar motor (brown), changing the direction of flagellar rotation from counterclockwise (CCW) to clockwise (CW), resulting in cell tumbling. Phosphorylated CheA also transfers a phosphate group to CheB (green), activating it to demethylate the receptor, countering the repellent signal and reseting the receptor to the prestimulus state. In the presence of an attractant, CheA, CheY and CheB are not phosphorylated and flagellar motor rotation remains CCW, producing smooth swimming. S-adenosyl-methionine (SAM) provides methyl groups for CheR (red) to methylate glutamic acid residues in the adaptation region of the kinase control module, countering the attractant signal and reseting the receptor to the prestimulus state. The lifetime of CheY-P is inversely proportional to the activity of the CheZ (white) phosphatase. The circles in the receptors represent glutamine (black circles) and glutamic acid residues (white circles). Abbreviations: IM, inner membrane; SAM, S-adenosyl methionine; CCW, counterclockwise; CW, clockwise.

P. aeruginosa has a chemotaxis system containing homologous protein

components to that of the *E. coli* chemotaxis system*.*

Adaptation

Chemoreceptors detect minuscule changes in stimulus concentration by

comparing a stimulus change against a constant background (Borroni *et al.*,

1988). The adaptation state of *E. coli* chemoreceptors are controlled by CheB

and CheR, whereas *P. aeruginosa* has the additional controller, CheD. In *E. coli*,

CheB and CheR bind to a C-terminal pentapeptide sequence that enhances the

catalytic reactions of CheR and CheB in the adaptation region of the kinase

control module (Fig. 2) (Barnakov *et al.*, 1999, Wu *et al.*, 1996). In the presence

of an attractant, S-adenosyl-methionine (SAM) provides methyl groups for CheR

to methylate the glutamic acid residues in the adaptation region, forming glutamyl

methyl esters (Fig. 3) (Boyd *et al.*, 1980, Terwilliger *et al.*, 1983). The addition of

methyl groups to the adaptation region renders the chemoreceptor more signal-

on (CW) biased (Starrett *et al.*, 2005), countering the smooth (signal-off) signal

sent by the attractant, and reseting cellular behavior to that of a random-walk

(Hazelbauer *et al.*, 2008, Macnab *et al.*, 1972). In the presence of a repellent,

activated CheA phosphorylates CheB (CheB-P) and CheB-P catalyzes the

hydrolysis of the methyl ester bond on the glutamyl methyl esters (Fig. 3) (Boyd

et al., 1980). Demethylation of the receptor triggers a conformational change in

the receptor that inactivates bound CheA and makes the receptor more signal-off

(CCW) biased; this counters the tumbling (signal-on) signal sent by the repellent,

and resets cellular behavior to that of a random-walk. Thus, receptor methylation establishes a bacterial short-term memory (of a few seconds) that keeps a record of the stimuli concentration (Berg *et al.*, 1975). By continually resetting the behavior to a random walk, small changes in stimuli can be monitored over a large range of concentrations (Macnab *et al.*, 1972, Hazelbauer *et al.*, 2008). Notably, *P. aeruginosa* has an alternative adaptation system that also incorporates CheD. Although the role of CheD in *P. aeruginosa* has not been demonstrated, studies on *Bacillus subtilis* CheD indicate that CheD is involved in the deamination of chemoreceptors (Glekas *et al.*, 2012). In *B. subtilis* this increases receptor-mediated kinase activity, but in *P. aeruginosa*, this decreases Aer2-mediated kinase activity.

E. coli Chemotaxis System

The chemotaxis system of *E. coli* is a well-studied chemosensory system that serves as a model for signal transduction. The *E. coli* chemotaxis system consists of five transmembrane chemoreceptors (Tsr, Tar, Trg, Tap, and Aer) that guide the cells toward optimal concentrations of life-sustaining nutrients and energy-generating environments (Fig. 4). The Tar and Tsr receptors are high abundance chemoreceptors making up 90% of chemoreceptors in the cell, while Trg, Tap, and Aer are low abundance chemoreceptors (Li *et al.*, 2004, Springer *et al.*, 1977). *E. coli* chemoreceptors are homodimers with similar structures. Tsr, Tar, Trg, and Tap all contain a periplasmic sensing domain, a TM region that anchors the receptor to the inner membrane, a cytoplasmic signal transduction

domain known as a HAMP domain, and a kinase control module (see Fig. 1). Tsr

senses the attractants serine and proton motive force (Clarke *et al.*, 1979,

Edwards *et al.*, 2006), Tar senses the attractants aspartate and maltose (Clarke

et al., 1979), Trg senses the attractants ribose, glucose, and galactose (Kondoh

et al., 1979), whereas Tap senses attractant peptides (Grebe *et al.*, 1998) (Fig.

4). Aer is different from the other chemoreceptors in that it has a cytoplasmic

sensor that is an FAD-containing PAS domain (Figs. 4 and 5). Aer is anchored to

the inner membrane by a TM domain, and is preceded by an F1 domain that

links the TM domain with the N-terminal PAS domain (Bibikov *et al.*, 1997a,

Bibikov *et al.*, 2000, Repik *et al.*, 2000b). The HAMP domain is C-terminal to the

TM domain and is connected to the kinase control module (Fig. 5). Aer is a redox

detector that indirectly senses O_2 by the reduction or oxidation of FAD bound to

the PAS domain (Rebbapragada *et al.*, 1997b, Bibikov *et al.*, 2000, Edwards *et*

al., 2006).
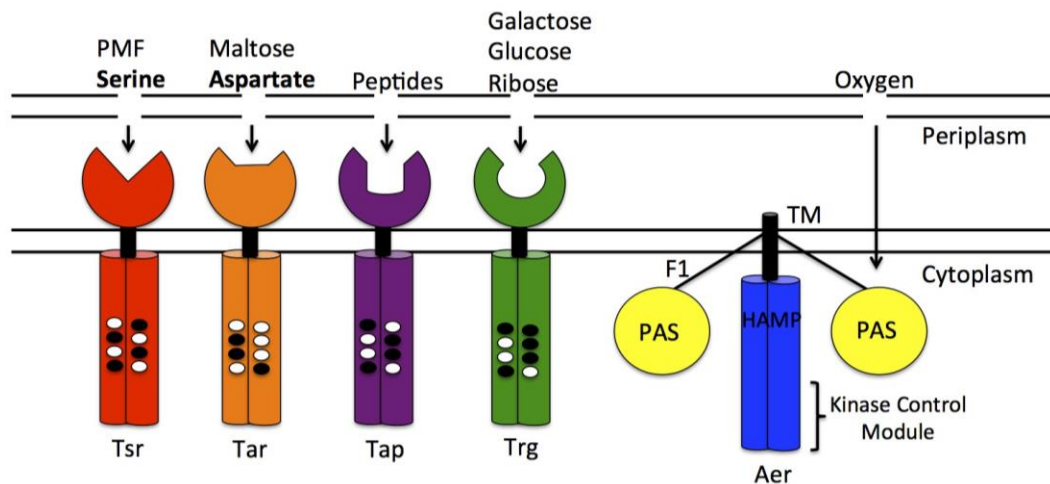
Figure 4. The five *E. coli* chemoreceptors. Serine and aspartate are the only *E. coli* attractants that do not require a binding protein to bind chemoreceptor ligand binding sites. Aer is the only *E. coli* chemoreceptor that infers ligand concentraction indirectly and lacks methylation sites. Reversible methylation of specific glutamic acid residues on the chemoreceptors is represented by black and white circles. Abbreviations: PMF, proton motive force.

Because the Tsr, Tar, Trg, and Tap receptors are methylated and demethylated by the adaptation enzymes CheB and CheR, they are also called methyl-accepting chemoreceptors, or MCPs (Grebe *et al.*, 1998). The high abundance receptors Tar and Tsr are the only *E. coli* receptors that have a C-terminal pentapeptide (NWETF) for binding CheR and CheB (Grebe *et al.*, 1998). Thus, *E. coli*'s low-abundance chemoreceptors are unable to directly bind CheR/B (Weerasuriya *et al.*, 1998, Feng *et al.*, 1997). Aer does not have a C-terminal pentapeptide or an adaptation region with methylatable residues. To compensate for this, Aer has a methylation-independent adaptation mechanism that has not been convincingly explained (Bibikov *et al.*, 2004, Niwano *et al.*, 1982). Aer signals may be dampened by the biasing influence of the MCPs, as

well as by unknown cellular compensatory changes in cellular redox (Bibikov *et al.*, 2004). In order for Trg and Tap to detect minuscule changes in attractants or repellents, they need adaptational assistance. Tar and Tsr provide such assistance by forming "assistance neighborhoods," (Hazelbauer *et al.*, 2008). Assistance neighborhoods are achieved through trimers of receptor dimers. The close proximity of the receptors in the trimer-of-dimers enables CheR and CheB to interact with the adaptation region of low-abundance chemoreceptors (Li *et al.*, 2005). Tar and Tsr contributes to the mobility of CheR within receptor clusters by allowing receptors lacking a pentapeptide to be methylated. The methylation sites are found within the adaptation region of the kinase control module with a sequence of Glu-Glu-X-X-Ala-Ser/Thr, with the second G residue being able to be methylated by CheR (Terwilliger *et al.*, 1986). CheR moves through receptor clusters like a "gibbon swinging through the branches of a tree" which is known as molecular brachiation (Levin *et al.*, 2002). Instead of moving through receptor clusters like CheR, the close proximity of the receptor units allows CheB to dock onto the pentapeptide of a high abundance receptor, resulting in an increased local CheB concentration that enables CheB to demethylate low abundance receptors. (Barnakov *et al.*, 1999).

E. coli Aerotaxis

Aerotaxis is the movement of microorganisms towards an optimal concentration of O_2 (Taylor, 1983). Aerotaxis in *E. coli* is mediated by both the Aer and Tsr chemoreceptors (Bibikov *et al.*, 1997a, Rebbapragada *et al.*, 1997a).

Aer and Tsr both require the electron transport system (ETS), and detect external

O_2 gradients either via changes in electron transport and redox (Aer) or by

changes in proton motive force (PMF) (Tsr) (Edwards *et al.*, 2006). In *E. coli*, a

substrate specific dehydrogenase accepts electrons from organic matter and

transfers them onto quinones. The quinones shuttle electrons through the

membrane, which are then passed to an electron acceptor by a terminal

reductase (Gennis *et al.*, 1996). As electrons move across the membrane via the

ETS, protons are translocated to the periplasmic space, which generates an

electrochemical gradient of protons (PMF) across the membrane (Krulwich *et al.*,

2011).
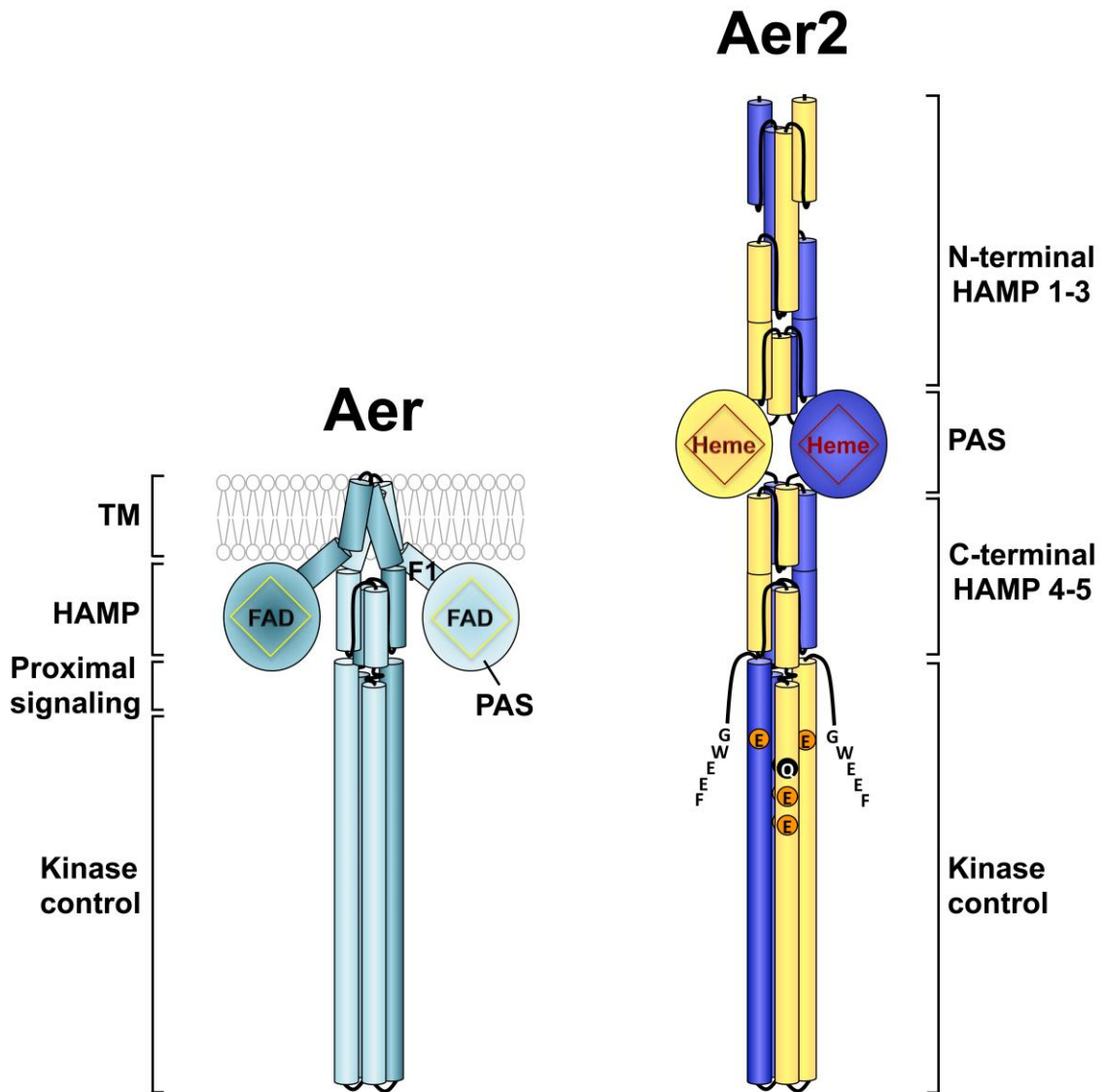
Figure 5. Comparison of the cellular location and structures of the Aer and Aer2 chemoreceptors. Aer consists of i) a transmembrane region (TM) that tethers the receptor to the inner membrane of the cell, ii) an F1 linker that connects the PAS domain to the transmembrane region, iii) a PAS domain with an associated FAD cofactor, iv) a HAMP domain, v) proximal signaling domain, and vi) a kinase control module. Aer2 consists of: i) three N-terminal and two C-terminal HAMP domains, ii) a PAS domain with a *b*-type heme cofactor, and iii) a kinase control module with methylation sites (QEEE) and a C-terminal pentapeptide (GWEEF) for binding adaptation enzymes. Abbreviations: TM, transmembrane; FAD, flavin adenine dinucleotide.

The terminal acceptor of electrons in aerobic respiration is O_2. Tsr mediates

aerotaxis by monitoring changes in PMF while Aer mediates aerotaxis by

responding to changes in redox (Edwards *et al.*, 2006). Notably, strong Aer

responses have been linked to redox changes in NADH dehydrogenase I,

although there is no absolute requirement (Edwards *et al.*, 2006).

P. aeruginosa Chemosensory Systems

Unlike *E. coli*, which has one chemosensory system and five

chemoreceptors, *P. aeruginosa* contains four chemosensory systems (gene

Clusters I-V) and 26 chemoreceptors. The four chemosensory systems include: i)

the Che system (gene Clusters I and V), which is involved in flagellar-mediated

chemotaxis (Kato *et al.*, 1999, Masduki *et al.*, 1995), ii) the Che2 system (Cluster

II), who's function remains to be elucidated (Guvener *et al.*, 2006, Hong *et al.*,

2004a, Ferrandez *et al.*, 2002), iii) the Wsp system (Cluster III), which regulates

biofilm formation (Kato *et al.*, 2008, Sampedro *et al.*, 2015), and the Pil-Chp

system (gene Cluster IV), which regulates pilus-mediated twitching motility

(Darzins, 1994, Kearns *et al.*, 2001). Although the function of the Che2 system

remains unknown, it contains a set of genes (*cheY2*, *A2*, *W2*, *R2*, *B2*, *D*) whose

products are expressed in stationary phase and are held together by the Che2

chemoreceptor, Aer2 (also known as McpB), at the cell pole (Guvener *et al.*,

2006, Hong *et al.*, 2005, Schuster *et al.*, 2004). With the exception of CheD, the

Che2 system proteins CheY2, CheA2, CheW2, CheR2, and CheB2 are

homologs of the *E. coli* chemotaxis proteins (Fig. 6).

16

The kinase control module of *P. aeruginosa* Aer2 is predicted to have four methylation sites (QEEE) and a C-terminal pentapeptide (GWEEF) (Fig. 5) (Watts *et al.*, 2011b). The Aer2 C-terminal pentapeptide sequence is speculated to bind the Che2 adaptation enzymes CheD, CheB2 and CheR2, which catalyze Aer2 deamidation, demethylation and methylation, respectively. The methyltransferase CheR2 has been shown to specifically methylate Aer2 (Garcia-Fontana *et al.*, 2014).The Che2 proteins do not interact with Che (chemotaxis) proteins, suggesting that the Che2 proteins form different signal transduction complexes (Guvener *et al.*, 2006).

Aer2 is a cytoplasmic receptor (Fig. 5) that was initially reported to be an aerotaxis receptor, but no aerotaxis response has been confirmed (Guvener *et al.*, 2006, Watts *et al.*, 2011b, Ferrandez *et al.*, 2002). The PAS sensing domain of Aer2 binds *b*-type heme, and the receptor can both bind and respond to oxy-gases like O_2, carbon monoxide (CO) and nitroc oxide (NO) (Watts *et al.*, 2011b). Interestingly, CheB2, which demethylates Aer2, is crucial to the virulence of *P. aeruginosa* in both a *Caenorhabditis elegans* infection model and a mouse lung infection model (Garvis *et al.*, 2009). Specifically, a deletion in CheB2 lowered the pathogenesis of *P. aeruginosa*. Thus, Aer2 may alter the virulence and in vivo survival of *P. aeruginosa*.
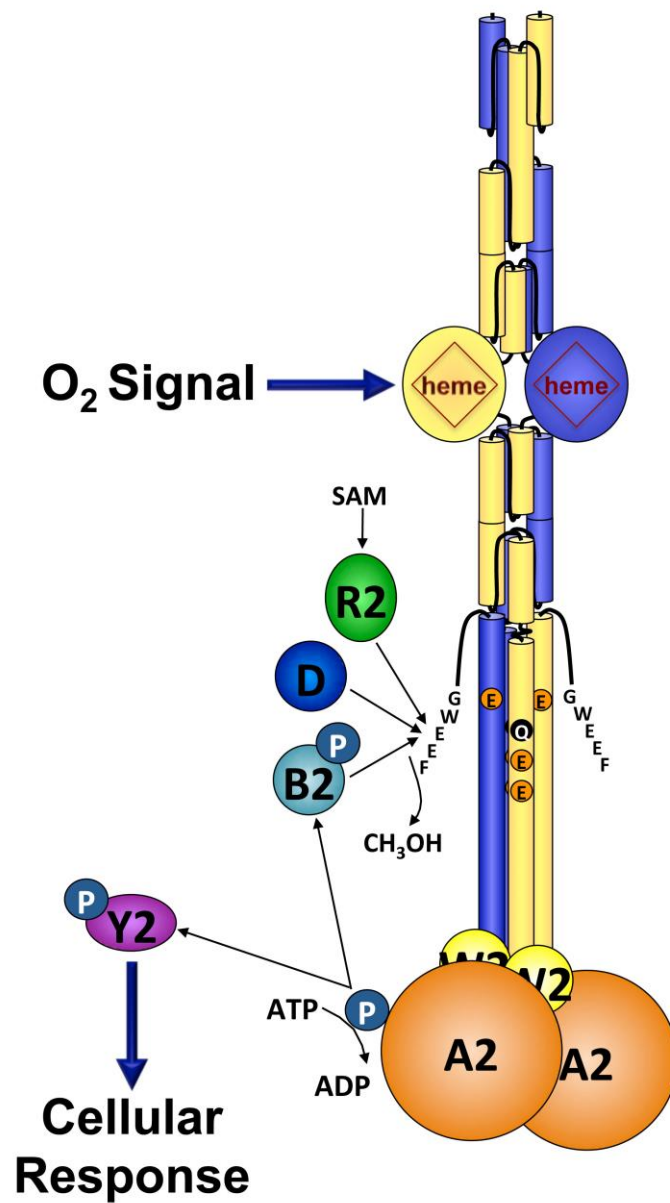
Figure 6. The Aer2 receptor and its associated Che2 proteins. The Che2 proteins CheR2, CheD, and CheB2 bind to the C-terminal pentapeptide sequence of Aer2 (GWEEF) for additional modification of specific glutamine and glutamic acid residues (QEEE). CheW2 docks CheA2 to the receptor. CheA2 transfers ATP-derived phosphate to CheY2. Phosphorylated CheY2 leads to a cellular response that remains to be elucidated. Abbreviations: SAM, S-adenosyl methionine.

PAS Domains: Signal Input Domains

Chemoreceptors sense chemoeffectors via their signal input domain. One signal input domain in chemoreceptors is the PAS (Per-Arnt-Sim) domain. The PAS acronym was created for the first three proteins in which PAS domains were discovered: a sensory protein in the fly clock protein **P**eriod (PER, involved in circadian rhythms) (Crews *et al.*, 1988), the mammalian transcription factor **A**ryl-hydrocarbon receptor nuclear translocator protein (ARNT, which participates in the activation of the xenobiotic response) (Hoffman *et al.*, 1991), and the **S**ingle-minded protein in insects (SIM, involved in cell fate determination) (Crews *et al.*, 1988). Currently, ~99,300 PAS domain containing proteins have been discovered in archaea, bacteria, eukaryotes, and viruses (http://smart.embl-heidelberg.de). PAS domains function as initiators of cellular signaling responses by monitoring changes in light, redox potential, gas molecules, small ligands, or the overall energy of the cell. PAS domains have been found in proteins such as transcriptional activators, histidine kinase sensor proteins, photoreceptors, clock proteins, and ion channels (Taylor *et al.*, 1999).

PAS Domains have a Conserved Structure

The prototype for the three-dimensional fold of the PAS domain superfamily is based on the crystal structures of five proteins: i) the full length photoactive yellow protein (PYP) of *Halorhodospira halophila* (Brudler *et al.*, 2000), ii) the heme domain of the FixL proteins from *Bradyrhizobium japonicum (Bj*FixL) (Gong *et al.*, 2000, Gong *et al.*, 1998, Hao *et al.*, 2002) and *Rhizobium meliloti* (*Rm*FixL)

(Miyatake *et al.*, 2000), iii) the N-terminal domain of the human ether-a-go-go

related gene (hERG) voltage-dependent potassium channel (Morais Cabral *et al.*,

1998), and iv) the flavin mononucleotide (FMN) containing LOV2 domain from

the plant blue-light receptor phy3 (Crosson *et al.*, 2001). Structural
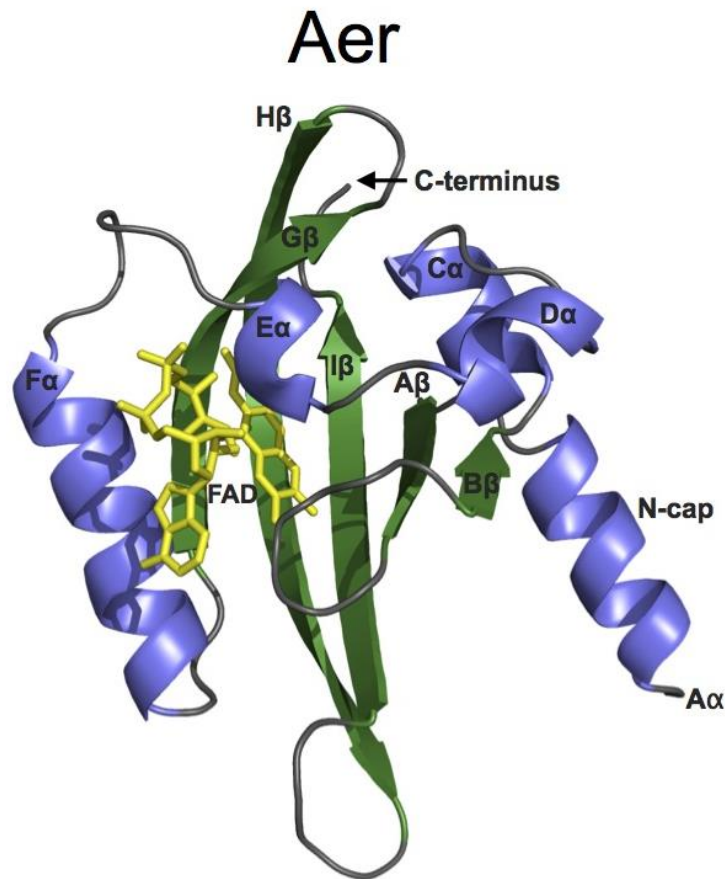
Figure 7. Aer PAS domain model based on the structure of *Azotobacter vinelandii* NifL [pdb 2GJ3, (Key *et al.*, 2007)]. α-helices in purple, β-strands in green, loops in grey, and FAD in yellow.

comparisons of resolved PAS domains reveal a conserved three-dimensional PAS fold that consists of: i) a β-scaffold that is comprised of five antiparallel β-strands, denoted Aβ, Bβ, Gβ, Hβ, and Iβ, and are in the topological order B-A-I-H-G or 2-1-5-4-3, ii) α-helices, denoted Cα, Dα, Eα, and Fα, that flank the β-sheet, iii) and a helical linker that connects the PAS core to the β-scaffold (Moglich *et al.*, 2009b, Taylor *et al.*, 1999) (Fig. 7). The PAS core creates a hydrophobic pocket on the β-sheet within which ligand or cofactor binding can occur. The PAS domain structure can be visualized as a left-handed glove. PAS domains can also have an N-terminal cap (N-cap) that is a helical lariat (helix-turn-helix) that is necessary for the stability and/or signaling of the PAS domain (Watts *et al.*, 2006b, Ke *et al.*, 2014).

PAS Domains Bind Diverse Cofactors and Ligands

Sequence alignments of PAS domains reveal variations in the structure and length of the PAS core region (Zhulin *et al.*, 1997, Zhulin & Taylor, 1998). These variations give PAS domains the ability to bind a wide range of ligands or cofactors (Moglich *et al.*, 2009b) (Fig. 8). PAS domains can have cofactors that act as sensors through cofactor modifications; for example, (FAD) in the Aer PAS domain is oxidized and reduced (Rebbapragada *et al.*, 1997a, Bibikov *et al.*, 1997a). PAS domains can also act as sensors through cofactors that bind ligands; for example, heme in the Aer2 PAS domain senses the binding of oxy-gases (Sawai *et al.*, 2012, Watts *et al.*, 2011b). Some PAS domains sense via the direct binding of ligands; for example, the PAS domain of the citrate sensor, CitA,

21

senses the binding of its ligand citrate (Reinelt *et al.*, 2003). However, many PAS

domains do not bind ligands or cofactors and are instead involved in signal

transduction and protein-protein interactions (Lindebro *et al.*, 1995).
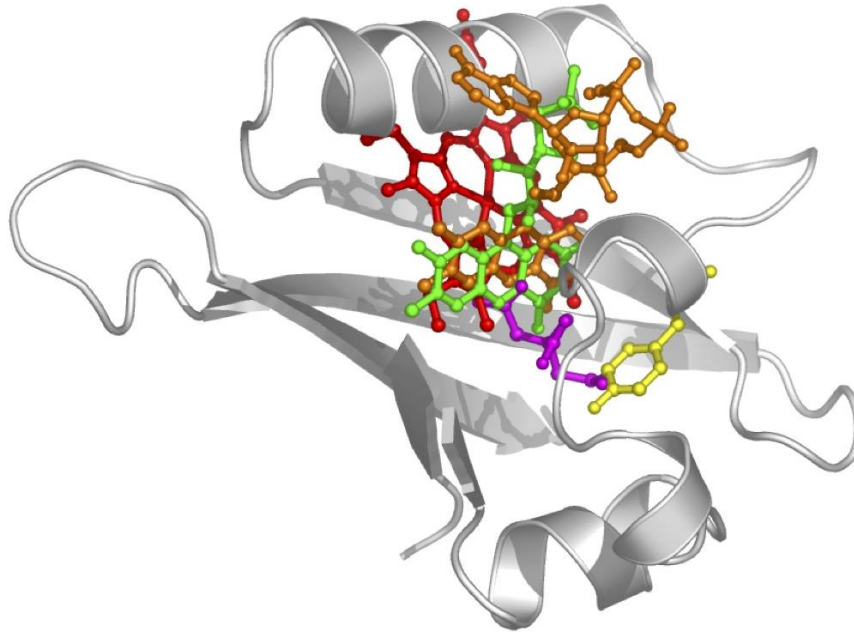
Figure 8. PAS domains accommodate diverse cofactors. The cofactors shown in this figure are FMN (green) from *Adiantum* Phy3 LOV2 PAS, heme (red) from *Sinorhizobium* FixL PAS, 4-hydroxycinnamic acid (yellow) from *Halorhodospira* PYP PAS, citrate (purple) from *Klebsiella* CitA PAS, and FAD (orange) from *Azotobacter* NifL PAS. Figure kindly provided by Dr. Sean Crosson, University of Chicago.

PAS Domain Localization

In bacterial proteins, PAS domains can be found in the cytoplasm,

periplasm, or extracytoplasmic locations (Henry *et al.*, 2011). However,

classifying extracytoplasmic PAS domains remains controversial due to slight

differences in their structure. Being localized in diverse places allows PAS

proteins to sense changes in intracellular or extracellular environments.

Approximately one third of PAS proteins contain multiple PAS domains (Henry *et*

al., 2011). Multiple PAS domains in a chemoreceptor can function as signal

sensors or serve as linkers to an effector region, another PAS domain, or to a

signaling domain (Little *et al.*, 2012). An example of a protein with multiple PAS

domains is plant phytochrome B. This photochrome contains one PAS domain in

the N-terminus and one in the C-terminus of the protein. The N-terminal PAS

domain is involved in light sensing (Oka *et al.*, 2008), whereas the C-terminal

PAS domain provides a nuclear localization signal where it is involved in

photoregulation of gene expression (Ni *et al.*, 1999).

PAS Domain Signaling Mechanisms

The signaling mechanisms used by PAS domains are thought to be

conserved among PAS domains. In general, PAS sensing domains sense a

stimulus and undergo global conformational changes in order to accommodate

and stabilize the ligand or cofactor modification (Rajagopal *et al.*, 2003, Key *et*

al., 2005). The conformational changes usually propagate to the β-sheet, and are

ultimately transmitted to other modules or domains (Moglich *et al.*, 2009b). The

transmission of the conformational changes acts as a signal to activate the

receptor and elicit a response to the stimulus.

Aer PAS Domain

Aer Binds FAD and Indirectly Senses O_2

The acronym for the aerotaxis receptor, Aer, stands for **a**ir, **e**nergy, and **r**edox. Aer guides *E. coli* cells to O_2 and energy rich niches. The Aer PAS domain senses redox changes via its non-covalently bound FAD cofactor (Bibikov *et al.*, 1997a, Rebbapragada *et al.*, 1997b, Edwards *et al.*, 2006). In PAS domains that contain FAD as a cofactor, the FAD is involved in sensing cellular redox and energy. The *Azotobacter vinelandii* NifL (*Av*NifL) PAS domain was the first FAD-bound PAS structure to be resolved (Key *et al.*, 2007). More recently, the crystal structure of the PAS-FAD domain from *Methylococcus capsulatus* MmoS was likewise solved (Ukaegbu *et al.*, 2009a). Despite the fact that the PAS structure of Aer has not yet been resolved, a series of conserved residues between Aer, NifL, and MmoS provide insight into possible Aer PAS residue interaction with FAD and signal transduction from FAD to the β-scaffold of the PAS domain.

Aer PAS Structure

The crystal structure of NifL and sequence similarities between the PAS domains of NifL and Aer has allowed a homology model to be created for the Aer PAS domain (Fig. 7). Based on this structural model, and sequence similarities between the Aer, NifL, and MmoS PAS domains, critical residues for FAD binding and signaling have been proposed. For Aer, this includes residues that bind FAD such as Asn85 (equivalent to NifL-N102 and MmoS-N164), which hydrogen bonds to the N3 and O4 atoms of the isoalloxazine ring of FAD (Zoltowski *et al.*,

24

2007, Key *et al.*, 2007, Ukaegbu *et al.*, 2009a), and Trp70 (equivalent to NifL-W87 and MmoS-W149), which forms stacking interactions with FAD and is used to predict whether a PAS domain binds FAD (Xie *et al.*, 2010, Key *et al.*, 2007, Ukaegbu *et al.*, 2009b). The residues that contact the isoalloxazine ring of FAD such as Arg57, His58, Asp60, and Asp68 are proposed to not only bind FAD, but participate in converting the redox state of FAD into conformational changes within the PAS domain (Repik *et al.*, 2000b).

Different States of FAD and the Aer Output Response

It is unknown how the FAD bound to Aer is reduced, but there are two possible scenarios in which a redox change could occur. The first possibility is that the Aer PAS domain is reduced by a cytoplasmic electron donor such as NADH. The second possibility is that the Aer PAS domain is reduced via direct interactions with the ETS (Edwards *et al.*, 2006). It is theoretically possible that the Aer FAD cofactor has three different redox states: an oxidized or quinone (FAD) state that occurs during starvation or high O_2 concentrations, ii) a semiquinone (FADH·) state which occurs when there is an electron donor and an electron acceptor such as O_2, and iii) a hydroquinone (FADH$_2$) state that occurs in anaerobic conditions (Fig. 9) (Repik *et al.*, 2000b). In one proposed model, the oxidized and fully reduced state of FAD renders the receptor kinase-on, which activates CheA; this results in CW flagellar rotation, causing cells to tumble (Fig. 3). The semiquinone state of FAD favors a kinase-off receptor leading to the inactivation of CheA, which results in CCW flagellar rotation and smooth

swimming. The three state model was used to explain why *E. coli* mutants with wild-type behavior were signal-off in response to increased O_2 levels, whereas an Aer-Y111C mutant had an inverted signal-on response (Repik *et al.*, 2000a). The Tyr111 side chain projects into the FAD pocket and might alter the redox potential of the FAD cofactor so that it is fully oxidized during maximal electron transport. Recently, the existence of the quinone and semiquinone states of the Aer FAD cofactor were biochemically confirmed in vitro (Fig. 9) (Samanta *et al.*, 2016); they were kinase-on and kinase-off respectively. However, the authors could not fully reduce Aer-FAD to the hydroquinone state, even though it must be formed in vivo. This conclusion is based on the fact that the in vivo receptor cycles between the kinase-off state aerobically (consistent with the semiquinone, not the quinone state), and the kinase-on state anaerobically (further reduction from the semiquinone state). Thus, other in vivo factors are most likely necessary to stabilize the fully reduced state of FAD.
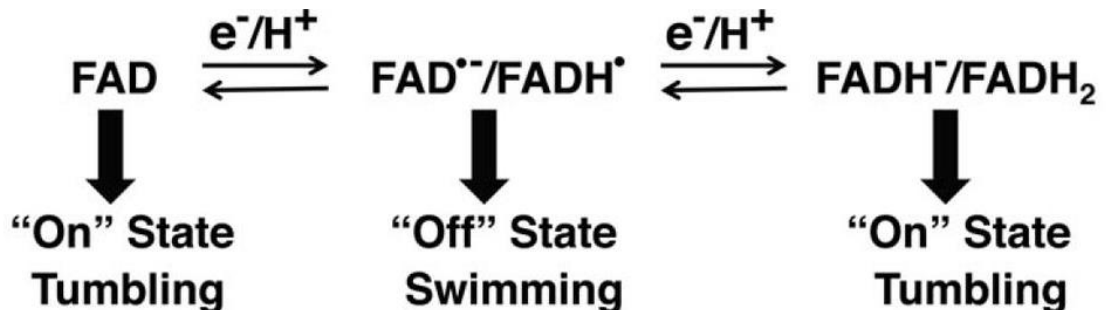
Figure 9. The different possible states of FAD in the Aer PAS domain. The quinone (FAD) and semiquinone (FAD$^{\cdot-}$/ FADH$^{\cdot}$) state of FAD have been biochemically confirmed to exist in Aer in vitro. The hydroquinone state (FADH$^-$/FADH$_2$) has not been confirmed (Samanta *et al.,* 2016).

Aer PAS Signaling Mechanism

In the Aer PAS domain, changes between the different redox states of FAD cause conformational changes. It is proposed that in the absence of O_2, FAD is in the hydroquinone state and the hydrogen bond network surrounding the FAD pocket is reorganized to allow a conformational signal to be propagated to the Aβ, Iβ, and Hβ strands that are located directly behind the FAD pocket (Key *et al.*, 2007, Zoltowski *et al.*, 2007). Genetic, biochemical, and behavioral studies have supported a role for the N-terminal (N-cap) helix in signaling (Watts *et al.*, 2006b). A similar N-cap displacement that is proposed for Aer is seen in PYP (Pellequer *et al.*, 1998), and in the LOV2 protein (Harper *et al.*, 2003), where a C-terminal helix displacement is involved in PAS signal transmission. In Aer, signal-on lesions have been discovered on the PAS Hβ and Iβ strands (Campbell *et al.*, 2010). Residues within the signal-on cluster could be crosslinked to the downstream HAMP domain, which transduces signals from the PAS domain to the kinase control module (Campbell *et al.*, 2010). This suggests that the PAS β-scaffold is the site that communicates with the downstream regions of Aer.

Aer2 PAS Domain

Aer2 PAS Cofactor and Ligand

PAS domains that bind *b*-type heme are most often O_2 sensors. Two well-known *b*-type heme binding PAS domains are found in the FixL protein from *Bradyrhizobium japonicum* (*Bj*FixL) and the *E. coli* direct O_2 sensor DOS

(*Ec*Dos). FixL is a signal-transducing protein that shuts down nitrogen fixation in response to the presence of O_2. DOS senses O_2 availability within biofilms and catalyzes the conversion of cyclic-di-GMP to linear di-GMP when there is an increase in O_2 (Shimizu, 2013), resulting in the repression of genes involved in biofilm formation (Tuckerman *et al.*, 2009). The PAS domain of Aer2 binds *b*-type heme (Fig. 10) and detects O_2, CO and NO (Watts *et al.*, 2011b).
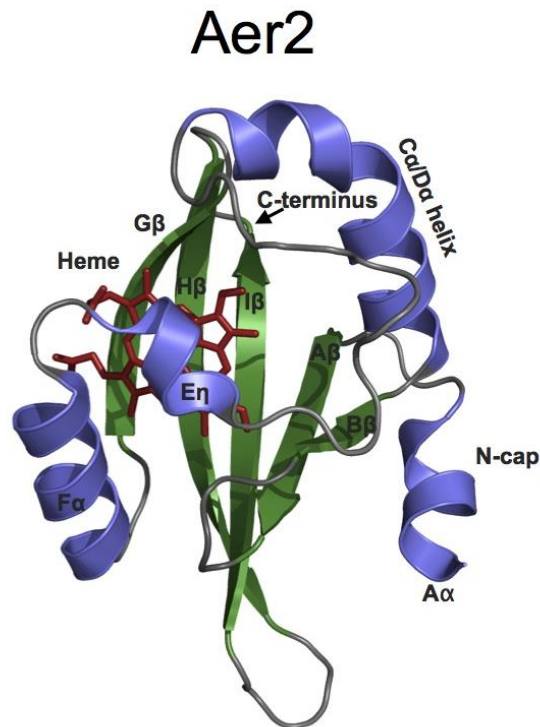
Figure 10. Structure of the Aer2 PAS domain [with cyanomet heme; pdb 3VOL, (Sawai *et al.*, 2012)]. α-helices in purple, β-strands in green, loops in grey, and heme in red.

Aer2 PAS Structure

Two crystal structures have been solved for the Aer2 PAS domain. One of

the structures is ligand-bound [cyanomet (Fe^{3+}- CN), Fig. 10] and the other is

unliganded [ferric (Fe^{3+})] (Fig. 11) (Sawai *et al.*, 2012, Airola *et al.*, 2013a). The

composition of the Aer2 PAS domain is somewhat unique compared with other

PAS-heme domains. Unlike FixL or DOS, structures of the Aer2 PAS domain

revealed an extended Cα/Dα helix and a short 3_{10} helix called Eη in place of the

Eα helix (Fig. 10). The heme-binding pocket of Aer2 is a hydrophobic cavity

surrounded by several helices. Although the Aer2 PAS domain has unique

features, it also shares similar structural features with the Aer PAS domain, e.g.,

a PAS β-scaffold that is predicted to relay signals from PAS to the downstream

domains of the receptor.

Aer2 PAS Heme Coordination

Heme coordination in PAS domains can be penta-coordinate (five

coordinate bonds to the heme iron) or hexa-coordinate (six coordinate bonds to

the heme iron) (Table 1). Heme coordination usually involves endogenous axial

ligands such as a proximal coordinating residue for penta-coordinated heme or

proximal and distal coordinating residues for hexa-coordinated heme. Heme

coordination usually involves a conserved histidine or cysteine residue (Rao *et*

al., 2011). In the reduced state of Aer2, the heme is penta-coordinate (Watts *et*

al., 2011b). In DOS and FixL, a histidine residue on the PAS Fα helix coordinates

heme-binding, and the same histidine is conserved in Aer2 (His239). However, in

Table 1. PAS domains with *b*-type heme.

Protein	Coordinating Residue		Gas Sensed	Coordination of Reduced Heme	O₂-Stabilizing Residue
	Proximal	Distal			
Aer2	Eη His	N/A	O_2	Penta-coordinate	Iβ Trp
FixL	Fα His	N/A	O_2	Penta-coordinate	Gβ Arg
PDEA-1	Fα His	N/A	O_2	Penta-coordinate	Gβ Arg
DOS	Fα His	FG loop Met	O_2	Hexa-coordinate	Gβ Arg
RcoM	Fα His	FG loop Met	CO	Hexa-coordinate	N/A
NPAS2-A	Cα loop His	Gβ His/Cys[b]	CO	Hexa-coordinate	N/A
YybT	N/A	N/A	NO	N/A	N/A
BdlA PAS-A	N/A	N/A	NO	N/A	N/A

[a]Data collected from (Gilles-Gonzalez *et al.*, 1994, Delgado-Nixon *et al.*, 2000b, Chang *et al.*, 2001, Gonzalez *et al.*, 2002, Kerby *et al.*, 2008, He *et al.*, 2009, Airola *et al.*, 2010a, Rao *et al.*, 2011, Watts *et al.*, 2011b, Petrova & Sauer, 2012, Sawai *et al.*, 2012, Uchida *et al.*, 2012, Airola *et al.*, 2013a).

[b]The distal coordinating residue for NPAS2-A is His in the ferrous state and Cys in the ferric state.

contrast to DOS and FixL, Aer2 PAS structures revealed a possible heme-coordinating residue on the short Eη helix (His234). There are several PAS domains that coordinate *b*-type heme differently to that of DOS and FixL (Table 1). The heme binding PAS domain of the YybT family of proteins lack a potential

proximal ligand for heme coordination and are proposed to coordinate *b*-type heme via bulky hydrophobic residues in the heme pocket (Rao *et al.*, 2011). Thus, an uncommon heme-binding mode exists for PAS domains besides the canonical heme-binding PAS domains of DOS and FixL.

Aer2 PAS O_2 Stabilization and Signaling

Overlaying the two Aer2-PAS structures revealed two highly conserved residues, Leu264 and Trp283, that appear to change orientations between liganded and unliganded PAS (Fig. 11). These residues are proposed to be involved in both ligand binding and PAS signaling (Airola *et al.*, 2013a, Sawai *et al.*, 2012). In the ligand bound state, Leu264 on the Hβ-strand is suspended over the heme, occupying the position where ligand will bind. Upon ligand binding, Leu264 shifts away from the heme, and Trp283 on Iβ rotates 90° to stabilize O_2 by forming a hydrogen bond. The suggestion that Trp283 stabilizes O_2 is completely novel to heme-binding PAS domains, as well as to non-PAS containing heme proteins. Other amino acids have been shown to stabilize O_2 in heme-binding PAS domains. For example, DOS and FixL use an arginine residue on Fα to stabilize O_2 (Table 1). Some non-PAS containing heme proteins including both the truncated hemoglobin (HbN) and DosT of *Mycobacterium tuberculosis,* as well as hemoglobin (Hb) of *Ascaris suum,* stabilize O_2 with a distal tyrosine residue (Huang *et al.*, 1996, Yeh *et al.*, 2000). In the vertebrate Hbs and myoglobin (Mb), a distal histidine residue stabilizes O_2 binding (Martinkova *et al.*, 2013).

HAMP domains: Signal Transducer Domains

In chemoreceptors, PAS domains often interact with a signal transducer known as a HAMP domain (Aravind *et al.*, 1999, Williams *et al.*, 1999). The HAMP acronym stands for **H**istidine kinases, **A**denylate cyclases, **M**ethyl accepting proteins of chemotaxis, and **P**hosphatases (Williams & Stewart, 1999, Aravind & Ponting, 1999), which were the first protein types discovered to contain HAMP domains. HAMP domains have been identified in ~93,500 proteins from bacteria, archaea and lower eukaryotes (http://smart.embl-heidelberg.de), where they mediate signal transduction between signal input and output domains.
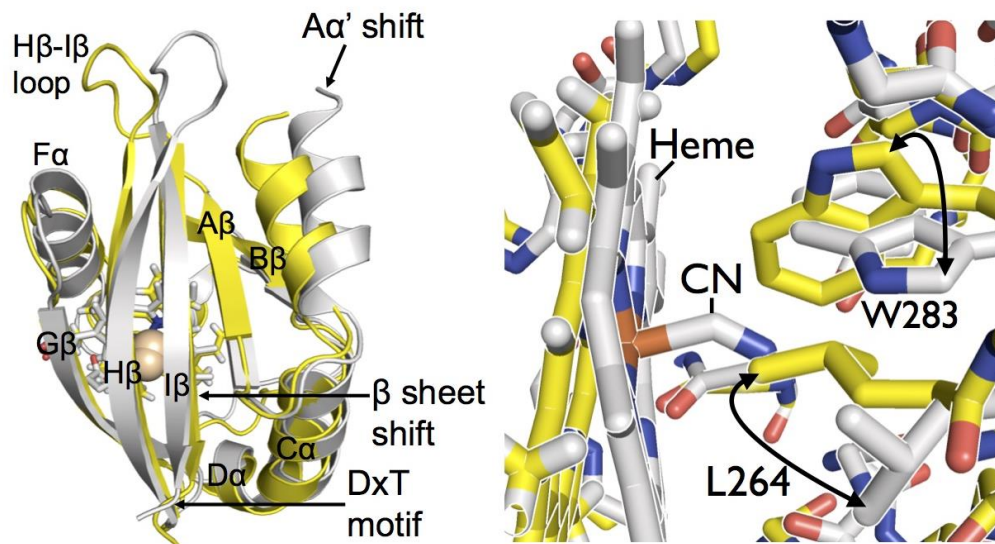
Figure 11. Overlay of unliganded (ferric heme, yellow) and liganded (cyanomet, grey) Aer2 PAS structures demonstrating a global conformational change with Trp283 rotating 90° for ligand stabilization and Leu264 moving away from the heme iron (Sawai *et al.*, 2012, Airola *et al.*, 2013a).

HAMP Structure

The first HAMP structure was solved for the *Archaeoglobus fulgidus*
Af1503 protein (Hulko *et al.*, 2006). HAMP monomers contain two amphipathic α-
helices (AS1 and AS2) that dimerize to form a parallel four-helix bundle (Fig. 12).
HAMP domains can be classified into canonical or divergent groups according to
their structure (Dunin-Horkawicz *et al.*, 2010). The canonical HAMP group
includes Aer and consists of a coiled coil structure with a DExG capping motif.
The DExG motif is located at the beginning of AS2 and is required for receiving
signals from the TM region (Dunin-Horkawicz *et al.*, 2010). In contrast, HAMP
domains from the divergent HAMP group, like those in Aer2, contain glycine
residues at the end of the AS1 helix and at the start of the AS2 helix (Dunin-
Horkawicz *et al.*, 2010). These conserved glycine residues enable HAMP
domains to associate and interact with each other as exemplified by
Debaryomyces hansenii Nik1 (DhNik1) histidine kinase, which has nine
successive HAMP domains (Meena *et al.*, 2010, Airola *et al.*, 2010d). In proteins
where there are successive HAMP domains, the HAMP domain that is proximal
to the membrane is usually from the canonical group and the distal ones are from
the divergent group (Natarajan *et al.*, 2014).

HAMP Signaling Mechanism

In membrane-bound chemoreceptors whose signal input domains are
periplasmic (Fig. 1), a conformational change is transduced through the TM
domain to cause a change in HAMP structure, thus allowing the signal from the

periplasm to be delivered to the output domain (Falke *et al.*, 2001). Biochemical

and structural studies of HAMP domains from different proteins suggest that

different signal transduction mechanisms may occur in HAMP domains. Models

proposing how the on and off states of the receptor alter the dynamics and

conformation of HAMP domains include: i) the gear-box model in which the

signaling state depends on rotation of the helices (Hulko *et al.*, 2006), ii) scissors-

like movement of the helices (Swain *et al.*, 2007), iii) tilting with rotation of the

helices (Airola *et al.*, 2013b, Matamouros *et al.*, 2015), and iv) a biphasic static-

dynamic signaling model in which the signaling state depends on four-helix

bundle stability (Zhou *et al.*, 2009). In chemoreceptors, the signaling state of the

HAMP domain is transmitted to the kinase control module where it modulates the

phosphorylation of bound CheA (Fig. 3).
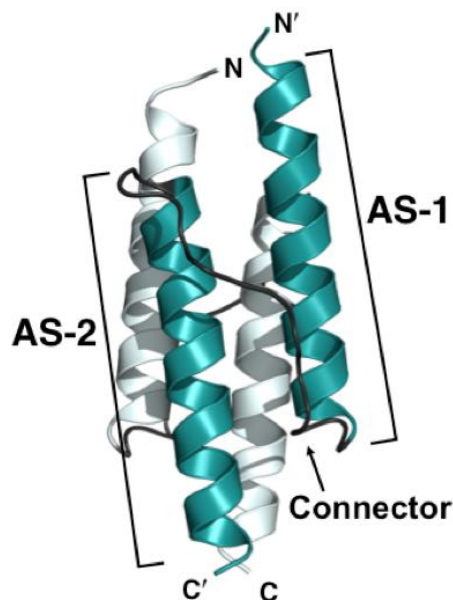
Figure 12. Model of the Aer HAMP domain based on the structure of Af1503 HAMP [pdb 2L7H, (Hulko *et al.*, 2006)]. The HAMP dimer is a parallel four-helix bundle with two amphipathic α-helices labeled AS-1 and AS-2 that are linked by a connector.

Aer and Aer2 HAMP Domains

Aer and Aer2 HAMP Structure

The HAMP domains of Aer and Aer2 differ in structure and number. Aer contains one canonical HAMP domain that follows the second transmembrane helix (Fig. 5). Although crystal structures have not been solved for the Aer HAMP domain, biochemical studies and in silico HAMP modeling indicate that the structure of the Aer HAMP domain is a four-helix bundle that is similar to the structure of Af1503-HAMP (Watts *et al.*, 2008, Hulko *et al.*, 2006) (Fig. 12). The Aer HAMP domain is also crucial for the folding and stability of the Aer PAS domain (Herrmann *et al.*, 2004, Ma *et al.*, 2005).

Aer2 contains three N-terminal HAMP domains (HAMP 1 through HAMP 3) and two C-terminal HAMP domains (HAMP 4 and HAMP 5) (Fig. 5) (Watts *et al.*, 2011a). Crystal structures of the three N-terminal HAMP domains revealed that HAMP 1 and HAMP 2 are separated by a helical linker, whereas HAMP 2 and 3 form an integrated di-HAMP structure (Airola *et al.*, 2010c). The HAMP 1 and HAMP 3 domains are structurally similar to Af1503-HAMP and appear to represent the structure of the signal-on state (Airola *et al.*, 2013a). HAMP 2 has an unusual trapezoidal four-helix bundle that represents the signal-off state (Airola *et al.*, 2010c, Airola *et al.*, 2013a). HAMP 4 and 5 share sequence similarities with HAMP 2 and 3, suggesting that they are likewise an integrated di-HAMP unit (Watts *et al.*, 2011b). In Aer2, the HAMP 4-5 unit precedes the kinase control module (Fig. 5). Unlike Aer, the HAMP domains of Aer2 are not needed for proper PAS folding and do not alter the heme environment (Airola *et al.*,

2013a).

The localization of the HAMP domains with respect to the PAS domain
differs between Aer and Aer2. The Aer PAS domain is separated from HAMP by
the intervening F1 and transmembrane domains (Fig. 5). In contrast, the Aer2
PAS domain is sandwiched between the three N-terminal and two C-terminal
HAMP domains in a linear arrangement (Fig. 5). However, in both receptors,
PAS sensing affects the structure of the C-terminal HAMP domain/s.

Aer and Aer2 PAS-HAMP Signaling Mechanisms

Aer Signaling Mechanism

Differences in the architectures of Aer and Aer2 may provide insight into
different signaling mechanisms between PAS and HAMP domains. In Aer,
signaling is initiated by the reduction of the PAS-FAD cofactor in the absence of
O_2 (Bibikov *et al.*, 1997b, Bibikov *et al.*, 2000, Repik *et al.*, 2000b). The PAS
domain then undergoes a global conformational change involving movement of
the N-cap, FAD binding cleft, and β-scaffold (Campbell *et al.*, 2011). This results
in a proposed lateral signaling mechanism involving residues on the β-scaffold
and HAMP residues on the AS2 helix (Watts *et al.*, 2004b, Ma *et al.*, 2005,
Campbell *et al.*, 2010). In the signal-on state, the HAMP domain undergoes a
conformational change that propagates to the kinase control module. In turn,
CheA transfers a phosphate group from ATP to CheY. Phosphorylated CheY
diffuses and binds to the flagella motor switch protein, FliM, resulting in a change
in flagellar rotation from CCW to CW. This change in flagella rotation allows the

cell to move away from the anaerobic environment and seek an aerobic

environment.

Aer2 Signaling Mechanism

Aer signaling is inhibited by the presence of O_2, whereas Aer2 signaling is

activated by O_2. The signaling mechanism of Aer2 is also different in that PAS

and HAMP interactions involve a linear pathway with limited PAS-HAMP

interaction (Fig. 5). In Aer2, an oxy-gas directly binds to the PAS heme cofactor

(Watts *et al.*, 2011b). Just like the PAS domain of Aer, the PAS domain of Aer2

undergoes a global conformational change that propagates from the ligand

binding cleft to the β-scaffold (Airola *et al.*, 2013a). Ligand binding may also

cause the PAS domain to transition from a dimer to a monomer (Airola *et al.*,

2013a). These PAS rearrangements allow the PAS domain to relay signals from

the C-terminal DxT motif to the AS1 helix of HAMP 4. Once the signal is received

by HAMP 4 and 5, it is then relayed to the kinase control module. The multiple

HAMP domains of Aer2 have distinct roles when it comes to signal transduction.

The role of HAMP 4 and 5 is to override the kinase-on state of the kinase control

module (Watts *et al.*, 2011b). In the presence of PAS ligand, HAMP 4 and 5 no

longer inhibits the kinase control module, resulting in a signal-on output. In

contrast, HAMP 2 and 3 do not directly transmit signals, but alter their

conformations to allow conformational changes of the PAS domain upon ligand

binding (Watts *et al.*, 2011b, Airola *et al.*, 2013a). In the presence of O_2, the

kinase control module of Aer2 increases the rate of CheA2 phosphorylation, with

37

subsequent phospho-transfer to CheY2. The output response of phosphorylated CheY2 has not yet been elucidated.

Purpose and Approach of this Dissertation

Studies on PAS domain sensing and signaling in chemoreceptors have been limited due to the difficulty of working in vitro with unstable membrane bound chemoreceptors like Aer. Therefore, molecular studies on Aer have required in vivo analyses. However, studies on the soluble Aer2 receptor overcome such limitations and also provide novel insights into PAS signaling mechanisms. The FAD-binding PAS domain of Aer is separated from its HAMP domain by a membrane anchor, while the heme-binding PAS domain of Aer2 is sandwiched between five HAMP domains. Due to their different domain arrangements, I propose that Aer utilizes a lateral PAS-HAMP signaling mechanism while the Aer2 receptor utilizes a linear PAS-HAMP signaling mechanism. In addition, since the PAS domains of Aer and Aer2 have related structure, I hypothesized that both PAS domains use similar signaling mechanisms involving residues on the β-scaffold to relay ligand binding to the HAMP domain.

The aim of the work in this dissertation is to define the PAS signaling mechanisms used by Aer and Aer2. To achieve this goal, I performed mutagenesis, biochemical and behavioral assays; to identifed PAS residues that are critical for lateral PAS-HAMP signaling in Aer, and characterized conserved residues that are needed for linear PAS-HAMP signaling in Aer2.

CHAPTER TWO

DELINEATING PAS-HAMP INTERACTION SURFACES AND SIGNALING-ASSOCIATED CHANGES IN THE AEROTAXIS RECEPTOR AER

Darysbel Garcia[1], Kylie J. Watts[1], Mark S. Johnson, and Barry L. Taylor*

Division of Microbiology and Molecular Genetics,

School of Medicine,

Loma Linda University.

Loma Linda, CA 92350. USA.

*Corresponding author.

[1]These two authors contributed equally to this investigation.

Telephone: (+1) 909 558 8544.

Fax: (+1) 909 558 0244.

Email: bltaylor@llu.edu.

Running Title: Direct PAS-HAMP interactions control Aer signaling

Key Words: PAS domain, HAMP domain, solvent accessibility, oxygen taxis, static-dynamic signaling.

This manuscript is based on experimental data acquired by Dr. Watts and myself. My contributions to this manuscript are listed below.

1) **I mapped the accessibility of the PAS domain.** I substituted 59 PAS residues with cysteine by site-directed mutagenesis. These residues were predicted to have surface-exposed side-chains (57 residues) or internal-facing side-chains (2 residues). The two interior residues (Ala97 and Ser113) served as inaccessible controls. The Cys codons were confirmed by DNA sequencing. The aerotaxis phenotypes of the Cys mutants were determined by measuring their expansion rates and ring formation in minimal soft agar plates. I then determined the accessibility of each PAS Cys mutant after permeabilizing cells with toluene/ethanol and treating with methoxypolyethylene glycol-maleimide 5000 PEG-mal. Aer and Aer PEG-mal adducts were analyzed by Western blot using anti-Aer$_{2-166}$ antisera. Cys mutants that reacted with PEG-mal were identified by an ~10kDa size increase on SDS-PAGE. I determined the extent of pegylation for each mutant by calculating the average PEGylation of the native sample and dividing it by the average PEGylation of the denatured samples.

2) **I revealed possible PAS-HAMP interaction surfaces.** I identified PAS-PAS' and PAS-HAMP interacting surfaces in vivo. To determine PAS-PAS' interaction surfaces, each of the PAS Cys mutants were crosslinked in vivo using copper phenanthroline (CuPhe). Crosslinked dimers were identified by their migration on Western blots using anti-Aer$_{2-166}$ antisera.

PAS-PAS' interaction surfaces were determined to be inter-dimeric by titrating cells with Tar chemoreceptor. To determine PAS-HAMP interaction surfaces I created di-Cys mutants by site-directed mutagenesis and crosslinked the receptor with CuPhe. Di-Cys combinations that crosslinked were retested after adding chloramphenicol to determine if crosslinking ocurred during protein folding.
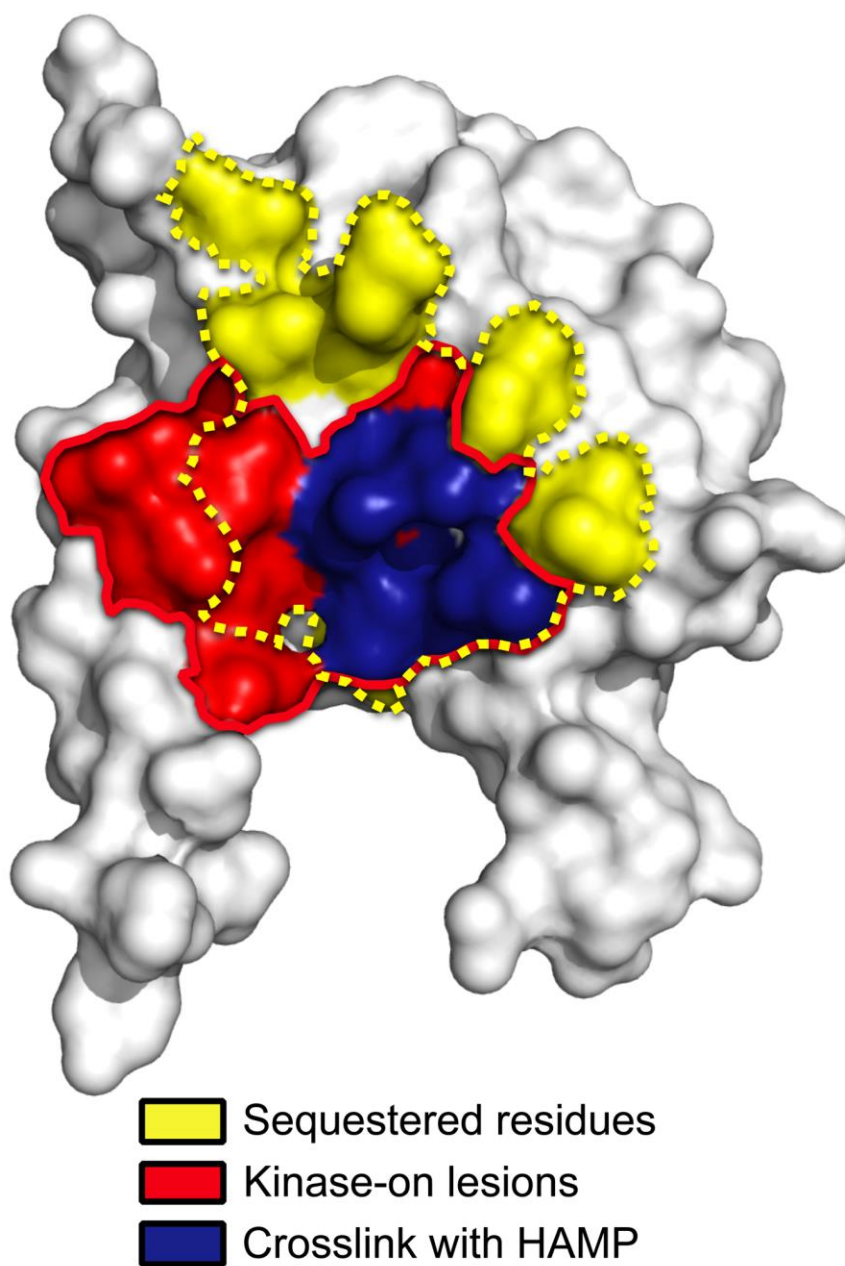
Figure 13. Graphical Abstract. Aer-PAS space-filled model overlaying a region of kinase-on lesions (within the red line) with residues shown in the current study to be either solvent-inaccessible (dotted yellow line), or preferentially crosslinked with the HAMP domain (blue).

Summary

The *Escherichia coli* aerotaxis receptor, Aer, monitors cellular oxygen and redox potential via FAD bound to a cytosolic PAS domain. Here we show that Aer-PAS controls aerotaxis through direct, lateral interactions with a HAMP domain. This contrasts with most chemoreceptors where signals propagate along the protein backbone from an N-terminal sensor to HAMP. We mapped the interaction surfaces of the Aer PAS, HAMP and proximal signaling domains in the kinase-off state by probing the solvent accessibility of 129 cysteine substitutions. Inaccessible PAS-HAMP surfaces overlapped with a cluster of PAS kinase-on lesions and with cysteine substitutions that crosslinked the PAS β-scaffold to the HAMP AS-2 helix. A refined Aer PAS-HAMP interaction model is presented. Compared to the kinase-off state, the kinase-on state increased the accessibility of HAMP residues (apparently relaxing PAS-HAMP interactions), but decreased the accessibility of proximal signaling domain residues. These data are consistent with an alternating static-dynamic model in which oxidized Aer-PAS interacts directly with HAMP AS-2, enforcing a static HAMP domain that in turn promotes a dynamic proximal signaling domain, resulting in a kinase-off output. When PAS-FAD is reduced, PAS interaction with HAMP is relaxed and a dynamic HAMP and static proximal signaling domain convey a kinase-on output.

Introduction

Microbial sensory systems include numerous combinations of common modular domains, enabling microbes to respond to a remarkable variety of environmental stimuli (Zhulin, 2001, Wuichet *et al.*, 2007). This has been likened to assembling sensory pathways from 'Lego®'-like modules (Schultz & Natarajan, 2013) that can be arranged into endless possible constructions, each maintaining function and a fine-tuned response. One of the best-characterized sensory systems is *E. coli* chemotaxis, where stimuli are integrated to modulate flagella rotation via a common phosphorylation cascade (Krell *et al.*, 2011, Parkinson *et al.*, 2015, Hazelbauer & Lai, 2010). Chemoreceptors regulate the cascade by controlling the autophosphorylation of the histidine kinase, CheA. Phospho-CheA in turn phosphorylates the response regulator, CheY, and phospho-CheY binds to the flagellar motor, thus altering the direction of flagella rotation and changing the direction of bacterial swimming. This is a versatile strategy that enables bacteria to collectively respond to numerous and diverse stimuli using variations on common mechanisms of intra-protein and inter-protein signaling.

Here we investigate another variation on the chemotaxis paradigm in the modular aerotaxis receptor, Aer (Fig. 14A), and examine common signaling mechanisms that underlie the different signaling pathways in aerotaxis and chemotaxis. The sensor for the aerotaxis receptor is an N-terminal PAS [Per-Arnt-Sim (Nambu *et al.*, 1991)] domain, which monitors cellular redox potential via a flavin adenine dinucleotide (FAD) cofactor [(Rebbapragada *et al.*, 1997a,

44

Bibikov *et al.*, 1997a, Taylor & Zhulin, 1999, Taylor, 2007), Fig. 14B]. PAS-FAD is

reduced under hypoxic conditions, eliciting a conformational cascade that

promotes the kinase-on state. We previously showed that the PAS sensor can

interact directly (Campbell *et al.*, 2010) with the Aer HAMP domain [HAMP is

found in histidine kinases, adenylyl cyclases, methyl-accepting chemotaxis

proteins, phosphatases, diguanylate cyclases and phosphodiesterases (Aravind

& Ponting, 1999, Dunin-Horkawicz & Lupas, 2010)]. From that study and

previous work we postulated that PAS modulates HAMP by direct PAS-HAMP

interactions.

In Aer, the PAS and HAMP domains are separated by the F1 linker

(Bibikov *et al.*, 2000, Campbell *et al.*, 2011) and the hairpin membrane anchor

[(Amin *et al.*, 2006), Fig. 14A]. This intervening sequence is not directly involved

in signaling, but the F1 linker supports maturation of the PAS and HAMP

domains (Buron-Barral et al., 2006, Campbell et al., 2011), and the membrane

anchor localizes Aer with other chemoreceptors (Amin *et al.*, 2006). The proximal

signaling domain [following HAMP; (Ma *et al.*, 2005), Fig. 14A] corresponds to

the adaptation region in methyl-accepting chemoreceptors. Although the proximal

signaling domain has no adaptation function in Aer (Bibikov *et al.*, 2004), it does

serve a critical role in Aer signaling (Bibikov *et al.*, 2004, Ma *et al.*, 2005, Buron-

Barral *et al.*, 2006b). Lastly, the C-terminal kinase control module controls the

rate of CheA phosphorylation. Here, each monomer forms antiparallel helices
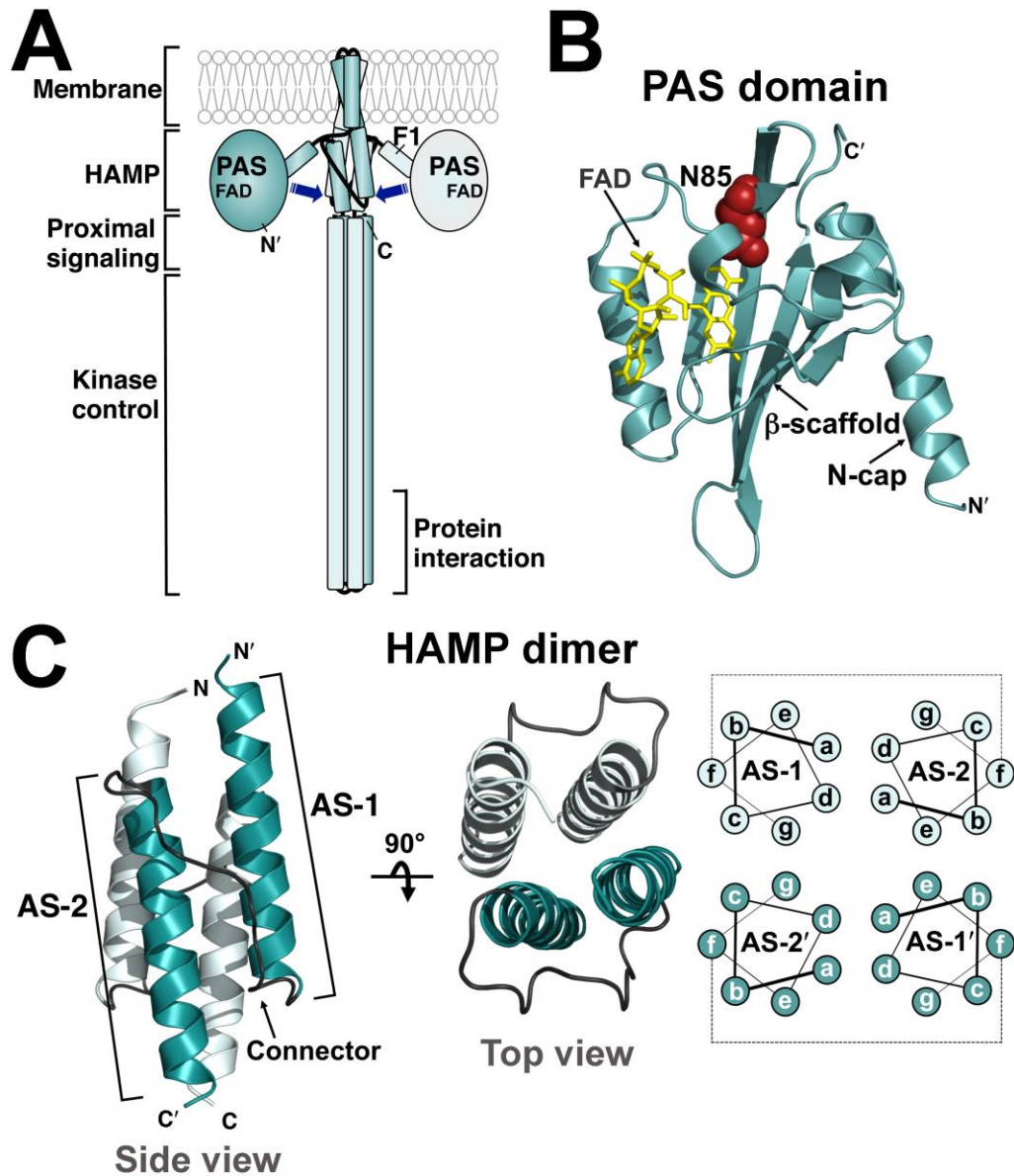
Figure 14. Models of the aerotaxis receptor, Aer, and the Aer PAS and HAMP domains. A. Cartoon of the domain organization of an Aer dimer. The PAS sensing domain is proposed to contact the downstream HAMP and proximal signaling domains (arrows). B. Aer PAS homology model (res. 5-122) based on the co-ordinates of the *Azotobacter vinelandi* NifL PAS domain (Key *et al.*, 2007) showing FAD (yellow) and the location of N85 (red spheres), which was substituted with serine to generate the kinase-on state of Aer. C. Aer-HAMP dimer model (res. 204-258) based on the co-ordinates of the *Archaeoglobus fulgidus* Af1503 HAMP domain (Hulko *et al.*, 2006). Each monomer is composed of two helices, AS-1 and AS-2, which are separated by a non-helical connector and arranged as a parallel four-helix bundle. Helical positions 'a' through 'g', and their proposed arrangement in the bundle are indicated. Abbreviations: FAD, flavin adenine dinucleotide; AS, amphipathic sequence.

with a U-turn at the tip, and together the two monomers form a long, supercoiled, four-helix bundle that extends into the proximal signaling domain (Fig. 14A).

In *E. coli* chemoreceptors, the HAMP domain is positioned in the cytosol between the cytoplasmic membrane and the kinase control module. Here it acts as a central processing unit, receiving input from an N-terminal sensor domain and relaying this information to the C-terminal kinase control domain (Parkinson, 2010). Each HAMP monomer is made up of two amphipathic α-helices (AS-1 and AS-2) (Butler & Falke, 1998, Watts *et al.*, 2008), and two HAMP monomers fold into a parallel four-helix coiled-coil [(Hulko *et al.*, 2006, Airola *et al.*, 2010b, Wang *et al.*, 2013, Mechaly *et al.*, 2014, Watts *et al.*, 2011a, Swain & Falke, 2007), Fig. 14C]. Our studies on Aer have shown that signals received by HAMP domains can be of two types. In many chemoreceptors, the HAMP domain is controlled by a periplasmic sensor domain, which transmits signals through the membrane to the HAMP domain [reviewed by (Parkinson, 2010)]; but in the aerotaxis receptor, Aer, the HAMP domain is controlled via direct lateral interactions with the cytosolic PAS sensing domain [(Herrmann *et al.*, 2004, Watts *et al.*, 2006a, Watts *et al.*, 2004a, Ma *et al.*, 2005, Buron-Barral *et al.*, 2006b, Campbell *et al.*, 2010), Fig. 14A]. HAMP domains are therefore able to convert two disparate conformational inputs into similar output controls.

Models to explain HAMP signaling range from those with static kinase-on and kinase-off conformations, such as the gearbox rotation model (Hulko *et al.*, 2006, Ferris *et al.*, 2011, Mondejar *et al.*, 2012), helix tilting models (Swain & Falke, 2007, Watts *et al.*, 2011a), and combined helix rotation with tilting models

(Airola *et al.*, 2010b, Wang *et al.*, 2012), to a biphasic static-dynamic signaling

model in which the signaling state depends on the structural stability of the

HAMP four-helix bundle (Zhou *et al.*, 2009, Zhou *et al.*, 2011, Airola *et al.*, 2013c,

Ames *et al.*, 2014, Lai & Parkinson, 2014, Klose *et al.*, 2014). In the static-

dynamic signaling model, the kinase-off conformation of the receptor is

associated with stable HAMP packing, in contrast to the kinase-on conformation,

which is associated with a more dynamic HAMP bundle. A loosely packed HAMP

domain (the kinase-on state) appears to be associated with a tightly packed

adaptation region in methyl-accepting chemoreceptors (regionally equivalent to

the Aer proximal signaling domain), causing a concomitant destabilization of the

distal kinase control region (the protein-interaction region; Fig. 14A) and

subsequent phosphorylation of CheA (Swain *et al.*, 2009, Parkinson, 2010, Zhou

et al., 2011, Falke & Piasta, 2014).

In this study, we investigate the signaling pathway from the PAS domain

to the HAMP and proximal signaling domains of Aer. Several previous studies

argued for direct signaling from the PAS to the HAMP domain: i) HAMP AS-2 is

required for PAS folding and for PAS FAD-binding (Herrmann *et al.*, 2004,

Bibikov *et al.*, 2000, Ma *et al.*, 2005, Buron-Barral *et al.*, 2006b), ii) PAS-N34D is

an allele-specific suppressor of HAMP-C253R, implying close proximity between

PAS-N34 and AS-2-C253 (Watts *et al.*, 2004a), and iii) specific cysteine

substitutions in the PAS β-scaffold crosslink with a cysteine substitution in the

HAMP domain, confirming close proximity of the PAS β-scaffold and HAMP

domain (Campbell *et al.*, 2010). Here, we extend previous studies by defining the

interacting surfaces of the Aer PAS, HAMP and proximal signaling domains. We first map the in vivo solvent accessibility of residues in these regions to identify hidden (contact) surfaces, and use cysteine crosslinking to uncover the orientation between the PAS and HAMP domains. We compare accessibilities in the kinase-on and kinase-off states and find signal-induced changes in the HAMP and proximal signaling domains that support the alternating static-dynamic signaling model. Our results suggest that HAMP domains employ a common signaling mechanism that can be modulated by either a lateral or linear sensory input.

Results

Mapping the in vivo Accessibility of Residues in Aer

We previously showed that under aerobic conditions the PAS and HAMP domains of Aer can physically interact (Campbell *et al.*, 2010). Under these conditions PAS-FAD remains oxidized and the output is kinase-off. Here, we examined the pathway through which the oxidized PAS domain controls the HAMP domain and stabilizes the kinase-off state. If PAS-HAMP interactions are stable, the contact surfaces should be sequestered and less accessible to solvent than non-contact surfaces. To identify putative contact regions on the PAS, HAMP and proximal signaling domains, we made single cysteine replacements throughout these domains, and then probed each protein under aerobic conditions with methoxypolyethylene glycol-maleimide 5000 (PEG-mal). PEG-mal is a bulky sulfhydryl-reactive reagent that preferentially reacts with

sulfhydryl residues that are accessible to solvent at the protein surface (Lu & Deutsch, 2001). The *E. coli* cells used for these experiments lacked both the Aer and Tsr aerotaxis receptors [BT3312 (*aer tsr*)]. BT3312 cells expressing each plasmid-encoded Aer-Cys protein were made permeable to PEG-mal by treatment with toluene and ethanol, and then incubated with 5 mM PEG-mal at 25°C for 15 min (see Experimental Procedures). To measure the PEGylation of native samples, reactions were stopped with excess β-mercaptoethanol before being boiled in sample buffer. To measure the maximum PEGylation of denatured samples, parallel reactions were continued by boiling in sample buffer without β-mercaptoethanol. The PEGylated samples were separated by SDS-PAGE, and a mobility shift of approximately 10 kDa on Western blots readily differentiated PEGylated from un-PEGylated Aer [Fig. 15, (Amin *et al.*, 2006)]. Under these conditions, the average chemical reactivity relative to denatured protein was below 50% and spanned a large dynamic range, ensuring that most reactions did not approach completion (compare Figs. 16A and 17B).

Accessibility of HAMP and Proximal Signaling Domain Residues in Aer

A library with serial cysteine replacements at each of 70 HAMP and proximal signaling domain residues was previously constructed [res. 206 to 276], and all but three of these cysteine mutants retained function (Watts *et al.*, 2008, Amin *et al.*, 2006). In the current study, the extent to which each residue reacted with PEG-mal was used as a measure of solvent accessibility (Fig. 16). In the first HAMP region, AS-1 (res. 207-223), the PEGylation pattern was inversely

related to previously determined disulfide crosslinking results (Watts *et al.*, 2008). Thus, PEGylation of the substituted cysteines increased as the extent of crosslinking decreased, and vice versa, which is consistent with prior conclusions that AS-1 is an α-helix. The most accessible AS-1 residues were located at the 'c' and 'f' positions of a helical wheel, where each position of the heptad repeat was designated by the letters a to g (Fig. 16B). In the membrane-proximal end of AS-1 (res. 206-211), PEGylation ratios were lower than the remainder of AS-1 (res. 212-223, located within the four-helix bundle) (Fig. 16A). This may be due to a local membrane effect, as this region precedes the HAMP four-helix bundle and anchors HAMP to the membrane at or near residue 206 (Amin *et al.*, 2006). The non-helical HAMP connector, which follows AS-1, generally showed greater PEGylation compared to AS-1 (Fig. 16A), but there was no discernible periodicity, nor did the data correlate well with the extent of disulfide formation previously determined in this region (Watts *et al.*, 2008).

Following the HAMP connector, HAMP AS-2 (res. 238-253) forms an α-helix with a crosslinking periodicity of 3.5 residues per turn, and 'a' and 'd' positions on the interior of the four-helix bundle (Watts *et al.*, 2008). In the current study, PEGylation was low for most of AS-2. This area is shaded yellow in Fig.16B and has a calculated surface area of 1180 Å^2.
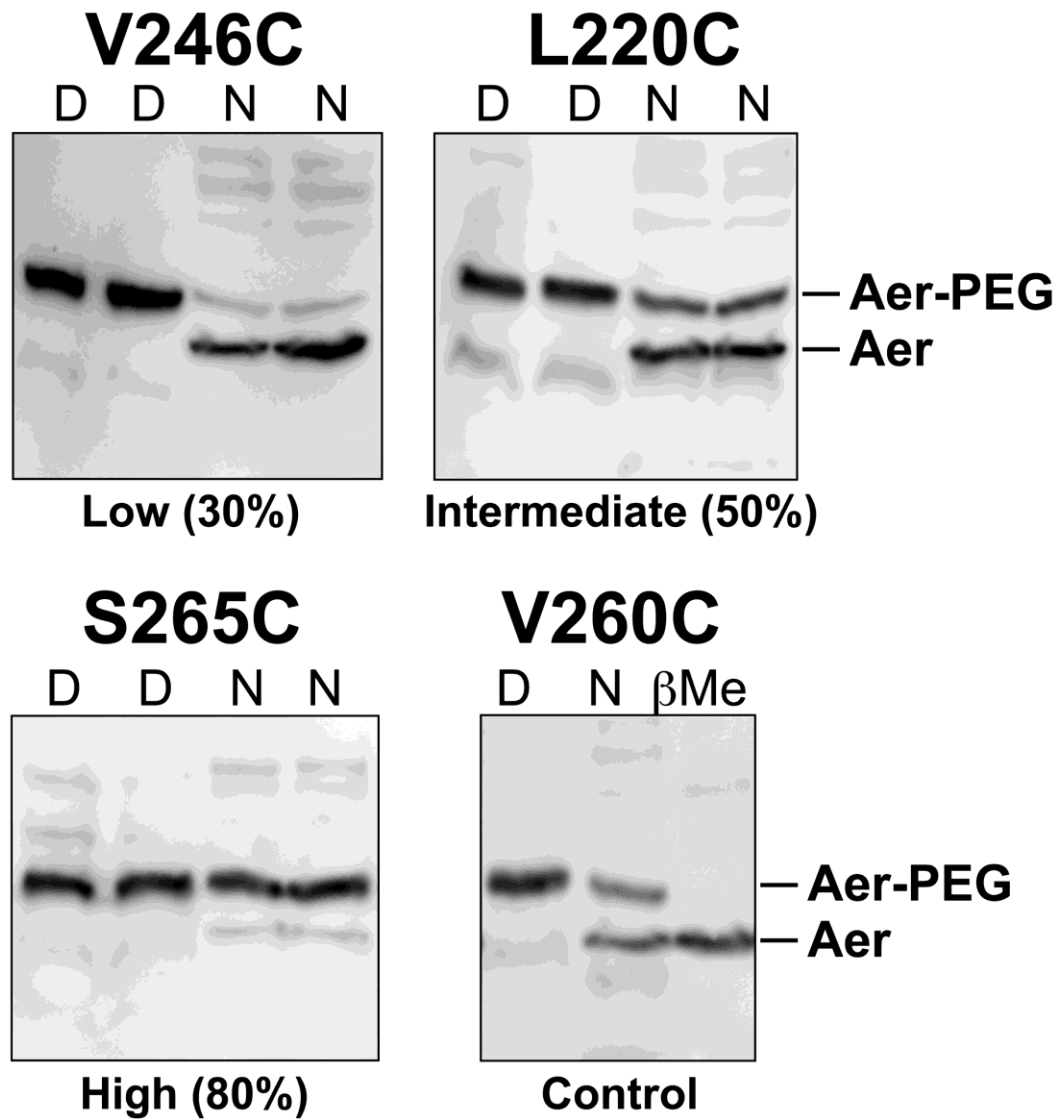
Figure 15. Western blots of Aer-Cys proteins showing examples of low (Aer-V246C), intermediate (Aer-L220C), and high (Aer-S265C) PEGylation under native (N) conditions. PEGylated Aer (Aer-PEG) has an apparent mass increase of ~10 kDa. Samples denatured (D) without β-mercaptoethanol quencher were PEGylated to apparent completion; samples pretreated with β-mercaptoethanol (before PEG-mal) were not PEGylated (see Aer-V260C, βMe lane). Faint bands migrating faster than an Aer monomer represent PEGylated Aer break-down product (Ma *et al.*, 2004). Abbreviations: D, denatured; N, native; β-Me, β-mercaptoethanol.
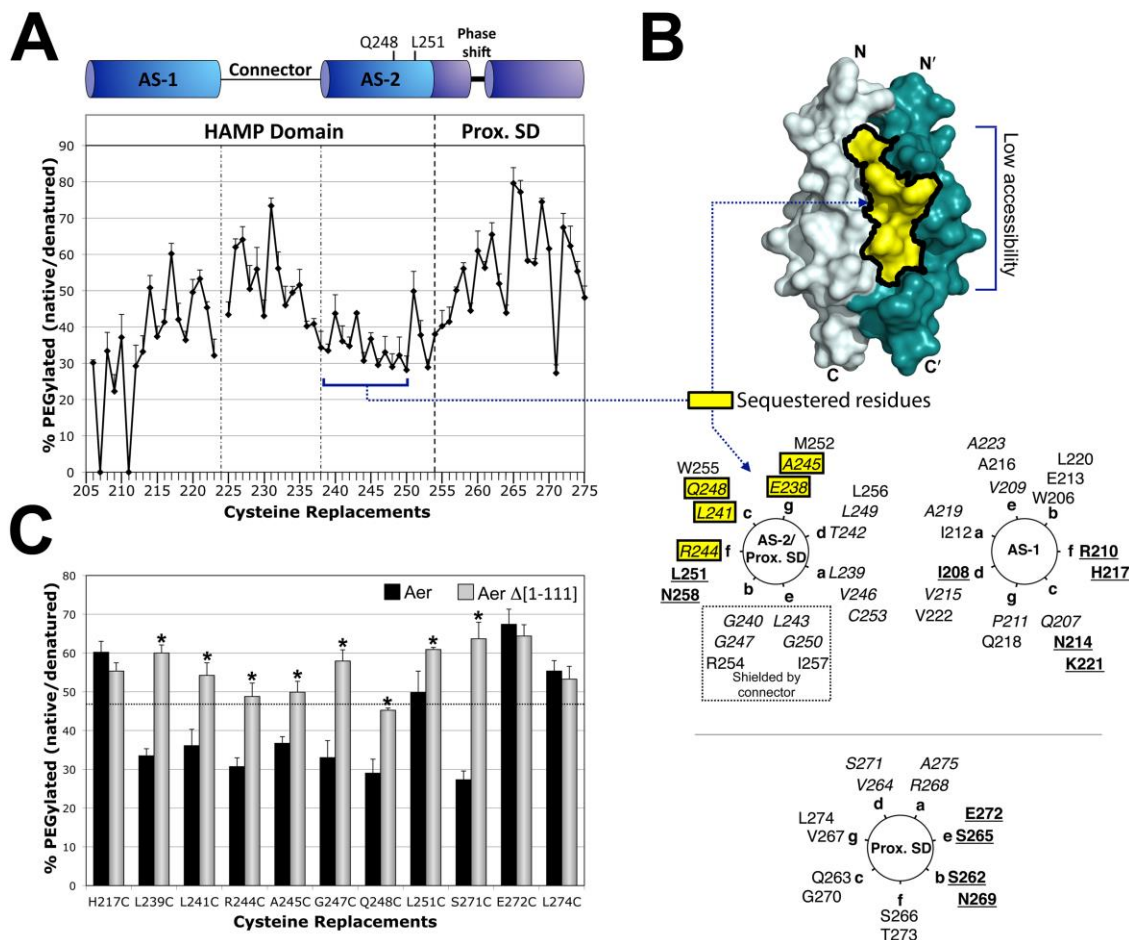
Figure 16. Accessibility of residues in the HAMP and proximal signaling domains as inferred from reactivity with PEG-mal. A. Extent of PEGylation for substituted cysteines at each residue of the Aer HAMP and proximal signaling domains. Error bars represent the standard deviation from multiple experiments. B. Sequestered AS-2 surface residues mapped onto a HAMP dimer model and a helical wheel. The hidden region was inferred by low accessibility to PEG-mal (A), and included residues 238 to 250 (shaded yellow). Helical wheels use the standard heptad repeat nomenclature (see Fig. 1), and include HAMP AS-1 (right panel), AS-2 (left panel) and the proximal signaling domain (Prox. SD). The proximal signaling domain is divided between two helical wheels due to the presence of a helical phase shift after residue 259, and the resumption of a helical accessibility pattern (with maximum accessibility every third and forth residue), at residue 262 (Watts *et al.*, 2008). AS-2 residues that are shielded by the connector in the HAMP model are indicated within a dotted box. Color code: bold and underlined, the most accessible residues in each region; italicized, the least accessible residues in each region; yellow boxes, residues predicted to be accessible but found to have low accessibility. C. Accessibility of HAMP and proximal signaling domain residues in the presence (black bars, full length Aer) and absence (gray bars, PAS-less Aer Δ[1-111]) of the Aer-PAS domain. Error bars represent standard deviations from multiple experiments. Asterisks indicate statistically significant differences in the absence of the PAS domain (p <0.05). The dotted line indicates the average accessibility of exposed AS-1 residues (the underlined residues in the AS-1 helical wheel shown in B).

53

The low accessibility was not likely caused by a membrane effect because AS-2 begins approximately 10 Å from the membrane. Of note, the interior facing 'a' and 'd' positions of AS-2 were not always the least accessible residues. This was because the 'b', 'c', 'e' and 'g' positions also had low accessibility (Fig.16). The HAMP connector is predicted to shield the 'b' and 'e' positions of AS-2, but the low accessibility of the 'c' and 'g' positions (and one 'f' position) suggested that this face was relatively hidden from solvent and may be shielded by another protein surface. In contrast, residues at the C-terminal end of AS-2 (res. 251-253) had PEGylation values that, like those in AS-1, inversely correlated with the extent of disulfide formation determined previously (Watts *et al.*, 2008).

The region immediately following HAMP AS-2 is the proximal signaling domain (res. 254-271), which links Aer-HAMP to the kinase control module (Ma *et al.*, 2005). The proximal end of this region showed a sequential increase in PEGylation values that did not inversely correlate with previously determined disulfide crosslinking results (residues 254 to 261, Fig. 16A). This was notable because we previously found a high extent of crosslinking in this region (Watts *et al.*, 2008). Specifically, Cys replacements at residues 256 and 260 had the greatest extents of disulfide bond formation of any cytosolic cysteine replacement in Aer (Watts *et al.*, 2008). Together these data raise the possibility that this segment is both accessible and flexible. Flexibility could result from the helical phase shift previously identified by disulfide crosslinking (Watts *et al.*, 2008) and narrowed to residues 259-262 in the current study. This experimentally determined phase shift represents a discontinuity in the heptad

repeat sequence and is five residues downstream of the HAMP-proximal signaling juncture. These junctures are notable because sequence analyses have revealed a phase stutter (a change in coiled-coil registry) at HAMP-output-helix connections (Parkinson, 2010). In this study, the Aer phase shift did not occur at the phase stutter (residues 254-256) but occurred between residues 259 and 262. Residue S262 is predicted to be in a 'c' position on the AS-2/proximal signaling domain helix (Fig. 16B, left helical wheel), but actually fits the accessibility pattern of an accessible 'b' position in the proximal signaling domain helix (Fig. 16B, bottom wheel). For the remainder of the proximal signaling domain and beyond (res. 262-275), PEGylation efficiency remained high, but the profile was inversely related to previously determined disulfide crosslinking values (Watts *et al.*, 2008). Therefore, residues following the putative phase shift appeared to form a 3.5 residue-per-turn α-helix, with the least accessible residues in the 'a' and 'd' positions and the most accessible residues in the 'b' and 'e' positions (Fig. 16B).

Comparison of HAMP Accessibility in the Presence and Absence of the PAS Domain

The simplest explanation for the sequestered surface of AS-2 (Fig. 16B, yellow residues) is that this region is shielded by another part of Aer. To determine whether the PAS domain shields HAMP AS-2, accessibility measurements were repeated in the presence (full-length Aer) or absence (Aer Δ[1-111]) of the PAS domain. Aer Δ[1-111] lacks all but eight C-terminal PAS

residues and forms a stable product (J. S. Parkinson, personal communication) that maintains near-normal steady-state levels under low induction (data not shown). Without the PAS domain, 'inaccessible' AS-2 residues became significantly more PEGylated, reaching levels routinely observed for surface-exposed AS-1 residues in full-length Aer (Fig. 16C). Control residues in AS-1 and the proximal signaling domain (with the exception of Aer-S271C at the interface of the proximal signaling domain) were not significantly more accessible in PAS-less Aer. Taken together, these data both provide evidence that the PAS domain shields HAMP AS-2, and potentially define a PAS-HAMP contact surface.

Mapping Inaccessible Surfaces of the PAS Domain

To identify surfaces on the PAS domain that may form stable interactions with HAMP or other domains, we probed predicted PAS surface residues with PEG-mal. Using an Aer-PAS homology model (Fig. 14B), we selected 57 surface-exposed PAS residues and two interior-facing PAS residues as inaccessible controls (A97 and S113, Fig. 17A). Each residue was individually replaced with cysteine, expressed in BT3312 and screened for phenotype in succinate minimal soft agar. Of the 59 Aer-PAS Cys mutants constructed, only Aer-W94C did not support aerotaxis in semi-solid agar at each expression level (see Fig. S1 for details).

The extent of PEGylation for each PAS cysteine replacement is shown in Fig. 17B. To search for inaccessible PAS surfaces, we first sorted the PAS PEGylation values into one of three categories: low accessibility (0-30%

PEGylation), intermediate accessibility (31-50% PEGylation) or high accessibility

(> 50% PEGylation). Each category was then mapped onto the Aer-PAS model

(Fig. 17D). As anticipated for residues shielded from PEG-mal, the two interior-

facing controls, A97C and S113C, had low accessibility (16% and 27%

PEGylation, respectively). Residues with high accessibility were scattered over

the PAS surface. A notable region of high accessibility was the PAS N-terminal

cap (N-cap, res. 1-19), where all residues tested (except T18C and T19C) had

high accessibility (Figs. 17B and D). This suggests that the PAS N-cap is

dynamic and does not stably interact with other domains in Aer, a conclusion that

is compatible with our previous finding that the N-cap can collide with

neighboring dimers (Watts *et al.*, 2006b). In contrast, a large area of low

accessibility measuring 1,370 $Å^2$ was present on the PAS β-scaffold (Fig. 20D,

yellow region outlined in black). This area was surrounded by residues with

intermediate accessibility (Fig. 17D), perhaps delineating the boundary of a PAS

contact surface.
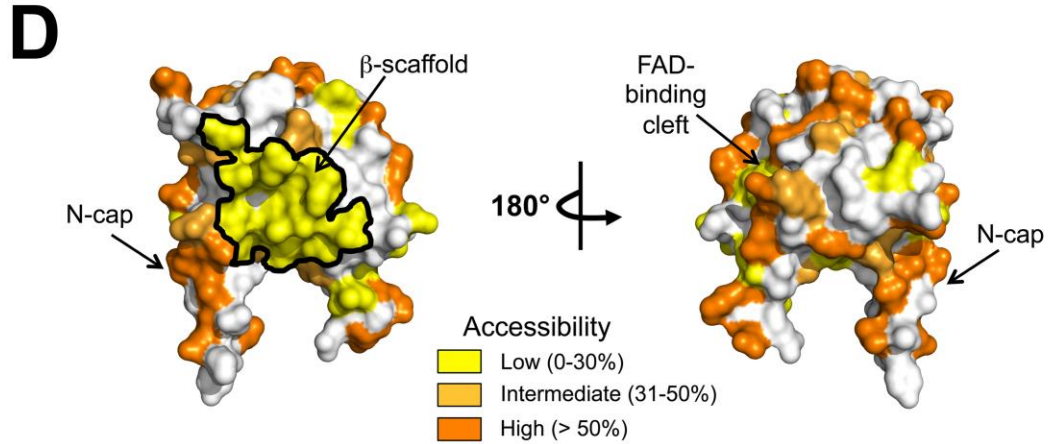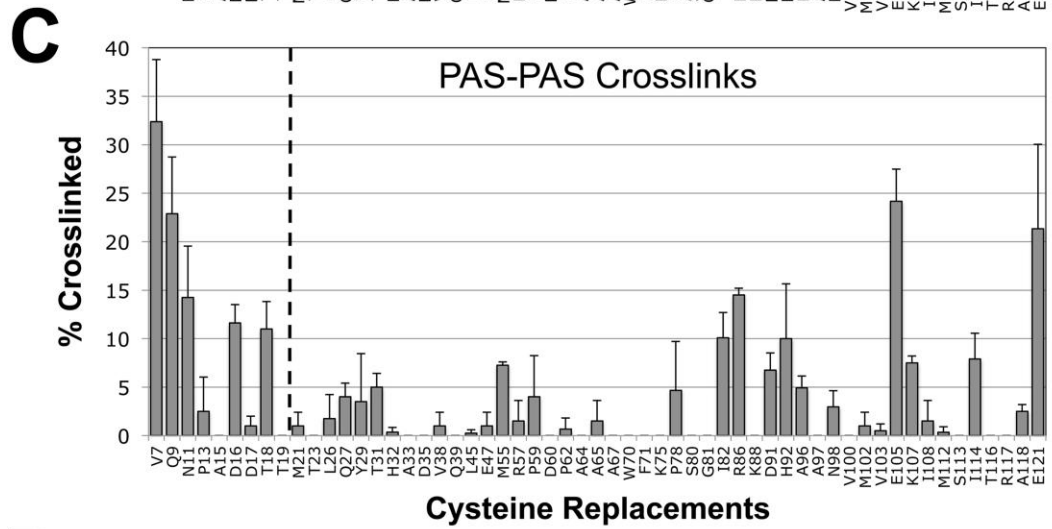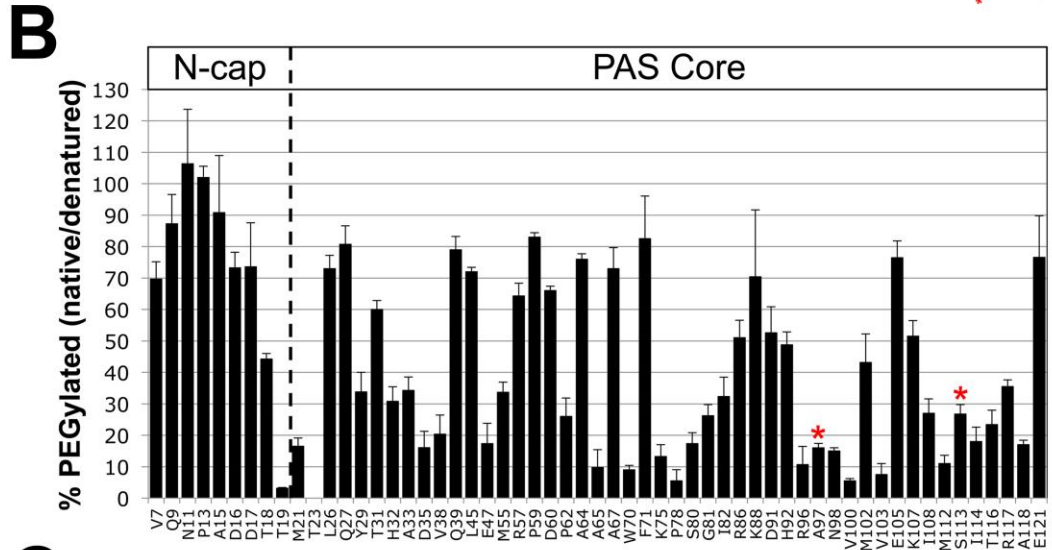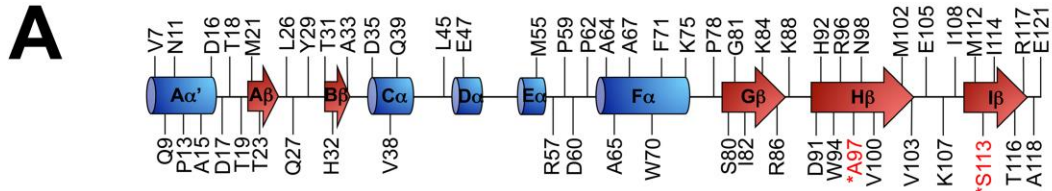
Figure 17. Probing the PAS domain for solvent accessibility and PAS-PAS proximity using PEGylation and disulfide crosslinking. A. Residues selected for cysteine replacement mapped onto the secondary structure of the Aer PAS domain. Residues in black font are predicted to be accessible on the surface of the Aer-PAS homology model; those in red font are predicted to face inwards towards the PAS interior, and were selected as surface-inaccessible controls.

B. Extent of PEGylation for substituted cysteines in the Aer PAS core and N-terminal cap (N-cap). Red asterisks identify the surface-inaccessible controls.

C. Extent of disulfide crosslinking between neighboring PAS domains. Error bars in B and C represent the standard deviation from multiple experiments.

D. Aer-PAS homology model showing the distribution of the tested residues based on whether they had low (yellow shading, 0-30% PEGylation), intermediate (light orange, 31-50% PEGylation) or high (orange, > 50% PEGylation) accessibility.

PAS-PAS Crosslinking

To determine if the area of low accessibility on the PAS β-scaffold was due to PAS-PAS interactions, each of the 59 PAS Cys substitutions that circumscribed the PAS domain was crosslinked in vivo by treating whole cells with 600 μM Cu(II)(1,10-phenanthroline)$_3$ (CuPhe) for 20 min. Crosslinked products were identified by their migration on SDS-PAGE and detected with anti-Aer$_{2-166}$ antisera. As anticipated, the interior-facing controls, A97C and S113C, did not crosslink (Fig. 17C). Notably, residues that clustered on the inaccessible PAS β-scaffold did not crosslink substantially (<8% dimers). This suggests that PAS-PAS interactions do not contribute to the inaccessible surface. The eight cysteine mutants that formed more than 10% dimers (Fig. 17C) also had high or intermediate accessibility to PEG-mal (Fig. 17B), indicating that some of these PAS-PAS interactions may have been transient, rather than stable. These residues included several in the flexible N-cap (V7C, Q9C, N11C, D16C and T18C), R86C in the β-scaffold, E105C in the PAS H-I loop, and E121C in the F1 loop (Fig. 17C).

In the PAS core, the greatest extent of PAS-PAS crosslinking was observed for E105C. Our previous studies predict that only flexible regions of PAS can form PAS-PAS crosslinks within an Aer dimer because the PAS domains are separated by the HAMP four-helix bundle. Non-flexible PAS regions are more likely to contact another dimer within the trimer-of-dimers hexameric structure of Aer (Campbell et al., 2011). To differentiate intra- from inter-dimeric contacts for E105C, the aspartate receptor, Tar, was over-expressed from a

compatible plasmid to form mixed trimers-of-dimers with Aer (Gosink *et al.*, 2006). In the presence of over-expressed Tar, Aer-E105C crosslinking decreased from 24% to 11%. This suggests that Aer-E105C crosslinking occurs between Aer dimers, a result that was also shown for E121C (Campbell *et al.*, 2011).

PAS-HAMP Interactions Defined by Disulfide Crosslinking

We previously demonstrated crosslinking between Cys replacements in the PAS and HAMP domains of Aer (Campbell *et al.*, 2010). For those experiments, Q248C was selected as the HAMP Cys probe because Q248C i) is located on the sequestered face of AS-2 (Figs. 16A and B), ii) is significantly more accessible in the absence of the PAS domain (Fig. 16C), and iii) does not significantly crosslink with itself within or between dimers [≤1% dimers, (Watts *et al.*, 2008)]. Those initial studies demonstrated in vivo PAS-HAMP crosslinking between HAMP-Q248C and PAS-N98C or PAS-I114C (Campbell *et al.*, 2010). The findings were possible because PAS-HAMP crosslinks can be differentiated from PAS-PAS and HAMP-HAMP crosslinks by their migration on SDS-PAGE. The different mobility is based on the N-terminal location of the PAS domain: Aer PAS-PAS crosslinked dimers migrate faster on SDS-PAGE than HAMP-HAMP crosslinked dimers, and PAS-HAMP crosslinked dimers have an intermediate mobility (Fig. 18A). Note that the latter point is only true if the PAS-HAMP crosslink forms between subunits, not within a subunit. An intra-subunit crosslink will migrate as a compact monomer (Bass *et al.*, 2007). In the current study, we

identify additional PAS-HAMP pairs that can crosslink and use these data to define the PAS-HAMP interaction surface. Q248C was paired with 25 different PAS Cys residues at sites circumscribing the PAS domain (see Experimental Procedures for details). The 25 di-Cys Aer constructs supported BT3312 aerotaxis in succinate minimal soft agar, with migration rates within the aerotactic range shown in Fig. S1. The Aer-Cys proteins were oxidized by treating whole cells with CuPhe as described above. Many of the substitutions produced small quantities of PAS-PAS and PAS-HAMP crosslinked dimers. However several residues preferentially produced PAS-HAMP crosslinked dimers: I82C, R96C, N98C, V100C, M112C and I114C on the PAS β-scaffold (Fig. 18A, right panel and Fig. 18B, left panel, gray bars) and V38C, in the N-cap hinge region. All of the PAS-HAMP crosslinks formed between, and not within, monomeric subunits.
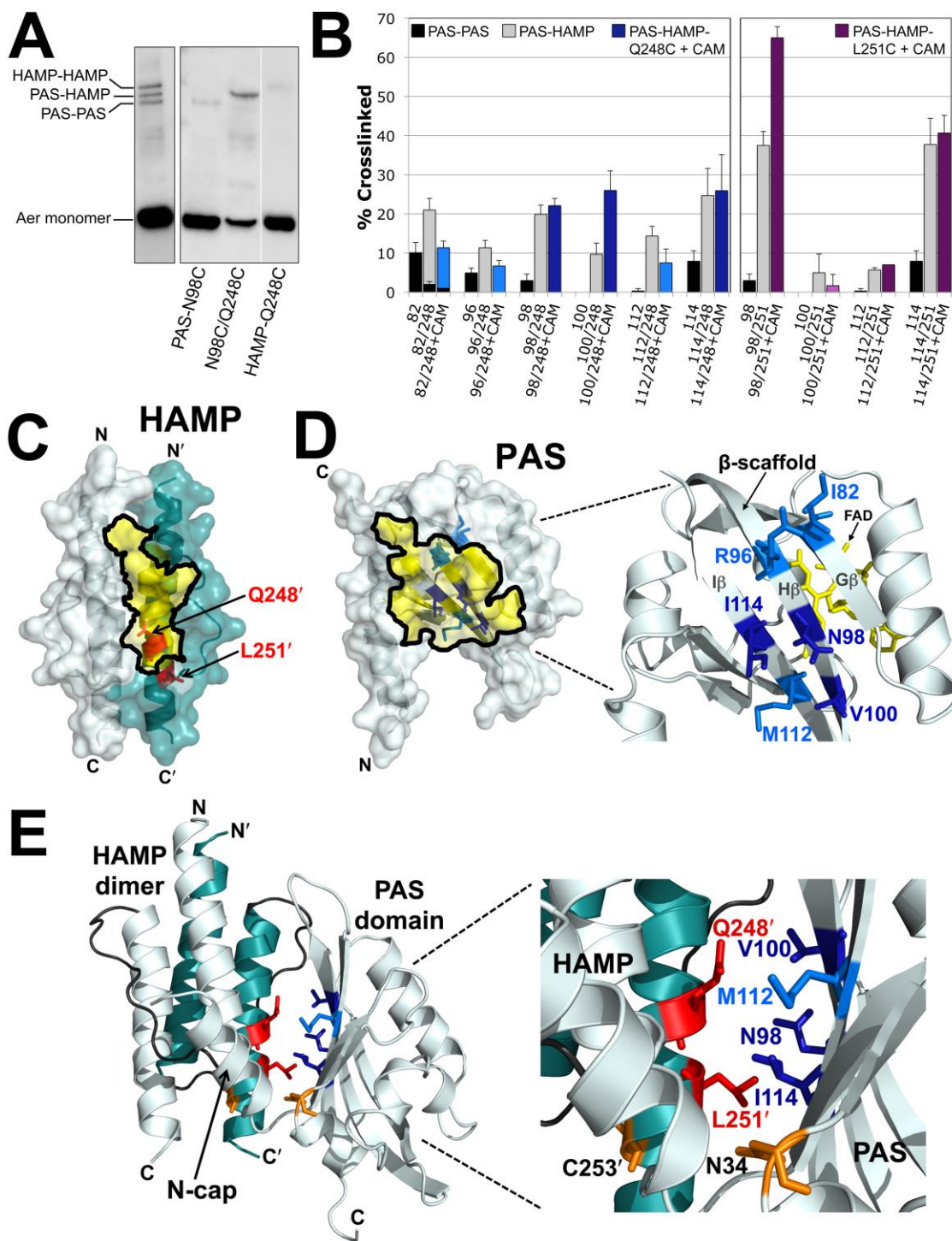
Figure 18. Disulfide crosslinking between the Aer PAS and HAMP domains.

A. Representative examples comparing SDS-PAGE mobilities for Aer dimers crosslinked between PAS-PAS, PAS-HAMP and HAMP-HAMP. The left panel illustrates the separation of the three crosslinked bands for a di-Cys mutant with similar band densities at each position (Aer-I82C/A245C). The right panel illustrates the separation of these bands for a di-Cys mutant with preferential PAS-HAMP crosslinking (Aer-N98C/Q248C). In all cases, uncrosslinked monomer bands are near the bottom of the gels. B. Extent of disulfide formation for PAS residues that preferentially crosslinked with HAMP-Q248C (left panel) and -L251C (right panel). PAS-PAS crosslinking is indicated by black fill, PAS-HAMP crosslinking by gray fill, PAS-Q248C crosslinking after treatment with chloramphenicol in blue fill and PAS-L251C crosslinking after treatment with chloramphenicol in purple fill. Dark blue or dark purple fill indicates that the extent of PAS-HAMP crosslinking did not significantly decrease after chloramphenicol treatment, whereas lighter blue or purple fill indicates a decreased extent of PAS-HAMP crosslinking after chloramphenicol treatment. HAMP-Q248C and -L251C controls routinely produced ≤1% dimers and are not shown. Error bars represent the standard deviation from multiple experiments. C. HAMP homology model showing the location of HAMP-Q248 and -L251, which crosslinked with PAS, in relation to the region that was sequestered from PEG-mal (Fig. 16B, yellow shading). D. PAS homology model showing the β-scaffold positions of the PAS residues that preferentially crosslinked with HAMP-Q248C in relation to the region that was sequestered from PEG-mal (Fig. 17D, yellow shading). Residue colors match those used in the left panel of B. E. PAS-HAMP dimer model showing the proposed orientation of the PAS and HAMP domains based on PEGylation and PAS-HAMP crosslinking data. For clarity, the model includes the PAS domain from just one subunit (res. 5-119) and a HAMP dimer (monomers from both subunits, res. 204-258). The PAS model was manually oriented relative to the HAMP AS-2 helix of the cognate monomer to account for the crosslinking (B) and sequestration (C and D) data. Residue colors match those used in B, C and D. The locations of PAS-N34D and HAMP-C253R, which were previously identified as site-specific suppressors (Watts *et al.*, 2004a), are shown in orange. Abbreviation: CAM, chloramphenicol.

Several of the residues, e.g., I82C, exhibited some PAS-PAS crosslinking, but the extent consistently decreased in the presence of HAMP-Q248C (Fig. 18B). This indicated that the side chains of the PAS residues collided more often with a HAMP domain than with another PAS domain. The PAS residues that preferentially crosslinked with HAMP-Q248C resided almost exclusively within the inaccessible region of the PAS β-scaffold (Fig. 18D). This region is notable because it includes the cluster of kinase-on lesions that we previously identified as components of the signaling pathway [(Campbell *et al.*, 2010), and the red area in Fig. 20].

Aer undergoes a complex maturation process in which proper folding of the Aer PAS domain requires the presence of the HAMP domain (Herrmann *et al.*, 2004). This process is easily destabilized by key mutations in either the PAS or HAMP domains (Buron-Barral *et al.*, 2006b, Campbell *et al.*, 2010). In the current study, we considered the possibility that some PAS-HAMP crosslinking occurred during the folding process before a mature Aer product was formed. To increase the fraction of mature Aer protein before crosslinking, new protein synthesis was inhibited with 500 µg ml^{-1} chloramphenicol for 15 min before adding CuPhe. After chloramphenicol treatment, three of the di-Cys mutants containing Q248C (N98C/Q248C, V100C/Q248C and I114C/Q248C) had an equivalent or increased proportion of PAS-HAMP crosslinked dimers (Fig. 18B, dark blue bars). This indicates that N98, V100 and I114, which are located on the PAS H and I β-strands (Fig. 18D), are each proximal to HAMP AS-2 in the folded protein. To test whether PAS-HAMP disulfide crosslinks formed within or

between dimers, Aer-I114C/Q248C was expressed with increasing concentrations of Tar. The amount of crosslinked I114C-Q248C product was unaffected by increased Tar expression (not shown), indicating that PAS-HAMP disulfide bonds most likely occurred between cognate monomers of the same dimer.

To identify HAMP residues other than Q248C that can crosslink with the PAS β-scaffold, we tested di-Cys combinations with several other HAMP residues (see Experimental Procedures for details). Of these, only HAMP-L251C (Fig. 18C) showed preferential PAS-HAMP crosslinking (Fig. 18B, right panel). Like Q248C, L251C has favorable properties in that it does not significantly crosslink with cognate L251C either within or between dimers [≤1% dimers, (Watts et al., 2008)]. In the presence of chloramphenicol, HAMP-L251C preferentially crosslinked with PAS-N98C, -M112C, and -I114C, but not with -V100C (Fig. 18B, purple bars). The extent of crosslinking between HAMP-L251C and either PAS-N98C or PAS-I114C was higher than that between HAMP-Q248C and these PAS residues (Fig. 18B). This indicates that these PAS residues are closer to HAMP-L251C than they are to HAMP-Q248C. In contrast, crosslinking between HAMP-Q248C and either PAS-V100C or PAS-M112C was higher than that between HAMP-L251C and these PAS residues (Fig. 18B). This suggests that these PAS residues are closer to Q248C than they are to L251C. Using this information, homology models of the Aer PAS and HAMP domains were manually manipulated to obtain the best fit (Fig. 18E). To fit the data, the PAS domain was rotated ~180° around the PAS-HAMP interface such that the

PAS-HAMP interaction surfaces are now flipped relative to our previous PAS-HAMP models [e.g., in (Campbell *et al.*, 2011, Watts *et al.*, 2008)]. The revised PAS-HAMP orientation resolves an unexplained anomaly that was present in previous models. Pseudoreversion analysis previously identified PAS-N34D as an allele-specific suppressor of HAMP-C253R (Watts *et al.*, 2004a). This implies close proximity between N34 and C253, but the previous PAS-HAMP models separated them. In the revised PAS-HAMP model, HAMP-C253 is in close proximity to PAS-N34 (Fig. 18E), resolving the anomaly.

Comparison of the Kinase-on and Kinase-off States

The solvent accessibility measurements in Figs. 19 and 20 were obtained under aerobic conditions and are expected to represent the kinase-off state of Aer (Repik *et al.*, 2000a). To gain insight into changes that might occur on HAMP surfaces as a result of signaling, we re-measured PEG-mal reactivities for 34 HAMP residues in the presence of the PAS kinase-on lesion N85S [(Campbell *et al.*, 2010), Fig. 19A]. N85 is located on the PAS Gβ strand, and its side chain is predicted to face the interior of the PAS domain, contacting the isoalloxazine ring of FAD [(Campbell *et al.*, 2010), Fig. 14B]. N85 is a possible link from the bound FAD to the β-scaffold, and the N85S substitution results in a kinase-on output. Residues that were significantly more accessible in the presence of N85S formed a patch on the HAMP surface that included both AS-1 and cognate AS-2′ residues (Fig. 19B, purple residues). This patch overlapped with AS-2 residues that were sequestered by the PAS domain in the kinase-off state (Fig. 16),

suggesting that the N85S lesion disrupts the interaction of PAS with HAMP. In contrast to the AS-1 and AS-2′ residues with increased accessibility, residues with decreased accessibility in this region were located on a different face from the more accessible patch (Fig. 19B). The decrease in accessibility was greatest at the phase shift, where the PEGylation of D259C decreased from approximately 45% in the unstimulated state to approximately 3% in the presence of PAS-N85S. However, the face on which residues after N258 were located could not be determined because the three-dimensional structure of the phase shift is unknown.

Notably, all residues that were significantly more accessible in the kinase-on state preceded the end of the HAMP domain (C253), while residues after the HAMP domain in the proximal signaling domain showed decreased accessibility. The proximal signaling and C-terminal kinase control domains are predicted to form an elongated antiparallel four-helix bundle in Aer (Fig. 14) that is analogous to the adaptation and protein interaction regions of other chemoreceptors (Falke & Piasta, 2014). Crosslinking studies of the proximal signaling domain indicate that this four-helix extends through the phase shift (res. 259-262). Our model pairs proximal signaling residue I257 with L505, and ends with H506 (aligned with L256) at the C-terminus of Aer [inferred from (Alexander & Zhulin, 2007), see Fig. 21]. Therefore, it is possible that residues following I257 that are less accessible in the kinase-on state form a more compact four-helix bundle. Conversely, increased accessibility in the HAMP domain in the kinase-on state may be associated with a more dynamic four-helix bundle.

Discussion

The Aer PAS-HAMP Interaction Surface

In this study, we investigated an unusual signaling mechanism in which a cytosolic PAS domain controls signaling by direct lateral interaction with a HAMP domain (Fig. 21). This differs from the prototypical membrane-bound chemoreceptor, in which HAMP is directly tethered through the membrane to a periplasmic sensor domain (Parkinson, 2010).
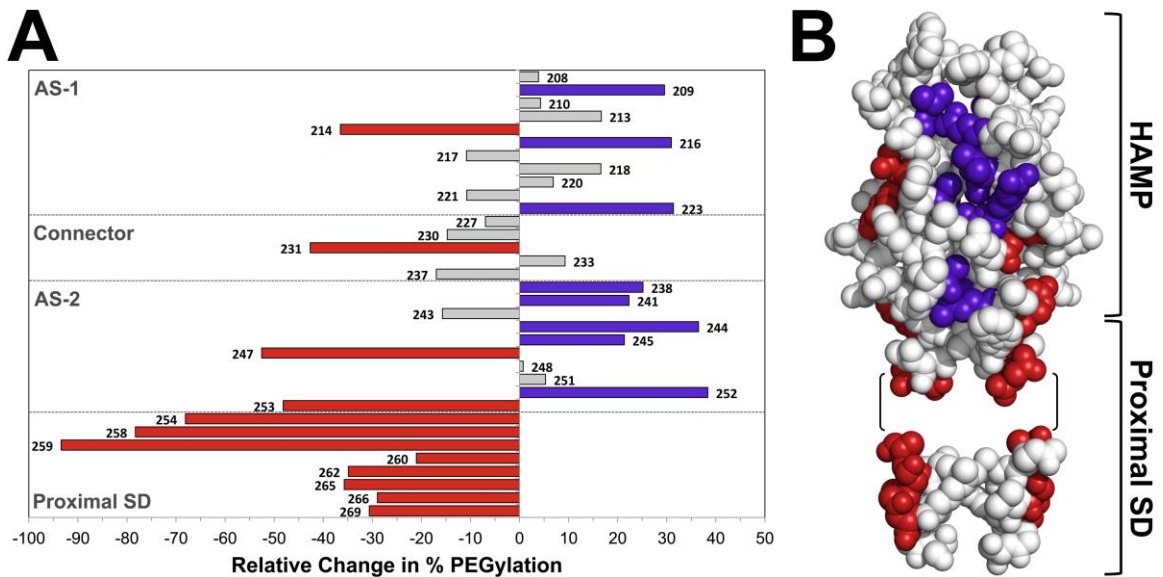
Figure 19. Influence of the PAS kinase-on lesion, N85S, on the accessibility of residues in the HAMP and proximal signaling domains to PEG-mal.

A. Histogram showing the average percent change in PEGylation for 34 Cys substitutions in Aer-N85S. Bars projecting to the right of the origin denote residues that became more accessible in the presence of N85S (significant increases are colored purple; $p < 0.05$). Bars projecting to the left denote residues that became less accessible (significant decreases are colored red; $p < 0.05$). Residues in gray had statistically insignificant changes.

B. Location of residues from A that showed significant changes in accessibility (in the kinase-on state) when mapped onto models of the Aer-HAMP domain and part of the proximal signaling domain. The models include residues 204-258 and 262-269. Residues 259-261 were omitted because of the phase shift in this region. Residues 262-269 are modeled onto a 3.5 residue per turn coiled coil α-helix; the precise orientation of this region relative to HAMP is unknown.

69
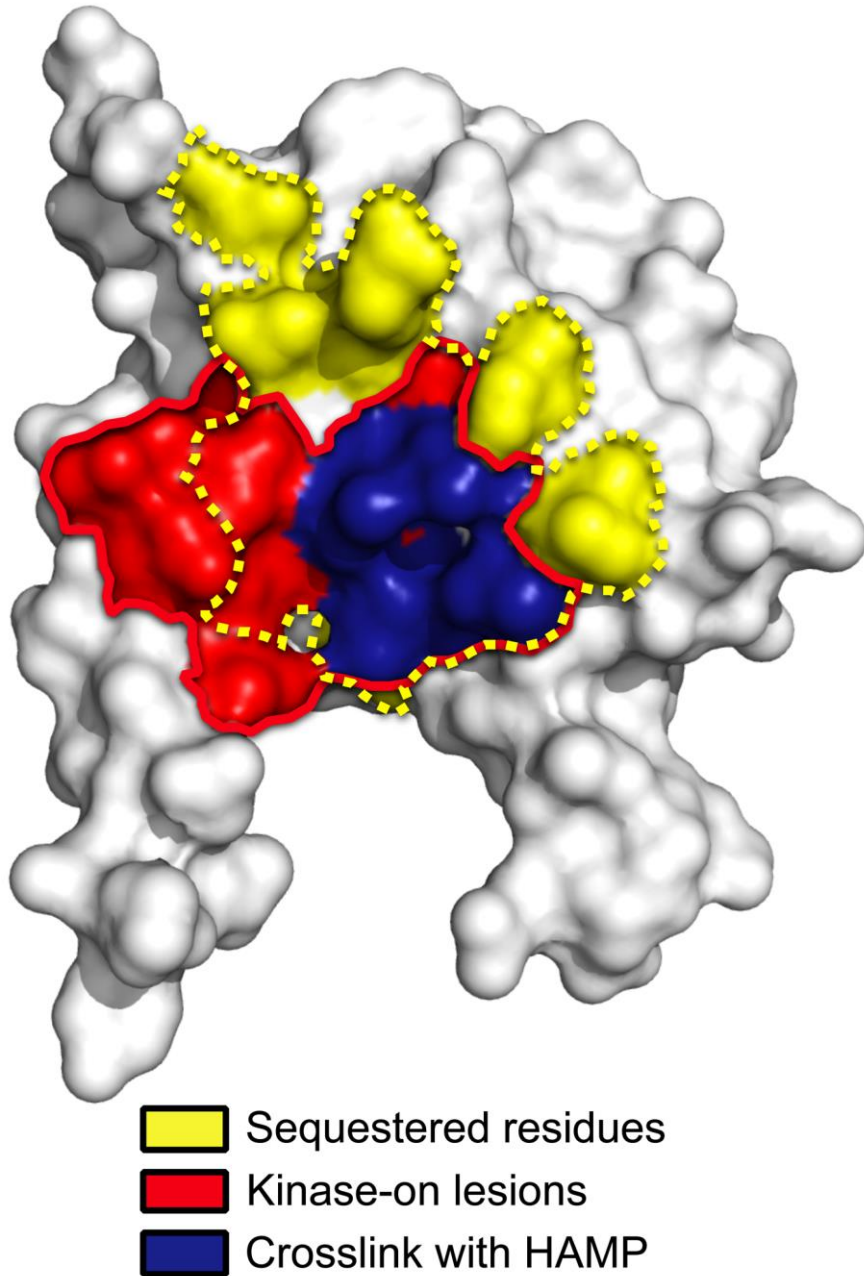
Fiure 20. PAS space-filled model overlaying a region of previously determined kinase-on lesions [(Campbell *et al.*, 2010), within the red line] with residues shown in the current study to be sequestered (dotted yellow line), or that preferentially crosslinked with the HAMP domain (blue).
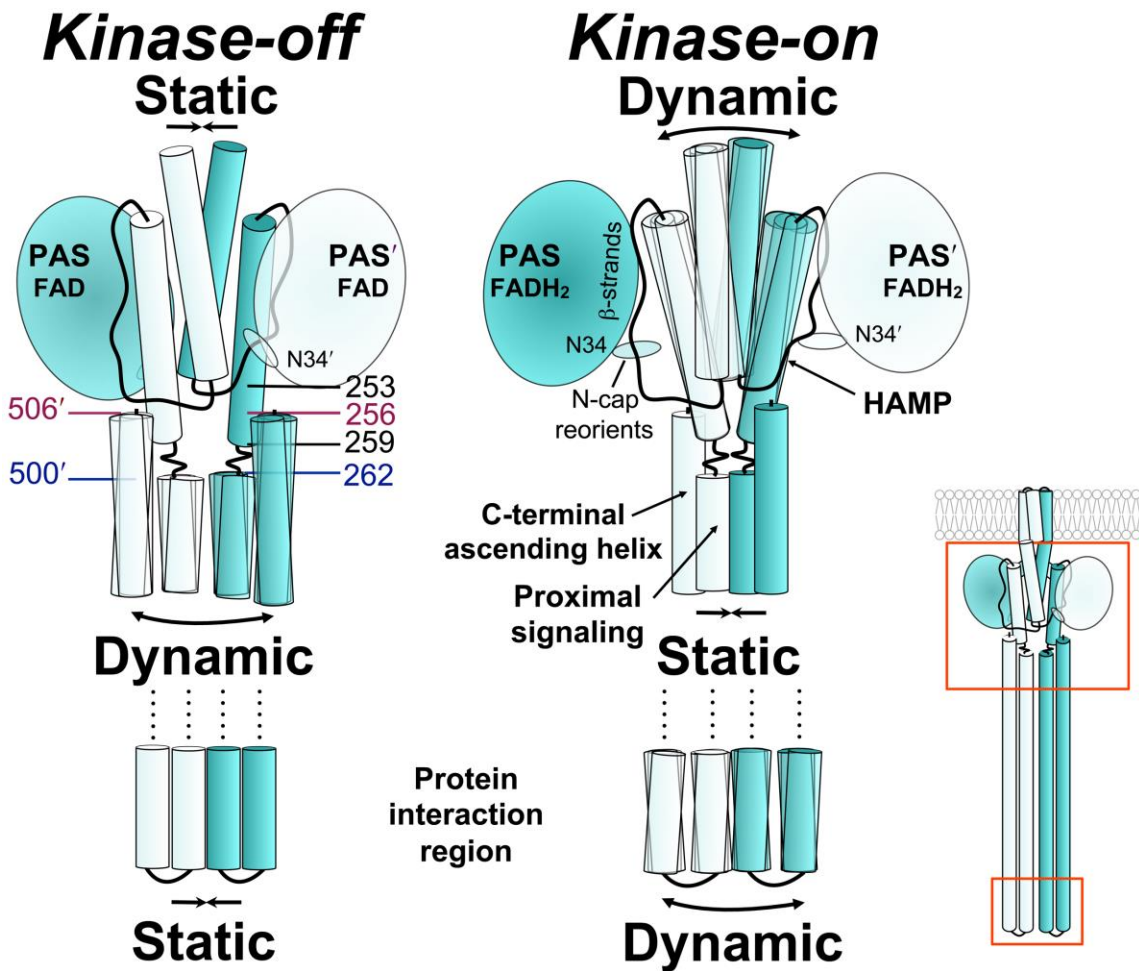
Figure 21. Working model of Aer showing the relationship between PAS and HAMP in the kinase-off and kinase-on states, based on current and previous data. Colors match those of Fig. 18. The reduction of PAS-bound FAD elicits a conformational change that decreases interaction between the PAS domain and the HAMP domain. The relative orientation between the N-cap and PAS core also changes, perhaps altering the stability of PAS-HAMP interactions. Decreased PAS-HAMP interactions are accompanied by tilting of the HAMP helices and a more relaxed, dynamic HAMP structure. The HAMP, proximal signaling domain and protein interaction regions are in opposition across contiguous boundaries such that a relaxed HAMP domain results in a static proximal signaling domain and a dynamic protein interaction region. Relevant residues: N34D, C253R, allele-specific suppressors; 259-262, phase shift; pairs 262/500 and 256/506 are highlighted to show their relative latitudes on descending and ascending helices. See Results and Discussion for details.

In Aer, the measured solvent accessibilities of the PAS, HAMP and proximal signaling domains (Figs. 16 and 17) defined potential PAS-HAMP interaction surfaces. Data from PAS surface residues showed a hidden region on the PAS β-scaffold (1,370 Å^2, Fig. 17D) that was consistent with a HAMP footprint rather than the footprint of a cognate PAS domain. Specifically, none of the sequestered residues crosslinked substantially with another PAS domain (Fig. 17C) and any such interactions may be transient rather than stable. Notably, the hidden region overlapped both with a cluster of PAS kinase-on lesions that we previously identified as part of the aerotaxis signaling pathway (Campbell *et al.*, 2010), and with PAS residues in this study that crosslinked with the HAMP domain (Fig. 17). Together, the data strongly support the hypothesis that the inaccessible PAS region forms the PAS component of the PAS-HAMP interface.

Of the 70 HAMP and proximal signaling domain replacements tested, accessibilities inversely correlated with disulfide crosslinking in two regions: HAMP AS-1 and the proximal signaling domain region that followed the phase-shift. In contrast, most of HAMP AS-2 and the N-terminal proximal signaling domain did not inversely correlate with crosslinking. Notably, 10 of 11 AS-2 residues residing on the HAMP exterior had low accessibility to PEG-mal (Fig. 16). Four of these were likely shielded by the HAMP connector (Fig. 16B), but five of the remaining residues were sequestered by the PAS domain (Fig. 16B, boxed residues shaded yellow) and are proposed to form the HAMP component of the PAS-HAMP interface (Fig. 21). In support of this, HAMP AS-2 substitutions

Q248C and L251C crosslinked with residues on the cognate PAS β-scaffold (Fig. 18). A best fit of the crosslinking data required that the PAS domain be rotated ~180° relative to a previous model (Campbell *et al.*, 2011, Watts *et al.*, 2008). The location of allele-specific suppressors PAS-N34D and HAMP-C253R are now shown in close proximity (Fig. 18E) and in harmony with genetic studies (Watts *et al.*, 2004a). PAS-HAMP crosslinking occurred between cognate subunits within dimers rather than between adjacent dimers because crosslinking was unaffected when collisions between Aer dimers were decreased by the presence of a second receptor (Tar). This is consistent with previous work indicating that HAMP dimers are centrally positioned, flanked by two PAS monomers (Campbell *et al.*, 2011), and are required for PAS folding and FAD binding (Herrmann *et al.*, 2004, Bibikov *et al.*, 2000, Ma *et al.*, 2005, Buron-Barral *et al.*, 2006b). Interestingly, an arrangement similar to the Aer PAS β-scaffold-HAMP AS-2 α-helix interface (Fig. 18E) has been described for several proteins including the periplasmic sensing domain of the *Sinorhizobium meliloti* C_4-dicarboxylate sensor DctB (Zhou *et al.*, 2008) and the *Vibrio harveyi* quorum sensor LuxQ (Neiditch *et al.*, 2006), where in both cases the β-scaffold of two PAS domains abuts a long α-helical spine.

Changes in PAS N-cap Orientation During Signaling

The PAS N-cap and the loop connecting the N-cap to the PAS core were highly accessible (Fig. 17) yet appear to be part of the Aer signaling pathway. Kinase-on lesions that define the Aer signaling pathway cluster not only on the PAS β-

scaffold and in the FAD cleft, but also in the N-cap (Campbell *et al.*, 2010, Watts

et al., 2006b). Truncating the first six N-cap residues bestows a kinase-on

phenotype, while deleting the first 14 residues yields an inverted response

phenotype (Watts *et al.*, 2006b). Aer-L14 is significant in that it likely hydrogen

bonds to N34, forming an unusual extended helix that is unbroken in structure,

but discontinuous in sequence (Etzkorn *et al.*, 2008, Key *et al.*, 2007, Campbell

et al., 2010, Watts *et al.*, 2006b). In DcuS-PASc, an N248D substitution that is

equivalent to Aer-N34D reorients the N-cap and activates the protein (Etzkorn *et

al.*, 2008). Notably, an N34D substitution in Aer is both kinase-on and an allele-

specific suppressor of HAMP-C253R (Watts *et al.*, 2004a). The crosslinking data

from the current study indicate that N34 and C253 are in close proximity (Fig.

18E), and by homology to DcuS-PASc, the N-cap may reorient when PAS is in

the kinase-on state (Fig. 21). In this scenario, N-cap reorientation would help

destabilize PAS-HAMP interactions (Fig. 21), giving the HAMP domain more

degrees of freedom and dynamic movement.

Changes in HAMP Conformation and PAS-HAMP Interactions During

Signaling

We previously found that the kinase-on substitution, PAS-N85S, altered

rates of crosslinking between HAMP AS-1 and AS-2′ helices (Watts *et al.*,

2011a). Rates decreased at the proximal end of HAMP, and increased at the

distal end of HAMP. This was interpreted as either i) tilting of AS-2 with respect

to AS-1′, or ii) a more relaxed HAMP structure [Fig. 21, (Watts *et al.*, 2011a)].

The data from the current study reveal changes in PAS-HAMP interactions that are correlated with these states: the kinase-on substitution (PAS-N85S) exposed a patch of HAMP residues that had been hidden in the kinase-off state by the PAS domain (Fig. 19). This is consistent with a decrease in the strength of the PAS-HAMP AS-2 interaction in the kinase-on state, and a less compact, more dynamic conformation of HAMP. The dynamic conformation is likely to be favored by Aer-HAMP because it lacks strong hydrophobic residues at several key packing positions in the HAMP bundle (Watts *et al.*, 2008, Parkinson, 2010). Still, some HAMP residues apparently remained in contact with PAS in the kinase-on state, because residues in the exposed patch remained less solvent accessible than they were in the PAS-less mutant (compare res. 241, 244 and 245 in Figs. 16C and 19A). However, PAS is effectively tethered to HAMP in the Aer dimer, so some collisional contacts are also expected.

The impact of PAS-N85S on AS-2 accessibility was not uniform. In contrast to AS-2 residues that exhibited increased accessibility with N85S, a patch of residues at the distal end of AS-2 through the proximal signaling domain had decreased accessibility (Fig. 19). The proximal signaling domain links HAMP AS-2 to the kinase control domain and has a helical phase shift between residues 259 and 262; the shift is five residues downstream of the phase stutter at the HAMP-output junction (Brown *et al.*, 1996, Parkinson, 2010). In Aer, the residues with decreased accessibility included not only residues throughout the proximal signaling domain toward the kinase control junction (N269), but also residues upstream, extending to the HAMP junction (C253) (Fig. 19). The

proximal signaling domain is also functionally distinguishable from the HAMP domain: missense mutations in the proximal signaling domain do not influence PAS-FAD binding (Ma *et al.*, 2005, Buron-Barral *et al.*, 2006b), nor are they suppressed by PAS suppressor lesions that rescue HAMP defects (Watts *et al.*, 2004a). This suggests that the proximal signaling domain, unlike HAMP, does not associate with the PAS domain.

The data from the current study are consistent with the dynamic bundle model (Parkinson, 2010, Zhou *et al.*, 2009), although they are not definitive. The broad changes in accessibility associated with signaling (Fig. 19) are more easily explained by dynamics [regulated unfolding, (Schultz & Natarajan, 2013)] than by conformational changes in semi-rigid structures that mimic a specific pattern of changes propagated by the transmembrane helix of a chemoreceptor. In Aer, signaling caused opposite accessibility changes in the HAMP and proximal signaling domains (Figs. 19 and 21). This suggests an inverse structural relationship between these domains, such that when one is compact the other is dynamic. Inverted shifting between compact and dynamic structures has been proposed for the other *E. coli* chemoreceptors, whereby three contiguous segments have opposite structural transitions: the HAMP domain, the adaptation region and the protein interaction region of the kinase control module (Falke & Piasta, 2014, Parkinson, 2010). The first inversion is associated with a helical phase shift at the juncture between HAMP AS-2 and the adaptation region. This shift couples the helical bundles in opposition, so that increasing the packing stability of one bundle decreases the stability of the other. The second inversion

may occur at a glycine hinge that is equivalent to Aer residues G330, G331 and G429. The behavioral output for Aer indicates that the structural state of the protein interaction region is similar to the state of HAMP, as it is in other chemoreceptors (Fig. 21B). Switching to a more static HAMP domain would reverse the states of the other two regions, so the HAMP and protein interaction regions continue to share the same conformational profile [(Falke & Piasta, 2014), Fig. 21].

Recent studies on the Tsr receptor suggest that the HAMP domain acts as a brake that inhibits the default kinase-on state of the receptor. Thus, the HAMP-independent output state of the Tsr kinase control module is kinase-on, and HAMP must actively override this state in response to attractant stimuli (Ames *et al.*, 2014). Given the homology among the Tsr, Tar, and Aer kinase-control modules, the default output for Aer is also likely to be kinase-on, although similar definitive analyses of Aer-HAMP deletions would be confounded by the requirement of HAMP for PAS maturation [(Herrmann *et al.*, 2004, Buron-Barral *et al.*, 2006b), J. S. Parkinson, personal communication].

Aer Signaling Model

From the present and previous studies, we propose a complete pathway for Aer-mediated aerotaxis. When *E. coli* swims into a region where the ambient oxygen concentration cannot maintain the electron transport system, FAD bound to the Aer-PAS domain is reduced and protonated. A hydrogen-bond network linked to FAD is reorganized, resulting in a conformational change in the PAS β-

scaffold at the PAS-HAMP AS-2 interface [(Campbell *et al.*, 2010); see also

(Campbell *et al.*, 2010, Key *et al.*, 2007, Ukaegbu & Rosenzweig, 2009b)].

Altered PAS-HAMP interactions switch a patch of HAMP surface residues from

low accessibility to high accessibility, consistent with decreased affinity between

the PAS and HAMP domains. We propose that interactions between oxidized

PAS and HAMP AS-2 promote a more ordered (static) HAMP structure and an

active kinase-off output, whereas weaker PAS-HAMP interactions in the reduced

state allow a more dynamic HAMP structure and kinase-on output (Fig. 21). Aer-

HAMP controls the proximal signaling domain, and in turn, the kinase control

domain. The tip of the kinase control domain is the protein interaction region,

which shares the same relative state as HAMP (dynamic or static) [reviewed by

(Falke & Piasta, 2014)]. After the bacteria approach the hypoxic region and FAD

is reduced, the cells tumble briefly and swim in a different direction. This avoids

anaerobiosis and ensures that cells move towards a higher oxygen

concentration. It is the movement up the oxygen gradient that is dominant in

determining net migration. In an aerobic environment, FAD becomes oxidized

and PAS-HAMP interactions strengthen, resulting in a static HAMP domain and a

kinase-off output. The static HAMP domain shifts the bias of the protein

interaction region, which inhibits CheA kinase and suppresses changes in

swimming direction.

The model for direct signaling between the PAS and HAMP domains of

Aer presents a new paradigm for controlling HAMP states. The paradigm

suggests that signal-sensitive, intra-dimeric contacts between PAS and HAMP

AS-2 controls the static or dynamic nature of HAMP. This mechanism likely occurs in other proteins that have laterally interacting PAS and HAMP domains, and may be the mechanism by which other sensing domains can control HAMP activity in a wide variety of systems.

SUPPLEMENTARY INFORMATION

DELINEATING PAS-HAMP INTERACTION SURFACES AND SIGNALING-ASSOCIATED CHANGES IN THE AEROTAXIS RECEPTOR AER

Darysbel Garcia[1], Kylie J. Watts[1], Mark S. Johnson, and Barry L. Taylor*

Division of Microbiology and Molecular Genetics,

School of Medicine,

Loma Linda University.

Loma Linda, CA 92350. USA.

*Corresponding author.

[1]These two authors contributed equally to this investigation.
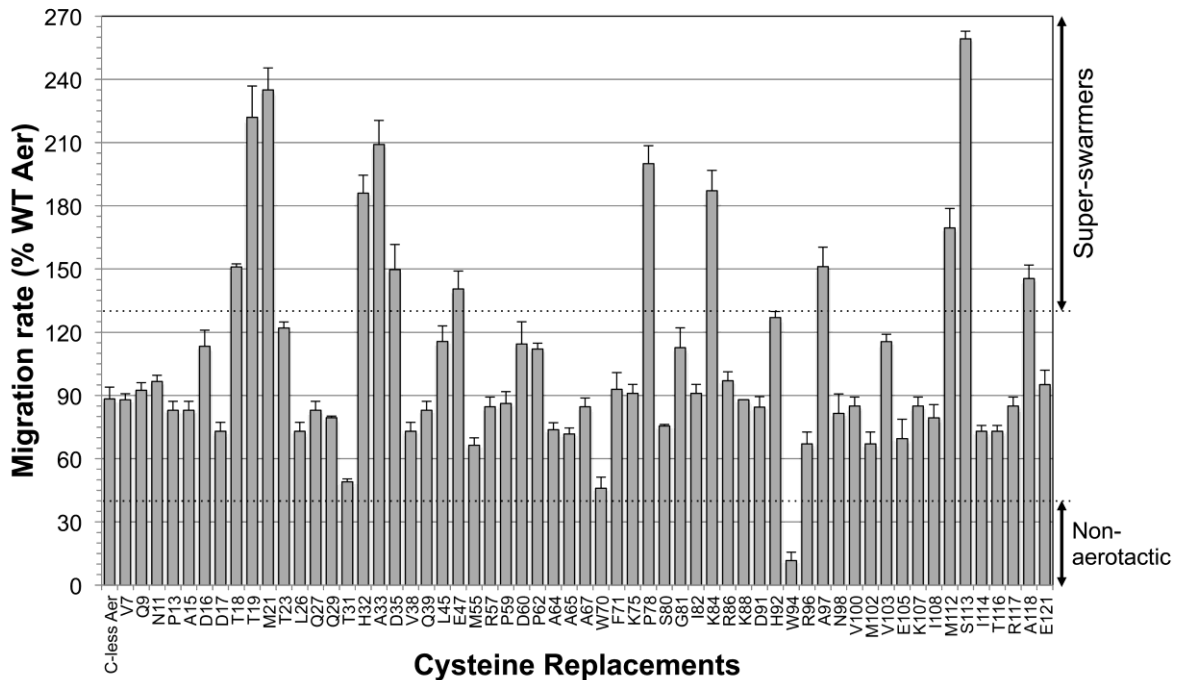
Figure S1. Influence of PAS-Cys substitutions on Aer-mediated behavior in *E. coli* BT3312 (*aer tsr*). Aer-Cys mutants were tested in succinate minimal soft agar containing 50 µg. ml^{-1} ampicillin. Colony expansion was determined after 15-20 hours of growth at 30°C and compared with wild-type Aer [as expressed from pGH1, (Rebbapragada *et al.*, 1997a)]. Mutants with average colony diameters greater than 130% of WT Aer were designated as 'superswarmers'. Mutants with average colony diameters less than 40% of WT have impaired behavior or are non-aerotactic (Watts *et al.*, 2008). Only cells expressing Aer-W94C fell in this category and were non-aerotactic in minimal soft agar. In a temporal aerotaxis assay (Taylor *et al.*, 2007), BT3312 cells expressing Aer-W94C were tumbly-biased in air, had a delayed response to nitrogen, and a showed a brief smooth-swimming response to oxygen.

Experimental Procedures

Bacterial Strains and Plasmids

Cysteine-less (C-less) Aer (Aer-C193S/C203A/C253A) was expressed from pMB1 (Ma *et al.*, 2004, Watts *et al.*, 2006b), a pTrc99A-derivative that expresses Aer under the control of an IPTG-inducible p_{trc} promoter. All Aer-Cys

mutants in this study were derived from pMB1. The WT Tar expression plasmid, pLC113, was a gift from John S. Parkinson and is a pACYC184-based plasmid that confers chloramphenicol resistance and carries a sodium salicylate-inducible promoter (Ames & Parkinson, 2006). Plasmids were expressed in *E. coli* BT3312, a strain that lacks the two aerotaxis receptors, Aer and Tsr [Δ*aer-1* Δ*tsr-7021*, (Repik et al., 2000] or in chemoreceptor-less BT3388 [*aer::erm* Δ*tsr-7021* Δ*tar-tap-5201 trg::Tn10*) (Yu *et al.*, 2002)].

Mutant Construction

A library of Aer mutants with single cysteine substitutions between residues 206 and 275 was previously constructed in pMB1 (Watts *et al.*, 2008, Amin *et al.*, 2006). Aer-N85S and additional Aer-Cys mutants were constructed by site-directed mutagenesis of pMB1 or pMB1-derived plasmids according to the instructions of the QuikChange® II site-directed mutagenesis kit (Agilent Technologies, Santa Clara, CA). The N85S codon was introduced into plasmids that contained a single Cys codon substitution, whereas di-Cys mutants were created from a pMB1-derivative that expressed either Aer-Q248C or Aer-L251C. Aer[112-506] mutants were created by amplifying the coding region for residues 112-506 from individual pMB1-derived plasmids using primers containing recognition sequences for AflIII and SalI, and ligating the products into pTrc99A with the NcoI-SalI DNA segment removed. Mutations were confirmed by sequencing the entire *aer* gene of each plasmid.

Expression and Aerotaxis Assays

Plasmids were introduced into BT3312 (*aer tsr*) and Aer expression was confirmed by Western blotting with a 1 in 133,000 dilution of anti-Aer$_{2\text{-}166}$ antisera (Repik *et al.*, 2000a). Aer[112-506] mutants express stable protein (K.K. Gosink and J.S. Parkinson, personal communication), but have fewer epitopes than full-length Aer, so were detected with a 1 in 50,000 dilution of anti-Aer$_{2\text{-}166}$ antisera. For Aer/Tar co-expression assays, Aer and Tar expression plasmids were introduced into BT3388 (*aer tsr tar trg tap*) and expressed as described (Campbell *et al.*, 2011). Tar expression was confirmed using a 1 in 10,000 dilution of anti-Tsr$_{290\text{-}470}$ antisera [a gift from J. S. Parkinson, (Ames & Parkinson, 1994)]. Aerotaxis phenotypes were determined for each Aer mutant by inoculating cells into succinate minimal soft agar containing 50 μg ml^{-1} ampicillin, incubating the plates at 30°C for 15-20 hours, and then observing colony morphologies (Taylor *et al.*, 2007).

In vivo Accessibility Assays using PEG-mal

In vivo PEGylation assays were performed using an unpublished permeabilized cell protocol developed by Claudia A. Studdert at the Universidad Nacional de Mar del Plata, Argentina, but modified in this study to work optimally for Aer. BT3312 cells expressing each of the Aer-Cys mutants were grown at 30°C to mid-log phase in tryptone broth containing 100 μg ml^{-1} ampicillin, and induced for 3 hours with 50 μM IPTG. Aer-P211C, Aer-R235C and Aer-G240C have lower steady-state accumulation levels (Watts *et al.*, 2008), as did Aer-

R57C, Aer-D60C and Aer-A97C (this study) and were induced with 100 µM IPTG. Two milliliters of each culture was centrifuged at 10,000 x g in each of two tubes (corresponding to denatured and native samples), then washed twice with 20 mM potassium phosphate [pH 7.0], 0.1 mM EDTA, and 0.1 mM MgCl$_2$ buffer. The cells in each tube were resuspended in 1 ml of wash buffer and permeabilized by adding 50 µl of 1:4 toluene:ethanol. After 15 min of vigorous mixing at room temperature on an Eppendorf mixer (Eppendorf model 5432, Hauppauge, NY), the cells were centrifuged, the supernatant and excess fluid were removed, and the pellets were resuspended in 50 µl of wash buffer. Five mM PEG-mal (Laysan Bio, Arab, AL) was thoroughly mixed with the cells, and the tubes were incubated at 25°C for 15 min. PEGylation reactions were stopped by adding 100 µl of sample buffer with excess β-mercaptoethanol (native samples, 1.43 M β-mercaptoethanol) or with no reducing agent (denatured samples). The samples were then boiled for four min and analyzed by SDS-PAGE. A quenching control, in which 1.43 M β-mercaptoethanol was added before PEG-mal, efficiently quenched the PEGylation reaction (see Fig. 2). Bands were visualized on Western blots and quantified on a BioSpectrum® digital imager (UVP, Upland, CA). For each residue, the proportion of PEGylated product was calculated by dividing the average density of the PEGylated band by the average densities of the non-PEGylated plus PEGylated fractions from duplicate lanes. Reactions were repeated on at least two, but usually three or more, occasions. To compare extents of PEGylation in the presence and absence of the PAS domain or PAS-N85S, statistical analyses were carried out

using a two-tailed Student's *t*-test. A *p* value of less than 0.05 was considered statistically significant.

In vivo Disulfide Crosslinking

BT3312 cells expressing each of the di-Cys and corresponding single-Cys mutants were grown to mid-log phase in H1 minimal salts medium supplemented with 30 mM succinate, 0.1% (w/v) casamino acids and 100 µg ml^{-1} ampicillin, before being induced for 3 hours with 50 µM IPTG. Crosslinking was performed at 25°C by exposing whole cells to 600 µM Cu(II)(1,10-phenanthroline)$_3$ (CuPhe) for 20 min, similar to that described previously (Amin *et al.*, 2006, Hughson & Hazelbauer, 1996, Watts *et al.*, 2008), but with modifications as described in (Lai & Hazelbauer, 2007, Taylor *et al.*, 2007). The following 25 PAS-Cys mutants were tested for crosslinking with Q248C in di-Cys receptors: T19C, M21C, T23C, H32C, N34C, D35C, T36C, V38C, L45C, M55C, K75C, P78C, S80C, I82C, K88C, N89C, R96C, N98C, V100C, V103C, I108C, M112C, I114C, A118C and E121C. PAS-Cys subsets were also tested for their ability to crosslink with R244C, G250C, M252C, C253, R254C and D259C. Aer-I114C/Q248C and Aer-E105C were also analyzed in BT3388, with Aer as the sole receptor, or in the presence of WT Tar (as expressed from pLC113) with no induction or with 1.2 µM sodium salicylate induction. Crosslinked products were separated from monomers by SDS-PAGE and quantified on the UVP digital imager after Western blotting. Percent crosslinking was calculated by dividing the intensity of the crosslinked dimer band by the sum of the intensities of the monomer and dimer

bands, multiplied by 100. Aer-V260C (Watts *et al.*, 2008) and C-less Aer (Ma *et al.*, 2004) were used as positive and negative crosslinking controls, respectively. Dimer bands were never evident with C-less Aer, whereas the extent of dimerization for Aer-V260C was routinely ≈65% after 20 min. Reactions were repeated on two or more occasions.

In silico Modeling

Aer PAS and HAMP domain models were previously created from the coordinates of NifL PAS (2GJ3) and Af1503 HAMP (2ASX), respectively (Campbell *et al.*, 2010, Watts *et al.*, 2008). PyMOL viewer (The PyMOL Molecular Graphics System, Version 1.0, Schrödinger, LLC) was used to manipulate models, map experimental data and determine surface areas. The experimental results were used as a guide to manually manipulate the positions of the PAS and HAMP domains in an Aer dimer to obtain the best fit (Figs. 5 and 8).

Acknowledgements

References

Airola, M.V., N. Sukomon, D. Samanta, P.P. Borbat, J.H. Freed, K.J. Watts and B.R. Crane, (2013) HAMP domain conformers that propagate opposite signals in bacterial chemoreceptors. *PLoS Biol* 11: e1001479.

Airola, M.V., K.J. Watts, A.M. Bilwes and B.R. Crane, (2010) Structure of concatenated HAMP domains provides a mechanism for signal transduction. *Structure* 18: 436-448.

Alexander, R.P. and I.B. Zhulin, (2007) Evolutionary genomics reveals conserved structural determinants of signaling and adaptation in microbial chemoreceptors. *Proc Natl Acad Sci USA* 104: 2885-2890.

Ames, P. and J.S. Parkinson, (1994) Constitutively signaling fragments of Tsr, the *Escherichia coli* serine chemoreceptor. *J Bacteriol* 176: 6340-6348.

Ames, P. and J.S. Parkinson, (2006) Conformational suppression of inter-receptor signaling defects. *Proc Natl Acad Sci USA* 103: 9292-9297.

Ames, P., Q. Zhou and J.S. Parkinson, (2014) HAMP domain structural determinants for signalling and sensory adaptation in Tsr, the *Escherichia coli* serine chemoreceptor. *Mol Microbiol* 91: 875-886.

Amin, D.N., B.L. Taylor and M.S. Johnson, (2006) Topology and boundaries of the aerotaxis receptor Aer in the membrane of *Escherichia coli*. *J Bacteriol* 188: 894-901.

Aravind, L. and C.P. Ponting, (1999) The cytoplasmic helical linker domain of receptor histidine kinase and methyl-accepting proteins is common to many prokaryotic signalling proteins. *FEMS Microbiol Lett* 176: 111-116.

Bass, R.B., S.L. Butler, S.A. Chervitz, S.L. Gloor and J.J. Falke, (2007) Use of site-directed cysteine and disulfide chemistry to probe protein structure and dynamics: applications to soluble and transmembrane receptors of bacterial chemotaxis. *Methods Enzymol* 423: 25-51.

Bibikov, S.I., L.A. Barnes, Y. Gitin and J.S. Parkinson, (2000) Domain organization and flavin adenine dinucleotide-binding determinants in the aerotaxis signal transducer Aer of *Escherichia coli*. *Proc Natl Acad Sci USA* 97: 5830-5835.

Bibikov, S.I., R. Biran, K.E. Rudd and J.S. Parkinson, (1997) A signal transducer for aerotaxis in *Escherichia coli*. *J Bacteriol* 179: 4075-4079.

Bibikov, S.I., A.C. Miller, K.K. Gosink and J.S. Parkinson, (2004) Methylation-independent aerotaxis mediated by the *Escherichia coli* Aer protein. *J Bacteriol* 186: 3730-3737.

Brown, J.H., C. Cohen and D.A. Parry, (1996) Heptad breaks in alpha-helical coiled coils: stutters and stammers. *Proteins* 26: 134-145.

Buron-Barral, M.D.C., K.K. Gosink and J.S. Parkinson, (2006) Loss- and gain-of-function mutations in the F1-HAMP region of the *Escherichia coli* aerotaxis transducer Aer. *J Bacteriol* 188: 3477-3486.

Butler, S.L. and J.J. Falke, (1998) Cysteine and disulfide scanning reveals two amphiphilic helices in the linker region of the aspartate chemoreceptor. *Biochemistry* 37: 10746-10756.

Campbell, A.J., K.J. Watts, M.S. Johnson and B.L. Taylor, (2010) Gain-of-function mutations cluster in distinct regions associated with the signalling pathway in the PAS domain of the aerotaxis receptor, Aer. *Mol Microbiol* 77: 575-586.

Campbell, A.J., K.J. Watts, M.S. Johnson and B.L. Taylor, (2011) Role of the F1 region in the *Escherichia coli* aerotaxis receptor Aer. *J Bacteriol* 193: 358-366.

Dunin-Horkawicz, S. and A.N. Lupas, (2010) Comprehensive analysis of HAMP domains: Implications for transmembrane signal transduction. *J Mol Biol* 397: 1156-1174.

Etzkorn, M., H. Kneuper, P. Dunnwald, V. Vijayan, J. Kramer, C. Griesinger, S. Becker, G. Unden and M. Baldus, (2008) Plasticity of the PAS domain and a potential role for signal transduction in the histidine kinase DcuS. *Nat Struct Mol Biol* 15: 1031-1039.

Falke, J.J. and K.N. Piasta, (2014) Architecture and signal transduction mechanism of the bacterial chemosensory array: Progress, controversies, and challenges. *Curr Opin Struct Biol* 29C: 85-94.

Ferris, H.U., S. Dunin-Horkawicz, L.G. Mondejar, M. Hulko, K. Hantke, J. Martin, J.E. Schultz, K. Zeth, A.N. Lupas and M. Coles, (2011) The mechanisms of HAMP-mediated signaling in transmembrane receptors. *Structure* 19: 378-385.

Gosink, K.K., M. del Carmen Buron-Barral and J.S. Parkinson, (2006) Signaling interactions between the aerotaxis transducer Aer and heterologous chemoreceptors in *Escherichia coli*. *J Bacteriol* 188: 3487-3493.

Hazelbauer, G.L. and W.C. Lai, (2010) Bacterial chemoreceptors: providing enhanced features to two-component signaling. *Curr Opin Microbiol* 13: 124-132.

Herrmann, S., Q. Ma, M.S. Johnson, A.V. Repik and B.L. Taylor, (2004) PAS domain of the Aer redox sensor requires C-terminal residues for native-fold formation and flavin adenine dinucleotide binding. *J Bacteriol* 186: 6782-6791.

Hughson, A.G. and G.L. Hazelbauer, (1996) Detecting the conformational change of transmembrane signaling in a bacterial chemoreceptor by measuring effects on disulfide cross-linking in vivo. *Proc Natl Acad Sci USA* 93: 11546-11551.

Hulko, M., F. Berndt, M. Gruber, J.U. Linder, V. Truffault, A. Schultz, J. Martin, J.E. Schultz, A.N. Lupas and M. Coles, (2006) The HAMP domain structure implies helix rotation in transmembrane signaling. *Cell* 126: 929-940.

Key, J., M. Hefti, E.B. Purcell and K. Moffat, (2007) Structure of the redox sensor domain of *Azotobacter vinelandii* NifL at atomic resolution: signaling, dimerization, and mechanism. *Biochemistry* 46: 3614-3623.

Klose, D., N. Voskoboynikova, I. Orban-Glass, C. Rickert, M. Engelhard, J.P. Klare and H.J. Steinhoff, (2014) Light-induced switching of HAMP domain conformation and dynamics revealed by time-resolved EPR spectroscopy. *FEBS Lett* 588: 3970-3976.

Krell, T., J. Lacal, F. Munoz-Martinez, J.A. Reyes-Darias, B.H. Cadirci, C. Garcia-Fontana and J.L. Ramos, (2011) Diversity at its best: bacterial taxis. *Environ Microbiol* 13: 1115-1124.

Lai, R.Z. and J.S. Parkinson, (2014) Functional suppression of HAMP domain signaling defects in the *E. coli* serine chemoreceptor. *J Mol Biol* 426: 3642-3655.

Lai, W.C. and G.L. Hazelbauer, (2007) Analyzing transmembrane chemoreceptors using in vivo disulfide formation between introduced cysteines. *Methods Enzymol* 423: 299-316.

Lu, J. and C. Deutsch, (2001) Pegylation: a method for assessing topological accessibilities in Kv1.3. *Biochemistry* 40: 13288-13301.

Ma, Q., M.S. Johnson and B.L. Taylor, (2005) Genetic analysis of the HAMP domain of the Aer aerotaxis sensor localizes flavin adenine dinucleotide-binding determinants to the AS-2 helix. *J Bacteriol* 187: 193-201.

Ma, Q., F. Roy, S. Herrmann, B.L. Taylor and M.S. Johnson, (2004) The Aer protein of *Escherichia coli* forms a homodimer independent of the signaling domain and FAD binding. *J Bacteriol* 186: 7456-7459.

Mechaly, A.E., N. Sassoon, J.M. Betton and P.M. Alzari, (2014) Segmental helical motions and dynamical asymmetry modulate histidine kinase autophosphorylation. *PLoS Biol* 12: e1001776.

Mondejar, L.G., A. Lupas, A. Schultz and J.E. Schultz, (2012) HAMP domain-mediated signal transduction probed with a Mycobacterial adenylyl cyclase as a reporter. *J Biol Chem* 287: 1022-1031.

Nambu, J.R., J.O. Lewis, K.A. Wharton, Jr. and S.T. Crews, (1991) The *Drosophila single-minded* gene encodes a helix-loop-helix protein that acts as a master regulator of CNS midline development. *Cell* 67: 1157-1167.

Neiditch, M.B., M.J. Federle, A.J. Pompeani, R.C. Kelly, D.L. Swem, P.D. Jeffrey, B.L. Bassler and F.M. Hughson, (2006) Ligand-induced asymmetry in histidine sensor kinase complex regulates quorum sensing. *Cell* 126: 1095-1108.

Parkinson, J.S., (2010) Signaling mechanisms of HAMP domains in chemoreceptors and sensor kinases. *Annu Rev Microbiol* 64: 101-122

Parkinson, J.S., G.L. Hazelbauer and J.J. Falke, (2015) Signaling and sensory adaptation in *Escherichia coli* chemoreceptors: 2015 update. *Trends Microbiol* 23: 257-266.

Rebbapragada, A., M.S. Johnson, G.P. Harding, A.J. Zuccarelli, H.M. Fletcher, I.B. Zhulin and B.L. Taylor, (1997) The Aer protein and the serine chemoreceptor Tsr independently sense intracellular energy levels and transduce oxygen, redox, and energy signals for *Escherichia coli* behavior. *Proc Natl Acad Sci USA* 94: 10541-10546.

Repik, A., A. Rebbapragada, M.S. Johnson, J.O. Haznedar, I.B. Zhulin and B.L. Taylor, (2000) PAS domain residues involved in signal transduction by the Aer redox sensor of *Escherichia coli*. *Mol Microbiol* 36: 806-816.

Schultz, J.E. and J. Natarajan, (2013) Regulated unfolding: a basic principle of intraprotein signaling in modular proteins. *Trends Biochem Sci* 38: 538-545.

Swain, K.E. and J.J. Falke, (2007) Structure of the conserved HAMP domain in an intact, membrane-bound chemoreceptor: a disulfide mapping study. *Biochemistry* 46: 13684-13695.

Swain, K.E., M.A. Gonzalez and J.J. Falke, (2009) Engineered socket study of signaling through a four-helix bundle: evidence for a yin-yang mechanism in the kinase control module of the aspartate receptor. *Biochemistry* 48: 9266-9277.

Taylor, B.L., (2007) Aer on the inside looking out: paradigm for a PAS-HAMP role in sensing oxygen, redox and energy. *Mol Microbiol* 65: 1415-1424.

Taylor, B.L., K.J. Watts and M.S. Johnson, (2007) Oxygen and redox sensing by two-component systems that regulate behavioral responses: behavioral assays and structural studies of Aer using in vivo disulfide cross-linking. *Methods Enzymol* 422: 190-232.

Taylor, B.L. and I.B. Zhulin, (1999) PAS domains: internal sensors of oxygen, redox potential, and light. *Microbiol Mol Biol Rev* 63: 479-506.

Ukaegbu, U.E. and A.C. Rosenzweig, (2009) Structure of the redox sensor domain of *Methylococcus capsulatus* (Bath) MmoS. *Biochemistry* 48: 2207-2215.

Wang, C., J. Sang, J. Wang, M. Su, J.S. Downey, Q. Wu, S. Wang, Y. Cai, X. Xu, J. Wu, D.B. Senadheera, D.G. Cvitkovitch, L. Chen, S.D. Goodman and A. Han, (2013) Mechanistic insights revealed by the crystal structure of a histidine kinase with signal transducer and sensor domains. *PLoS Biol* 11: e1001493.

Wang, J., J. Sasaki, A.L. Tsai and J.L. Spudich, (2012) HAMP domain signal relay mechanism in a sensory rhodopsin-transducer complex. *J Biol Chem* 287: 21316-21325.

Watts, K.J., M.S. Johnson and B.L. Taylor, (2006a) Minimal requirements for oxygen sensing by the aerotaxis receptor Aer. *Mol Microbiol* 59: 1317-1326.

Watts, K.J., M.S. Johnson and B.L. Taylor, (2008) Structure-function relationships in the HAMP and proximal signaling domains of the aerotaxis receptor Aer. *J Bacteriol* 190: 2118-2127.

Watts, K.J., M.S. Johnson and B.L. Taylor, (2011) Different conformations of the kinase-on and kinase-off signaling states in the Aer HAMP domain. *J Bacteriol* 193: 4095-4103.

Watts, K.J., Q. Ma, M.S. Johnson and B.L. Taylor, (2004) Interactions between the PAS and HAMP domains of the *Escherichia coli* aerotaxis receptor Aer. *J Bacteriol* 186: 7440-7449.

Watts, K.J., K. Sommer, S.L. Fry, M.S. Johnson and B.L. Taylor, (2006b) Function of the N-terminal cap of the PAS domain in signaling by the aerotaxis receptor Aer. *J Bacteriol* 188: 2154-2162.

Wuichet, K., R.P. Alexander and I.B. Zhulin, (2007) Comparative genomic and protein sequence analyses of a complex system controlling bacterial chemotaxis. *Methods Enzymol* 422: 1-31.

Yu, H.S., J.H. Saw, S. Hou, R.W. Larsen, K.J. Watts, M.S. Johnson, M.A. Zimmer, G.W. Ordal, B.L. Taylor and M. Alam, (2002) Aerotactic responses in bacteria to photoreleased oxygen. *FEMS Microbiol Lett* 217: 237-242.

Zhou, Q., P. Ames and J.S. Parkinson, (2009) Mutational analyses of HAMP helices suggest a dynamic bundle model of input-output signalling in chemoreceptors. *Mol Microbiol* 73: 801-814.

Zhou, Q., P. Ames and J.S. Parkinson, (2011) Biphasic control logic of HAMP domain signalling in the *Escherichia coli* serine chemoreceptor. *Mol Microbiol* 80: 596-611.

Zhou, Y.F., B. Nan, J. Nan, Q. Ma, S. Panjikar, Y.H. Liang, Y. Wang and X.D. Su, (2008) C4-dicarboxylates sensing mechanism revealed by the crystal structures of DctB sensor domain. *J Mol Biol* 383: 49-61.

Zhulin, I.B., (2001) The superfamily of chemotaxis transducers: from physiology to genomics and back. *Adv Microb Physiol* 45: 157-198.

CHAPTER THREE

GAS SENSING AND SIGNALING IN THE PAS-HEME DOMAIN OF THE

PSEUDOMONAS AERUGINOSA AER2 RECEPTOR

Darysbel Garcia, Emilie Orillard, Mark S. Johnson and Kylie J. Watts[#]

Running title: Signaling in the PAS-Heme Domain of *P. aeruginosa* Aer2

Division of Microbiology and Molecular Genetics

Loma Linda University

Loma Linda, CA, 92350, USA

[#]*Corresponding author:*

Telephone: +1 (909) 558-1000 x83394

Fax: +1 (909) 558-4035

Email: kwatts@llu.edu

KEY WORDS*: Chemoreceptor; PAS domain; signal transduction; *Pseudomonas aeruginosa*; heme; oxygen

This manuscript is based on experimental data acquired by Drs. Watts, Orillard, Johnson and myself. The work that I did not produce in this paper include; i) experiments on the proximal coordinating histidine, which were performed by Dr. Watts, ii) a few of the mutants were created by Drs. Watts and Orillard, and iii) determination of heme content using the pyridine hemochrome assay, which was performed by Drs. Johnson and Watts. A number of the experiments were performed by me after I left the lab. This was necessary in order to improve experimental standards deviations, and to acquire more reliable data using a new non-defective anaerobic hood.

Abstract

The Aer2 chemoreceptor from *Pseudomonas aeruginosa* contains a PAS sensing domain that coordinates *b*-type heme and signals in response to the binding of O_2, CO or NO. PAS-heme structures suggest that Aer2 uniquely coordinates heme via a His residue on a 3_{10} helix (H234 on Eη), stabilizes O_2 binding via a Trp residue (W283), and signals via both W283 and an adjacent Leu residue (L264). Ligand binding may displace L264 and reorient W283 for hydrogen-bonding to the ligand. Here we clarified the mechanisms by which Aer2-PAS binds heme, regulates ligand-binding, and initiates conformational signaling. H234 coordinated heme, but additional hydrophobic residues in the heme cleft were also critical for stable heme-binding. O_2 appeared to be the native Aer2 ligand (K_d of 16 μM). With one exception, mutants that bound O_2 could signal, whereas many mutants that bound CO could not. W283 stabilized O_2-binding, but not CO-binding, and was required for signal initiation; W283 mutants that could not stabilize O_2 were rapidly oxidized to Fe(III). W283F was the only Trp mutant that bound O_2 with WT affinity. The size and nature of residue 264 was important for gas binding and signaling: L264W blocked O_2 binding, L264A and L264G caused O_2-mediated oxidation, and L264K formed a hexa-coordinate heme. Our data suggest that when O_2 binds to Aer2, L264 may move concomitantly with W283 to initiate the conformational signal. The signal then propagates from the PAS domain to regulate the C-terminal HAMP and kinase control domains, ultimately modulating a cellular response.

Importance

Pseudomonas aeruginosa is a ubiquitous environmental bacterium and opportunistic pathogen that infects multiple body sites including the lungs of cystic fibrosis patients. *P. aeruginosa* senses and responds to its environment via four chemosensory systems. Three of these systems regulate biofilm formation, twitching motility and chemotaxis. The role of the fourth system, Che2, is unclear but has been implicated in virulence. The Che2 system contains a chemoreceptor called Aer2, which contains a PAS sensing domain that binds heme and senses oxygen. Here we show that Aer2 uses unprecedented mechanisms to bind O_2 and initiate signaling. These studies provide both the first functional corroboration of the Aer2-PAS signaling mechanism previously proposed from structure, as well as a signaling model for Aer2-PAS receptors.

Introduction

Pseudomonas aeruginosa is a common environmental bacterium and a significant cause of opportunistic human disease. It survives in complex environments with the aid of 26 chemoreceptors and four chemosensory systems that collectively sense environmental conditions and modify bacterial behavior. The roles of three of these chemosensory systems are known: one modulates type IV pili production and twitching motility (Pil-Chp system), another controls biofilm formation (Wsp system), and a third regulates flagella-mediated chemotaxis (Che system) (Kato *et al.*, 2008, Sampedro *et al.*, 2014). The role of the fourth chemosensory system, Che2 (PA0173-PA0179), is currently unknown.

Che2 expresses a complete set of chemosensory proteins (CheY2, CheA2, CheW2, CheR2, CheD and CheB2), including a chemoreceptor (PA0176) called Aer2 (previously called McpB). Aer2 was so named because it, along with classical Aer, was observed to mediate aerotaxis by *P. aeruginosa* (Hong *et al.*, 2004b). However, we, and others, have not observed Aer2-mediated chemotaxis or aerotaxis in *P. aeruginosa* (Watts *et al.*, 2011b, Guvener *et al.*, 2006). Moreover, it is now understood that the response regulators (CheY proteins) of Che2-like systems do not bind to the bacterial flagella motor protein, FliM, to modulate swimming behavior [(Biswas *et al.*, 2013, Hyakutake *et al.*, 2005, Dasgupta & Dattagupta, 2008) and Watts *et al.,* unpublished data]. This suggests that the primary role of Che2 is something other than the control of chemotaxis or aerotaxis. Notably, a role for Che2 in virulence has been suggested (Garvis *et al.*, 2009, Schuster *et al.*, 2004).

The Che2 chemoreceptor, Aer2, has no membrane-spanning segments. However, during the early stationary phase of *P. aeruginosa* growth, Che2 proteins form a cluster at the cell pole that is held together solely by Aer2 (Guvener *et al.*, 2006, Schuster *et al.*, 2004). Importantly, Che2 proteins do not co-localize with Che (chemotaxis system) proteins (Guvener *et al.*, 2006). Aer2 has an unusual architecture with a PAS sensory domain sandwiched between three N-terminal and two C-terminal HAMP domains (Fig. 22a). These domains precede a kinase control module that is typical of methyl-accepting chemoreceptors. The kinase control module has four predicted methylation sites (QEEE) and a C-terminal pentapeptide (GWEEF) for binding the adaptation

98

enzymes CheR2, CheB2 and CheD [Fig. 22a, (Garcia-Fontana *et al.*, 2014)]. In

P. aeruginosa, receptor deamidation/demethylation by CheB2 (and possibly

CheD), as well as methylation by CheR2, is expected to fine-tune Aer2-mediated

responses. The kinase control module of Aer2 has significant sequence identity

with the kinase control modules of the major *Escherichia coli* chemoreceptors.

Thus, Aer2 is able to control the *E. coli* chemotaxis pathway through direct

interactions with the *E. coli* adapter protein, CheW, and the histidine kinase,

CheA (Watts *et al.*, 2011b). When Aer2 is expressed in otherwise

chemoreceptor-less *E. coli*, it mediates repellent tumbling (signal-on) responses

to O_2, CO and NO (Watts *et al.*, 2011b). Gas-bound Aer2 causes rapid

autophosphorylation of bound CheA with subsequent

phospho-transfer to CheY. Phospho-CheY in turn binds to the *E. coli* flagellar

switch protein, FliM, causing a directional change in flagellar rotation from

counterclockwise to clockwise, resulting in *E. coli* tumbling.

The Aer2 gas response is initiated in the PAS (Per-ARNT-Sim) domain,

which itself binds penta-coordinate *b*-type heme (Watts *et al.*, 2011b). PAS

domains are common sensing and signaling domains in nature. They have a

broadly conserved structure that consists of a central antiparallel β-sheet with

five β-strands (Aβ, Bβ, Gβ, Hβ, and Iβ) flanked by several α-helices (Cα, Dα, Eα,

and Fα) (Moglich *et al.*, 2009b).
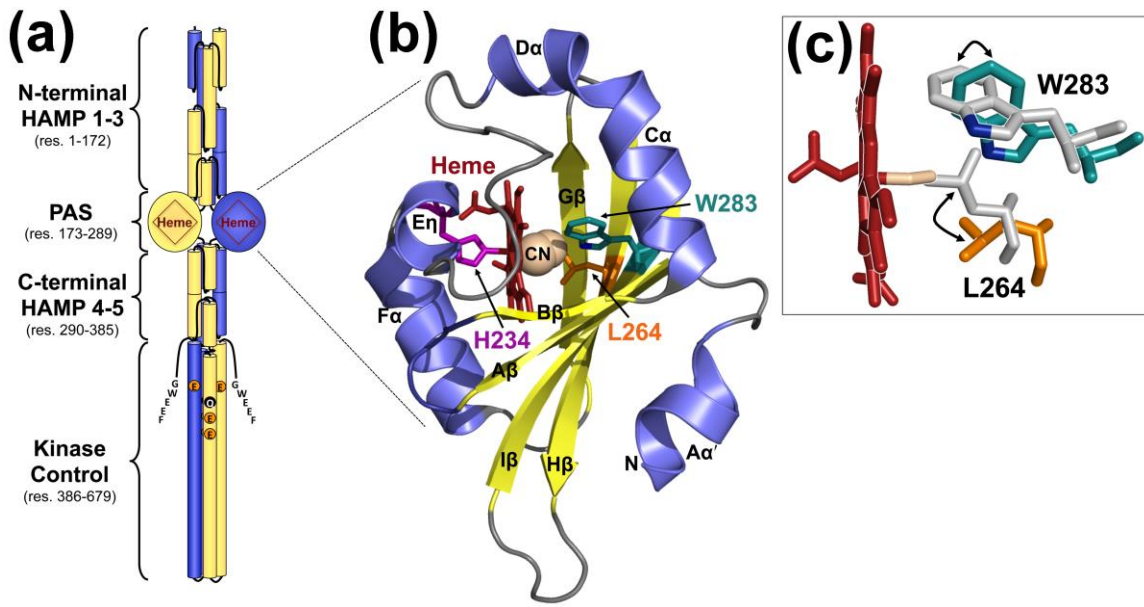
Figure 22. *P. aeruginosa* Aer2 and the structure of its PAS domain. (a) Model of an Aer2 dimer showing the PAS domain sandwiched between three N-terminal and two C-terminal HAMP domains. The C-terminal kinase control domain has four predicted methylation sites (QEEE) and a C-terminal pentapeptide (GWEEF) for binding adaptation enzymes. (b) Crystal structure of the Aer2 PAS domain in cartoon form with heme cofactor (shown as red sticks) and bound cyanide (shown as spheres) (PDB: 3VOL, (Sawai *et al.*, 2012)). The Fe-CN bond angle is 137° (Sawai *et al.*, 2012). The side chains of three amino acids relevant to this study, H234, L264 and W283 are shown as sticks. For clarity, the PAS structure is shown rotated 180 degrees around the x-axis compared with the orientation in Fig. 22a. (c) Cyanide-bound heme and a structural overlay showing the locations of the L264 and W283 side chains in both the unliganded (Fe^{3+} heme, grey side chains, PDB: 4HI4, (Airola *et al.*, 2013a)) and liganded (Fe^{3+}-CN heme, colored side chains (Sawai *et al.*, 2012)) Aer2 PAS domain. The position of the W283 nitrogen, which is predicted to bond with O_2, is shown in blue. Abbreviations: res, residue; CN, cyanide.

There are currently two structures for the Aer2 PAS domain: one contains cyanide bound to ferric heme [cyanomet, Fe^{3+}-CN, PDB: 3VOL, (Sawai *et al.*, 2012), Fig. 22b], and the other contains unliganded ferric heme [Fe^{3+}, PDB: 4HI4, (Airola *et al.*, 2013a)]. These structures revealed several unusual PAS features, including an extended Cα/Dα helix, a short 3_{10} helix called Eη (that replaces Eα),

100

heme coordination via a His residue on Eη, and potential O_2 stabilization via the indole group of a Trp residue on Iβ (Fig. 22b). In contrast, other PAS domains with *b*-type heme, like those in *E. coli* DOS (*Ec*DOS) or *Sinorhizobium meliloti* FixL (*Rm*FixL), coordinate heme with a His residue on the Fα helix, and stabilize O_2-binding via an Arg residue on Gβ (Gilles-Gonzalez & Gonzalez, 2005). The two Aer2 PAS structures represent non-physiological heme states (cyanomet and ferric heme), but they do represent structures with and without ligand, and overlaying these two structures highlights several residues that may be important for conformational signaling. In the absence of ligand, the Iβ Trp residue W283 appears to rotate ~90°, and an adjacent Leu residue, L264 on Hβ, contracts towards the heme iron center to occupy the position where CN^- was bound [Fig. 25c, (Airola *et al.*, 2013a)]. The heme itself appears to shift ~2.0 Å upon ligand binding and the heme pocket adjusts accordingly (Airola *et al.*, 2013a).

The Aer2 PAS domain is flanked on either side by poly-HAMP units (Fig. 22a). Individual HAMP domains form parallel four-helix bundles that are commonly found in prokaryotic proteins as signal-transducing modules (Dunin-Horkawicz & Lupas, 2010). In Aer2, there appears to be minimal PAS-HAMP interactions and, overall, Aer2 assumes a linear domain arrangement [Fig. 22a, (Airola *et al.*, 2013a)]. This contrasts with the aerotaxis receptor, Aer, where side-on PAS-HAMP interactions allow PAS to control HAMP signaling state through direct interactions (Garcia *et al.*, 2016). For Aer2, several structures have been solved for the N-terminal HAMP domains (Airola *et al.*, 2013c, Airola *et al.*, 2010b). Those structures show that HAMP 1 is separated from HAMP 2-3 by a

helical extension (Airola *et al.*, 2010b, Airola *et al.*, 2013c). HAMP 1 is also

largely dispensable for Aer2 function (Watts *et al.*, 2011b). In contrast, N-terminal

HAMP 2-3, and C-terminal HAMP4-5, each form integrated di-HAMP units that

are indispensable for Aer2 function (Airola *et al.*, 2010b, Watts *et al.*, 2011b). The

HAMP 1 and HAMP 2 structures represent signal-on and signal-off states,

respectively (Airola *et al.*, 2013c), lending support to the hypothesis that poly-

HAMP chains relay signals by inter-converting HAMP signaling states along the

HAMP chain.

Based on experimental evidence, our current signaling model for Aer2

includes the following features: Aer2 PAS-heme binds O_2, generating a

conformational signal that is transmitted to the PAS Iβ strand (Airola *et al.*,

2013a, Watts *et al.*, 2011b, Sawai *et al.*, 2012). N-terminal HAMP 2-3 do not

transmit signals, but function to stabilize the PAS signaling state by altering their

conformations in response to PAS ligand binding (Watts *et al.*, 2011b, Airola *et

al.*, 2013c). The PAS conformational signal is transmitted to C-terminal HAMP 4-

5, which together function as a unit to inhibit signaling from the kinase control

module (Watts *et al.*, 2011b). Therefore, without a PAS ligand, the kinase control

module conveys the signal-off state; but in the presence of PAS ligand, HAMP 4-

5 no longer inhibits the kinase control module, resulting in a signal-on output and

the autophosphorylation of bound CheA2. Without HAMP 4-5, the default state of

the isolated kinase control module is signal-on (Watts *et al.*, 2011b). The purpose

of the current study is to clarify the mechanisms used by the Aer2 PAS domain to

bind heme, regulate ligand binding, and initiate conformational signaling. We

provide evidence that i) the Eη His coordinates heme binding, ii) the hydrophobic heme pocket is crucial for stable heme binding, iii) O_2 is the native ligand of the Aer2 PAS domain, iv) the unprecedented Iβ Trp stabilizes O_2-binding but not CO-binding, and plays a pivotal role in signal initiation, and v) the Hβ Leu and other conserved PAS residues are important for heme binding, stable gas binding and signal transduction.

Results

Aer2 PAS Coordinates Heme with a Uniquely Positioned Histidine Residue

Structural studies suggest that the Aer2 PAS domain from *P. aeruginosa* coordinates *b*-type heme via a His residue (H234) that resides on a short Eη helix [Fig. 22b, (Sawai *et al.*, 2012, Airola *et al.*, 2013a)]. In contrast, other PAS domains coordinate *b*-type heme with a His residue on the PAS Fα helix (Gilles-Gonzalez & Gonzalez, 2005, Kerby *et al.*, 2008). Notably, Eη and Fα His residues are both highly conserved in Aer2-PAS homologs (Figs. 23a and S2). To test the contributions of each histidine to heme binding in *P. aeruginosa* Aer2, H234A (Eη His), H239A (Fα His) and H234A/H239A, were introduced into the PAS peptide, Aer2[173-289]. Aer2[173-289] is expressed with an N-terminal 6x-His tag and contains all necessary PAS heme-binding components (Watts *et al.*, 2011b). The purified PAS-H234A peptide showed a significant heme-binding defect, whereas PAS-H239A retained wild-type (WT) heme content (Figs. 23b and c). This confirms that the Eη His is the predominant means of coordinating heme in Aer2. However, 20% of PAS-H234A molecules retained heme, and

PAS-H234A/H239A exhibited a significant decrease in heme content versus H234A alone (Fig. 23c, 6% heme, p <0.05). The dual His replacement peptide thus has a lower heme affinity, suggesting that H239 might contribute to heme coordination in the absence of H234.

To determine the effect of the His substitutions on Aer2 signaling, mutations encoding H234A and H239A were introduced separately into full-length *aer2* in an *E. coli* expression plasmid. Both Aer2 mutants had steady-state expression levels comparable with WT Aer2 (Fig. 24a). When WT Aer2[1-679] is expressed in chemoreceptorless *E. coli* BT3388, it directs *E. coli* to tumble in the presence of O_2 because Aer2 signaling activates the *E. coli* chemotaxis cascade (Watts *et al.*, 2011b). When O_2 is replaced with N_2, Aer2 no longer signals, and after 5-10 sec, BT3388 cells resume smooth-swimming behavior (~2% of the cells tumble at any time) (Watts *et al.*, 2011b). BT3388 cells expressing Aer2-H239A behaved like cells expressing WT Aer2: cells tumbled in air (20.9% O_2) and had smooth-swimming behavior in N_2. In contrast, Aer2-H234A orchestrated tumbling in air like WT Aer2, but cells remained tumbling-biased in N_2 (~60% of cells tumbled in N_2 versus ~2% for WT Aer2). Aer2-H234A therefore has a signal-on bias (Fig. 25a). The partial response may reflect the ability of a small proportion of heme-retaining molecules to respond to O_2 changes.
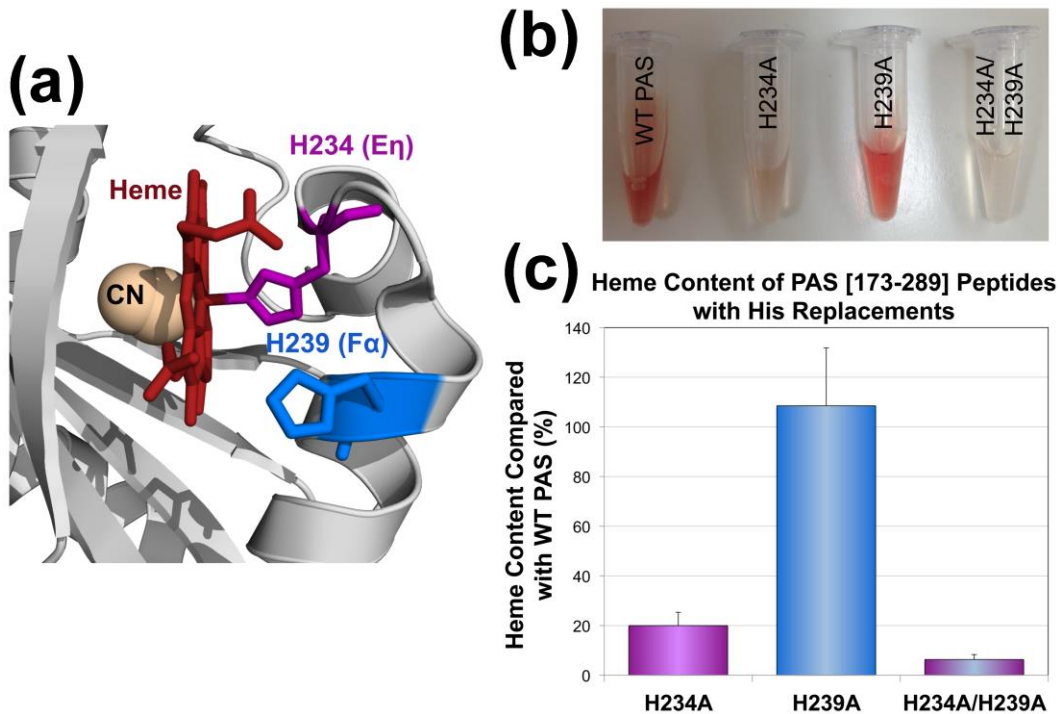
Figure 23. Heme coordination in the Aer2 PAS domain. (a) Location of the Eη (H234) and Fα His (H239) side chains in the cyanomet structure of the Aer2 PAS domain (Sawai *et al.*, 2012). Aer2-PAS structures indicate that the Eη His coordinates heme (Sawai *et al.*, 2012, Airola *et al.*, 2013a), whereas the Fα His coordinates heme in other PAS-heme proteins (Gilles-Gonzalez & Gonzalez, 2005, Kerby *et al.*, 2008). Both His residues are highly conserved in Aer2-PAS homologs (see Fig. S2). (b) Purified Aer2 PAS[173-289] peptides (imidazole bound, 2.6 to 4 mg ml^{-1}) showing less red color in Aer2-H234A and Aer2-H234A/H239A compared with WT Aer2 and Aer2-H239A. (c) Heme content of PAS peptides with Eη and Fα His replacements, given as a percentage of WT PAS heme content, corrected for peptide concentration (see Materials and Methods). Abbreviations: CN, cyanide; WT, wild-type.

When WT Aer2 is expressed in *E. coli*, cells respond to both O_2 and CO (Watts *et al.*, 2011b). To test for a CO response, *E. coli* BT3388 cells expressing Aer2 are monitored in CO temporal assays. In these assays, cells are perfused with N_2 (to remove O_2) until they resume smooth swimming, after which CO is perfused for 10 seconds. If the receptor can respond to CO, cells tumble, and continue to tumble for up to 30 sec after CO has been removed (Watts *et al.*, 2011b). To

determine if Aer2-H239A can respond to CO, cells expressing Aer2-H239A were perfused with CO under anaerobic conditions. Similar to WT Aer2, cells expressing Aer2-H239A responded to CO by tumbling, and the tumbling persisted for ~30 seconds after CO was removed. However, a CO response could not be determined for Aer2-H234A, because cells expressing Aer2-H234A tumbled too extensively in the absence of O_2.

PAS Structures Suggest a Possible Signaling Mechanism

Two PAS domain structures currently exist for Aer2, one with cyanide bound to ferric heme [cyanomet, Fe^{3+}-CN (Sawai *et al.*, 2012)], and another containing ferric heme without ligand [ferric heme, Fe^{3+} (Airola *et al.*, 2013a)]. The ligand-bound structure suggests that Aer2 stabilizes O_2 binding via a Trp residue on the PAS Iβ strand [W283, Fig. 23, (Sawai *et al.*, 2012)]. Moreover, an overlay of the two PAS structures suggests that both the Iβ Trp and an adjacent Leu residue on Hβ (L264) reorient in response to ligand binding. In the absence of ligand, the indole group of the Iβ Trp may rotate ~90°, whereas the adjacent Hβ Leu residue contracts towards the heme iron center to occupy the position where CN^- was bound [Fig. 23c, (Airola *et al.*, 2013a)]. To determine the importance of W283 and L264 for Aer2 sensing and signaling, we performed site-directed random mutagenesis on each residue and analyzed the effects on receptor function, heme binding and ligand binding.
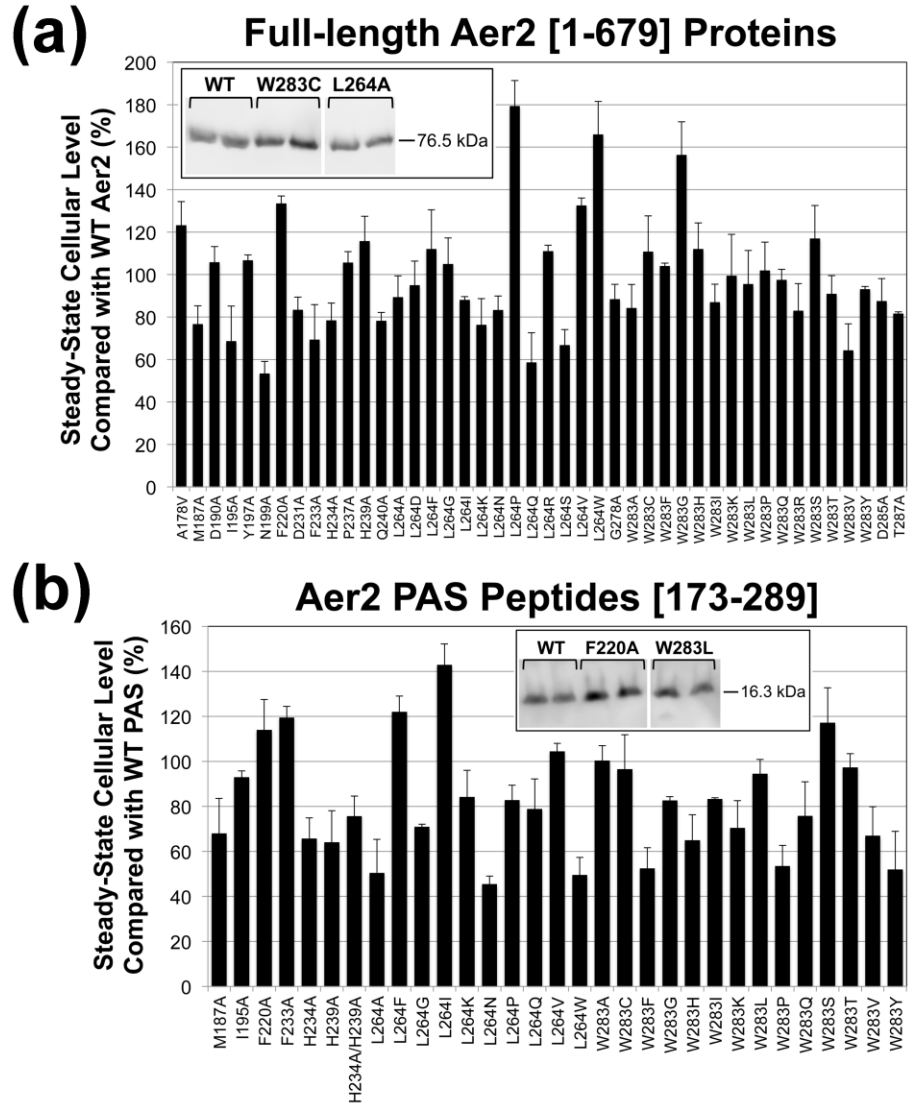
Figure 24. Steady-state cellular levels of full-length Aer2 proteins and PAS peptides in *E. coli*. (a) Steady-state levels of full-length Aer2 proteins compared with WT Aer2[1-679] in *E. coli* BT3388. Aer2 expression was induced with 50 µM IPTG and protein levels were determined from Western blots, an example of which is shown in the inset box. Lanes are from the same gel; intervening lanes are represented by white space. (b) Steady-state levels of PAS peptides compared with WT PAS[173-289] in *E. coli* BL21(DE3). Aer2 peptide expression was induced with 100 µM IPTG and protein levels were determined from Western blots (see the example in the inset box. Lanes are from the same gel; intervening lanes are represented by white space). Error bars represent the standard deviation from multiple experiments.
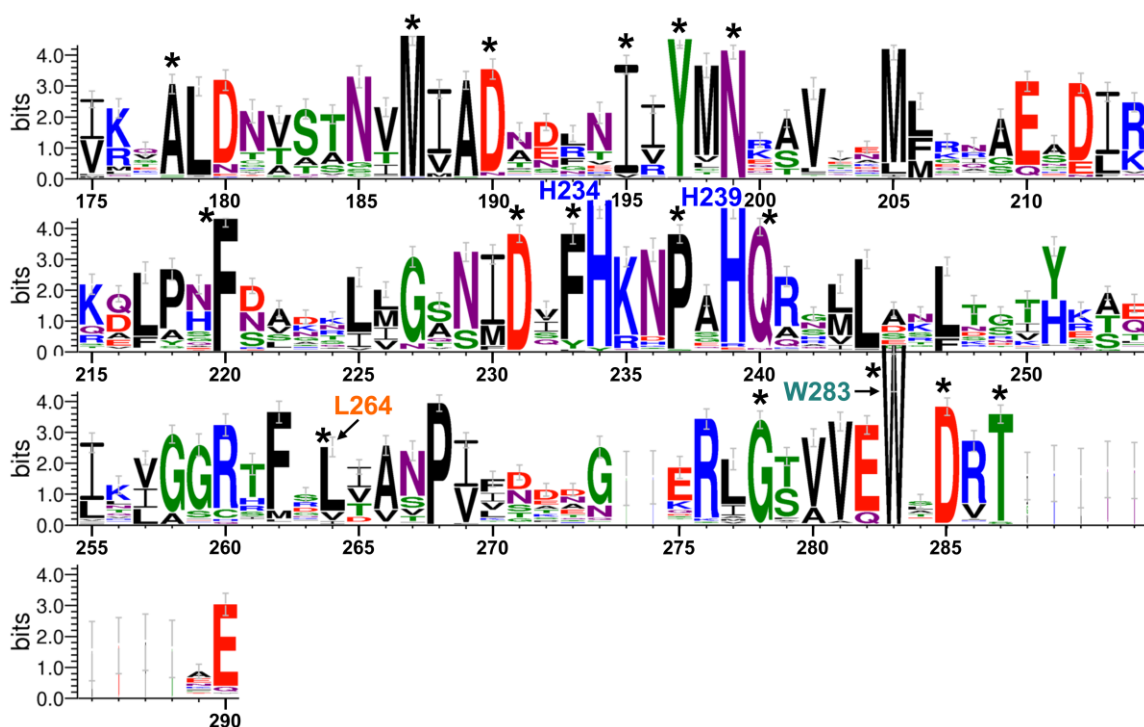
Figure S2. WebLogo sequence alignment of 100 Aer2 PAS domain-like sequences. Sequence homologs were acquired by performing an NCBI protein BLAST search (http://blast.ncbi.nlm.nih.gov/Blast.cgi?PAGE=Proteins) against *P. aeruginosa* PAO1 Aer2 residues 175-290, and the top 100 sequences were aligned to create a WebLogo (http://weblogo.berkeley.edu (Crooks *et al.*, 2004)). The overall height of each letter stack indicates the sequence conservation at that position (measured in bits), while the height of each letter within the stack indicates the relative frequency of each amino acid at that position. Error bars are provided at twice the height of sample correction for positions with limited sequence information. Asterisks indicate the 16 conserved residues that were selected for site-directed alanine mutagenesis.

The Iβ Trp is Important for Gas Binding and Signal Initiation

The PAS Iβ Trp is 100% conserved in 100 Aer2 PAS-like sequences (Fig. S2) and may be essential for stabilizing heme-O_2 binding. To determine the role of the Iβ Trp in *P. aeruginosa* Aer2, we performed site-directed random mutagenesis on the W283 codon in the construct that expresses full-length Aer2.

Expression was induced in *E. coli* BT3388 with 200 μM IPTG and individual

mutants were screened under the microscope for behavioral defects. Mutants

with non-WT behavior were sequenced to determine the amino acid substitution

at W283. After several rounds of mutagenesis and screening, 12 amino acid

changes were identified at W283 that altered behavior (Fig. 25a). W283H and

W283Y were not identified during the screen, but they were specifically

engineered since these amino acids stabilize O_2-binding in other heme proteins

(Podust *et al.*, 2008, Kloek *et al.*, 1994, Olson *et al.*, 1988). W283A was similarly

not identified during screening, but was created as part of the PAS alanine

mutagenesis described below. All 15 of the W283 mutant proteins were stably

expressed in *E. coli* BT3388 (Fig. 24a), but 12 of the receptors were signal-off

receptors that did not respond to the addition or removal of O_2 (Fig. 25a). Cells

expressing these receptors swam smoothly in both the presence and absence of

O_2, even after induction with 1 mM IPTG to produce high cellular levels of Aer2.

In contrast, cells expressing Aer2-W283F, L or I retained some functionality (Fig.

25a). Aer2-W283F and Aer2-W283L were signal-on biased mutants that

orchestrated tumbling in air like cells expressing WT Aer2, but when air was

removed, 50-80% of the cells continued to tumble (Fig. 25a). Cells expressing

Aer2-W283I had an inverted phenotype where ~50% of the cells tumbled in N_2,

but became smooth swimming after ~30 seconds in air. Heme-CO binding does

not require amino acid stabilization and should not require W283. However, only

two of the 15 W283 mutants, Aer2-W283I and Aer2-W283V, responded to CO

(Fig. 25a).Cells expressing these mutants tumbled when CO was added in either

N$_2$ or air. It was not possible to determine whether cells expressing Aer2-W283F or Aer2-W283L responded to CO, because cells expressing these mutants tumbled too extensively to determine a CO response.
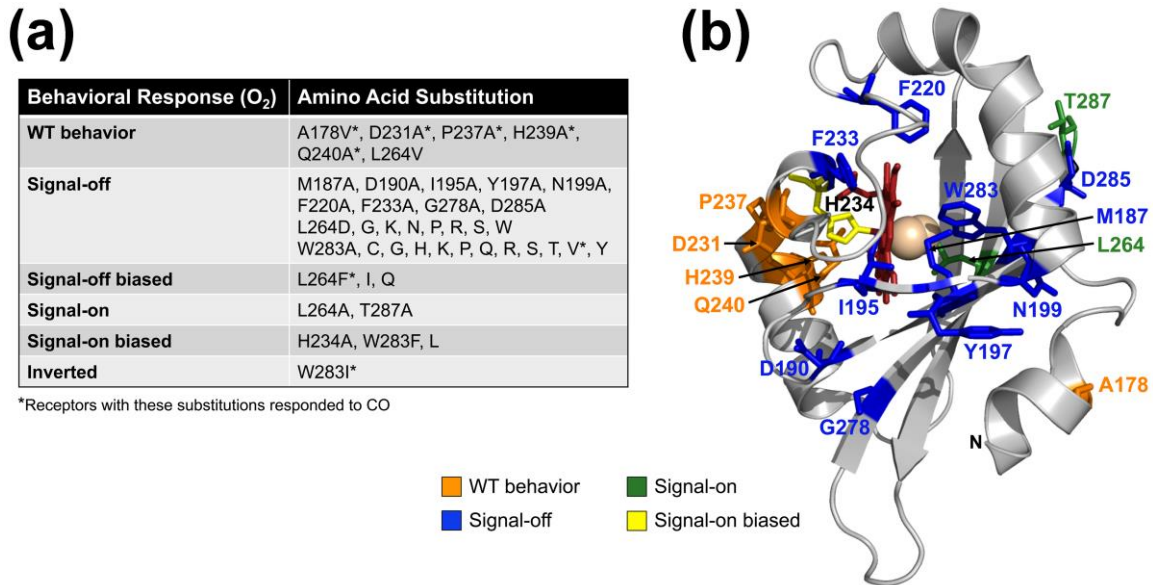
Figure 25. Aer2 mutant phenotypes in temporal assays. (a) Effects of amino acid substitutions on Aer2-mediated behavior in *E. coli* BT3388. Signal-off mutants exhibited random swimming behavior (~2% tumbling) in both air and N$_2$, whereas signal-on mutants tumbled constantly in both air and N$_2$. Neither signal-off nor signal-on mutants responded to the introduction or removal of O$_2$. Signal-off biased mutants responded to the introduction of O$_2$ but adapted, unlike WT Aer2 in BT3388, which remains signal-on in the presence of O$_2$. Signal-on biased mutants responded to the removal of O$_2$, but at least 50% of the cells continued to tumble in N$_2$. Residue substitutions marked by an asterisk resulted in receptors that could respond to CO, i.e., they directed cell tumbling in the presence of CO. CO responses could not be determined for signal-on biased and signal-on mutants. (b) Alanine mutants mapped onto the cyanomet structure of Aer2. Original side chains are shown as color-coded sticks based on the O$_2$ responses listed in Fig. 25a.

To determine the O$_2$ and CO binding affinities of W283 mutants, W283-encoding mutations were transferred into the Aer2-PAS expression construct,

Aer2[173-289], and the PAS peptides were purified on Ni-NTA agarose. W283

mutants that were analyzed included those that responded to O_2 or CO, and 11

of the signal-off mutants; these were compared with WT Aer2 (which was

determined to have an O_2 K_d of 16 μM, and a CO K_d of 2 μM; see Fig. S3 for WT

O_2 and CO titrations). Unexpectedly, PAS peptides for nine of the 11 W283

signal-off mutants exhibited very low heme content when purified (3-37.5% of WT

heme levels, Fig. 26a) and gas-binding affinities could not be determined. To test

whether these heme-binding defects were also present in full-length receptors,

we purified full-length Aer2-W283Y and Aer2-L264N (see below), both of which

had PAS peptides with heme-binding defects (Fig. 26a). Neither of the purified

full-length receptors showed heme binding (data not shown). The other signal-off

mutants, W283C and W283V, had sufficient heme content to analyze (Fig. 26a).

Aer2-W283C and Aer2-W283V did not respond to O_2 and did not bind it; during

O_2 titrations, both mutants exhibited met-heme spectra with rapid oxidation from

Fe(II) to Fe(III) heme (Fig. S3c; met-heme spectra were independently verified by

oxidizing proteins with potassium ferricyanide and comparing with the spectra

from O_2 titrations). However, both mutants bound CO with WT affinity, and Aer2-

W283V was able to respond to it (Figs. 25a and 26b). Of the three W283 mutants

that responded to O_2 in the behavioral assay (Aer2-W283F, L and I), only Aer2-

W283F appeared to bind O_2, and its O_2 affinity was similar to that of WT Aer2-

PAS (Fig. 26b). In contrast, Aer2-W283L and Aer2-W283I both responded to O_2,

but purified PAS peptides with these substitutions did not bind O_2 (Figs. 25 and

26b) and were rapidly oxidized from Fe(II) to Fe(III) heme. Sawai et al. similarly

reported that purified full-length Aer2-W283L does not bind O_2 (Sawai *et al.*,

2012).

PAS Peptide [173-289]	$O_2\ K_d$ (µM)	CO K_d (µM)
WT PAS	16	2
M187A	14	0.7
F220A	-	2
L264A	-	1
L264F	8	1
L264G	-	0.6
L264I	9	4
L264K	-	-
L264V	9	3
L264W	-	3
W283C	-	2
W283F	13	1
W283I	-	2
W283L	-	2
W283V	-	2
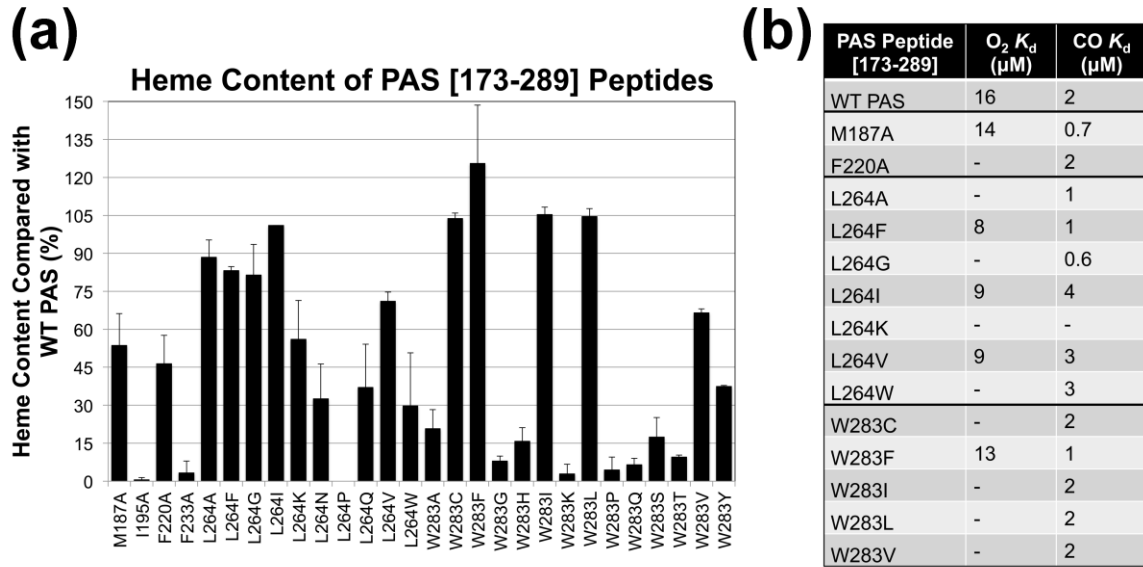
Fig. 26. PAS peptide heme content and gas binding affinities. (a) Heme content of PAS peptides with amino acid substitutions, given as a percentage of WT PAS heme content, corrected for peptide concentration (see Materials and Methods). Values below 40% indicate a substantial heme-binding defect. Aer2[173-289]-L264P contained no measureable heme. (b) PAS peptide O_2 and CO binding affinities. A dash (-) indicates that O_2- or CO-bound spectra were not observed, so binding affinities could not be determined.

It is possible that O_2 binding to these mutants is too transient to observe during in

vitro O_2 titrations, but sufficiently stable in vivo to generate a behavioral

response. All of the W283 mutants tested bound CO, and with similar affinities to

WT Aer2 (Fig. 26b), irrespective of whether the corresponding full-length

receptors responded to CO or not (Fig. 25). Overall, these data indicate that the

Iβ Trp is important for stable heme- and O_2-, but not CO-binding, and is important

for signal initiation in the Aer2 PAS domain.
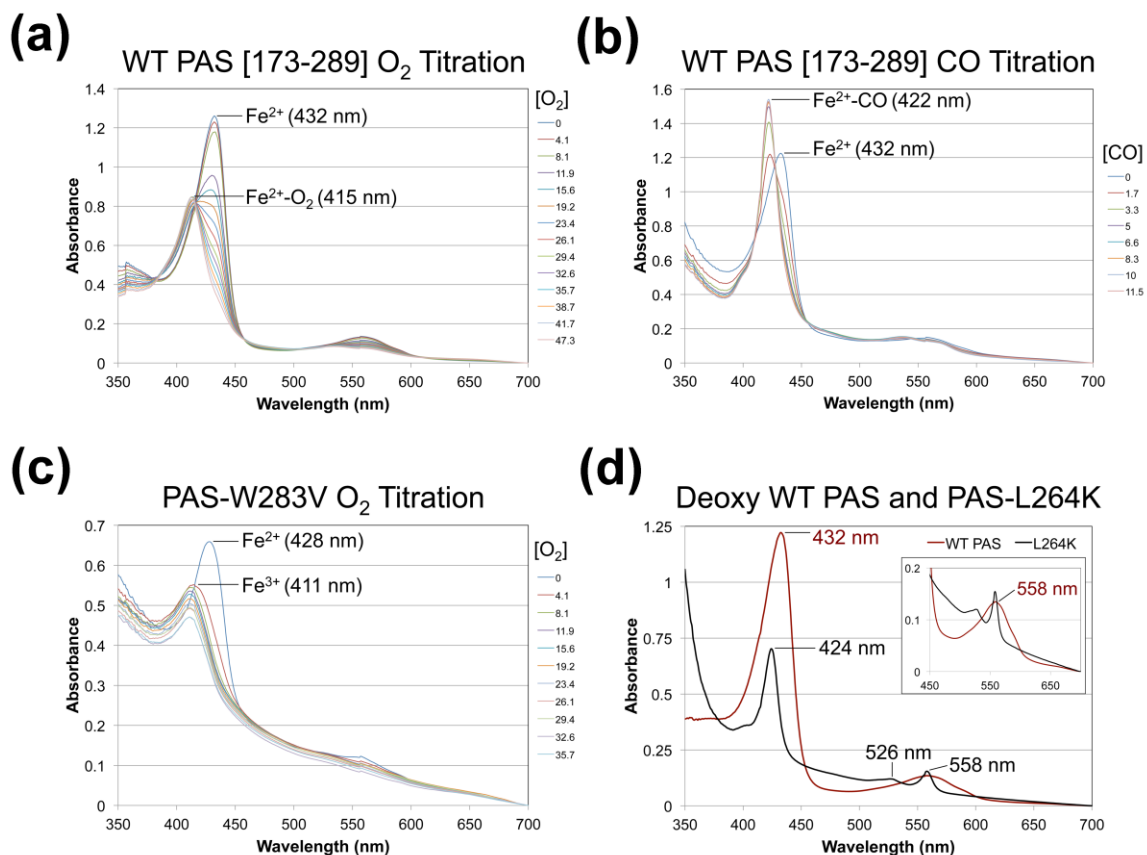
Figure S3. Examples of gas titrations using 10 μM purified Aer2[173-289] PAS peptides. (a-b) WT deoxy PAS peptide titrated with O_2 (a) and CO (b). (c) Deoxy PAS-W283V peptide titrated with O_2, showing rapid met-heme formation. The designation of met-heme instead of oxy-heme was verified spectrophotometrically after oxidizing PAS peptides with potassium ferricyanide and comparing the spectra. (d) Deoxy spectra of WT Aer2-PAS and Aer2-L264K. Aer2-L264K exhibits β and α bands (526 and 558 nm, respectively), which is indicative of hexa-coordinate heme, whereas WT Aer2 has a single broad band with a 558 nm maxima (see enlarged inset), which is indicative of penta-coordinate heme.

Substitutions at the Hβ Leu Alter Gas Binding and Signaling

Aer2 PAS structures suggest that the Hβ Leu residue, L264, may be involved in initiating PAS signaling (Airola *et al.*, 2013a). The L264 side chain appears to occupy the PAS ligand-binding site but swings out of the site when ligand binds [Fig. 22c, (Airola *et al.*, 2013a)]. The Hβ Leu is well conserved in

Aer2 PAS-like sequences, but other hydrophobic amino acids are also found at the same position, primarily Val and, to a lesser extent, Ile (Fig. S2). To determine if Aer2 can function with Val at 264, Aer2-L264V was engineered by site-directed mutagenesis. Full-length Aer2-L264V mediated an O_2 response, but exhibited a 30 second delayed smooth-swimming response in N_2, and did not respond to CO. Therefore, Aer2 can function with Val at 264, but the behavioral response is restricted to O_2. Notably, PAS-L264V bound O_2 and CO with affinities that were similar to WT (Fig. 26b).

To determine whether other replacements at L264 affect the O_2 response, we performed site-specific random mutagenesis on the L264 codon and screened for defective mutants as outlined for W283 above. L264A was not identified during the screen, but was created as part of the PAS alanine mutagenesis described below. After several rounds of mutagenesis and screening, 12 amino acid substitutions were identified at L264 that altered the O_2 response (Fig. 25a). All of these mutants were stably expressed in *E. coli* BT3388 (Fig. 24a). Eight of the mutants were non-functional, signal-off mutants (Fig. 25a), even after induction with 1 mM IPTG. In contrast, Aer2-L264A was locked signal-on, causing cells to tumble constantly in air and in N_2 (Fig. 25a). The remaining three mutants, Aer2-L264F, I and Q, were signal-off biased mutants that responded to O_2 (Fig. 25a; Ile shows some conservation at this position, see Fig. S2). Cells expressing Aer2-L264I and Aer2-L264Q had WT O_2 responses, whereas cells expressing Aer2-L264F had a reduced tumble response to O_2 (~60% of cells tumbled). However, all three mutants adapted to

114

O$_2$ (cells became less tumble-biased) over the course of several minutes. Only one of the L264 mutants, Aer2-L264F, tumbled in response to the addition of CO (Fig. 25a; this mutant also responded to O$_2$). A CO response could not be determined for Aer2-L264A because cells expressing this Aer2 variant tumbled constantly in the presence and absence of O$_2$.

To determine the O$_2$ and CO binding affinities of the L264 mutants, L264-encoding mutations were transferred to the Aer2 PAS peptide Aer2[173-289] and the peptides were purified on Ni-NTA agarose. L264 mutants that were analyzed included those that responded to O$_2$ or CO, the signal-on mutant Aer2-L264A, and five of the signal-off mutants; these were compared with WT Aer2-PAS (Fig. 26). Four of the mutants expressed PAS peptides that contained very low heme content when purified. This included three of the signal-off mutants, L264N, P and W, and one of the functional mutants, L264Q (0-37% of WT heme levels, Fig. 26a). Gas-binding affinities could not be determined for PAS-L264N, P and Q, but were determined for PAS-L264W, due to higher peptide purity. PAS-L264P showed no detectable heme spectra, even after scanning concentrated (135 μM) protein. There was no defect in the steady-state cellular expression level of PAS-L264P (Fig. 24b). Of the remaining L264 mutants, three bound O$_2$ and CO (L264F, I and V), three bound CO but not O$_2$ (L264A, G and W), and one bound neither gas (L264K) (Fig. 26b). The three L264 mutants that bound O$_2$ (L264F, I and V) also responded to it. In contrast, PAS-L264G, I, V, and W all bound CO, but did not respond to it. Of the L264 mutants that did not stably bind O$_2$, PAS-L264A and PAS-L264G were rapidly oxidized by O$_2$, and PAS-L264K

was slowly oxidized by O_2. In contrast, PAS-L264W showed no shift in its soret

maxima during O_2 titrations, suggesting the absence of heme-O_2 interactions.

This finding lends support to the hypothesis that L264 must move out of the

ligand-binding site to allow for O_2 binding. However, L264W still allowed CO-

binding, indicating that the CO-binding angle (perpendicular to the plane of the

heme) was permitted (Fig. 26b).

Of all the mutants in this study, the signal-off mutant, Aer2-L264K, was the

only mutant that did not bind either O_2 or CO. Moreover, the deoxy spectra of

PAS-L264K contained a β band and a prominent α band (Fig. S3d), suggesting

the formation of a hexa-coordinate heme. This would entail coordination to H234

on the proximal side of the heme, as well as coordination on the distal side, quite

possibly by the amino group of lysine [e.g., Lys can coordinate heme in place of

Met in cytochrome *c*-550 (Worrall *et al.*, 2005)]. This differs from WT deoxy-Aer2,

which contains penta-coordinate heme [Fig. S3d, (Watts *et al.*, 2011b)].

Aer2 Signaling is Disrupted by Alanine Replacements at Conserved Residues

To complement the mutagenesis experiments on W283 and L264, 16

residues that are highly conserved in Aer2 homologs (Fig. S2, marked by

asterisks), were selected for site-directed alanine mutagenesis (A178 was

instead substituted with Val). Conserved Gly residues that are structural

elements at turns were excluded. The results for L264A and W283A were

discussed above. Most of the mutants exhibited stable steady-state expression

levels in *E. coli* BT3388 (Fig. 24a). However, 10 of the 16 Ala mutants were

signal-off mutants and did not respond to either O_2 or CO (Fig. 25). This included

the four heme cleft mutants that were tested: M187A, I195A, F220A, and F233A.

In contrast, Aer2-A178V, Aer2-P237A, and Aer2-Q240A mediated WT responses

to both O_2 and CO (Fig. 25). Aer2-D231A similarly orchestrated WT-like

responses to O_2 and CO, but had a 30 second delayed smooth-swimming

response in N_2 after O_2 was removed. Overall, the Ala mutants that had WT or

signal-on biased behavior congregated on the Eη and Fα helices (Fig. 25b,

orange and yellow residues). Very few signal-on mutants were identified in this

study. Aer2-T287A, like Aer2-L264A, was a signal-on mutant that caused cells to

tumble constantly in both air and N_2. Because of this, a CO response could not

be determined for Aer2-T287A. L264 and T287 both reside on the PAS β-sheet,

which is the signal-output surface of the PAS domain (Airola *et al.*, 2013a,

Moglich *et al.*, 2009b).

To determine gas-binding affinities for the four heme-pocket mutants

(M187A, I195A, F220A, and F233A), relevant mutations were transferred to the

construct expressing Aer2[173-289] and the PAS peptides were purified. PAS

peptides with I195A and F233A had severe heme-binding defects (Fig. 26a),

even though neither of these mutants had steady-state expression defects (Fig.

24b). In contrast, PAS peptides with M187A and F220A both bound heme (Fig.

26a), and could bind CO (Fig. 26b), yet neither mutant responded to CO. Aer2-

F220A neither bound nor responded to O_2, whereas Aer2-M187A bound O_2 with

WT affinity, but was also rapidly oxidized by O_2 (Fig. 26A). Sawai et al. similarly

117

reported that full-length Aer2-M187A binds O_2 (Sawai *et al.*, 2012). Aer2-M187A was the only mutant in this study that bound, but did not respond, to O_2.

Signal-on Behavior is Independent of Aer2 Methylation

When WT Aer2 is expressed in *E. coli*, it does not adapt to O_2. This is because Aer2 is methylated by the *E. coli* methyltransferase, CheR, but it is not demethylated by the *E. coli* methylesterase, CheB (Watts *et al.*, 2011b). When WT Aer2 is expressed in an *E. coli* strain lacking CheR and CheB, Aer2 remains unmethylated and the cells have a low tumbling frequency [~5% of cells tumble in O_2, (Watts *et al.*, 2011b)]. Hence, robust signal-on behavior requires receptor methylation. In this study, two locked signal-on mutants (L264A and T287A) and three signal-on biased mutants (H234A, W283F and W283L) were identified. To determine if their phenotypes were dependent on receptor methylation, full-length receptors containing each of these amino acid substitutions were expressed in *E. coli* UU2610, which lacks all *E. coli* chemoreceptors, as well as CheR and CheB (Zhou *et al.*, 2011). In UU2610, the tumbling bias of Aer2-L264A decreased ~20% in both air and in N_2. However, the tumbling biases of the other four mutants were not diminished by the lack of receptor methylation in UU2610. This suggests that the signal-on biases of these receptors are primarily due to the amino acid changes in the PAS domain and not receptor methylation status.

Discussion

The Eη Histidine Coordinates Heme in the Aer2 PAS Domain

Crystal structures of the Aer2 PAS domain identify the Eη His (H234) as the proximal heme coordinating ligand (Sawai *et al.*, 2012, Airola *et al.*, 2013a). This differs from the PAS domains of *Rm*FixL, *Ec*DOS, *Acetobacter xylinium* PDEA-1 (*Ax*PDEA-1), and *Burkholderia xenovorans* RcoM, where, in each case, an Fα His residue coordinates *b*-type heme (Gilles-Gonzalez & Gonzalez, 2005, Kerby *et al.*, 2008). Although the Fα His is well conserved in Aer2-PAS homologs (Fig. S2), in *P. aeruginosa* Aer2 it resides ~10 Å from the heme Fe, in contrast to the Eη His, which lies ~2 Å away. In the current study, the Fα His substitution, H239A, did not affect PAS heme content or behavioral responses. In contrast, the Eη His substitution, H234A, imposed substantial heme-binding and behavioral defects (Fig. 23), confirming that it is the proximal coordinating His of Aer2. However, Aer2-H234A had a signal-on bias, unlike all other heme-binding mutants in this study, which were signal-off or signal-off biased. In addition, the 80% heme-loss in PAS-H234A is less than that observed for other PAS-heme domains when the proximal coordinating His is replaced. For example, His substitutions in RcoM result in <1% heme (Kerby *et al.*, 2008) and a His to Ala substitution in the Aer2 PAS-2 domain from *Vibrio cholerae* results in 2% heme (Watts *et al.,* unpublished). In Aer2-PAS, it is unclear how heme might be coordinated in the absence of H234, particularly since H239 lies at a more remote location at the entrance of the heme cleft. A dual PAS-H234A/H239A mutant had significantly less heme than PAS-H234A (Fig. 23), suggesting that

119

Fα-H239 might contribute to heme coordination in the absence Eη-H234. Alternatively, the dual His replacements might distort the heme pocket in a way that prevents heme retention. Heme might instead be retained by PAS-H234A through hydrophobic pocket interactions. Hydrophobic interactions are sufficient to bind *b*-type hemes in the YybY family proteins from *Bacillus* and *Geobacillus*, which have no natural proximal heme-coordinating residue in their PAS domains (Tan *et al.*, 2013, Rao *et al.*, 2011).

The Hydrophobic Heme Cleft is Critical for Stabilizing Heme Binding in Aer2

In Aer2-PAS, the heme cleft is a hydrophobic pocket in which the imidazole ring of H234 coordinates the heme-Fe, and H251 hydrogen-bonds to the heme-7-proprionate (Sawai *et al.*, 2012). In this study, replacing heme-coordinating H234 caused a substantial heme-binding defect (PAS-H234A retained 20% heme, Fig. 23). However, other amino acid substitutions in both the proximal (I195A and F233A) and distal (L264N, P, Q and W; W283A, G, H, K, P, Q, S, T and Y) heme cleft likewise caused substantial heme-binding defects (0-37.5% of WT heme content, Fig. 26a). Remarkably, some of these defects were greater than that caused by H234A. This suggests that hydrophobic heme cleft interactions are critical for stabilizing heme binding in Aer2. On the proximal side of the cleft, I195 and F233 both reside ~4Å from, and parallel to, the heme; the severe defects caused by Ala substitutions at these residues (0.6-3% heme content) shows that moderate perturbations in the PAS heme pocket can alter

heme binding. Moreover, perturbations in O_2-stabilizing and signaling residues, W283 and L264, also affected heme binding. In *Bradyrhizobium japonicum* FixL, replacing the distal O_2-stabilizing Arg residue with Ala relaxes heme-protein coupling (Dunham *et al.*, 2003); a similar event could be responsible for heme-loss in PAS-W283 mutants.

Oxygen is the Native Ligand of the Aer2 PAS Domain

In the absence of imidazole, *P. aeruginosa* Aer2 purifies in the oxy-bound state (Sawai *et al.*, 2012). However, Aer can signal in response to the binding of O_2, CO and NO (Watts *et al.*, 2011b). This is atypical for heme sensors; they often bind all three gases, but typically respond to only one. For example, the histidine kinase FixL is inhibited by O_2, but not by CO or NO, even though it binds these two more tightly (Gilles-Gonzalez *et al.*, 2008). Protohemes generally bind O_2, CO and NO with relative affinities of $1:10^3:10^6$ (Tsai *et al.*, 2012a, Tsai *et al.*, 2012b). In this study, we determined that the O_2 and CO affinities of the isolated Aer2 PAS domain are 16 μM and 2 μM, respectively (Fig. 26b). The O_2 affinity of Aer2-PAS is comparable with the O_2 affinities of the PAS-heme O_2 sensors *Ec*DOS (13 μM), *Ax*PDEA-1 (~10 μM), and *Rm*FixL (31 μM) (Delgado-Nixon *et al.*, 2000a, Gilles-Gonzalez & Gonzalez, 2005). In the DOS, PDEA-1 and FixL PAS domains, a Gβ Arg residue interacts directly with bound O_2: substitutions at this residue substantially lower O_2 but not CO affinities and affect O_2-regulated behavior (Tanaka *et al.*, 2007, Dunham *et al.*, 2003). In Aer2, substitutions at the Iβ Trp likewise prevented O_2 but not CO binding (Fig. 29b, W283C, I, L and V).

Because changes in highly conserved residues predominately affect O_2 binding properties and responses, these data suggest that O_2 is the native ligand of the Aer2 PAS domain. We did not test NO binding in this study. However, unlike Aer2, heme-NO sensors usually exclude O_2-binding; e.g., H-NOX (Heme-Nitric oxide/OXygen) proteins that lack hydrogen-bond donors bind NO instead of O_2 (Karow *et al.*, 2004, Kosowicz & Boon, 2013), the PAS-heme domain of YybY is rapidly oxidized by O_2 (Rao *et al.*, 2011), and nitrophorins exclude O_2 by maintaining their heme in the Fe(III) state (Jain & Chan, 2003).

The Role of Aer2 PAS Residues in Ligand Binding and Signal Transduction

The data from this study indicate that the Iβ Trp, W283, stabilizes O_2 binding to the Aer2 PAS-heme domain. Twelve of 15 W283 mutants, including those with amino acids that commonly stabilize O_2 binding to other heme proteins [His, Tyr and Arg, (Martinkova *et al.*, 2013)], resulted in signal-off Aer2 receptors that did not respond to O_2. For W283 mutants that did not stably bind O_2 in vitro (W283C, I, L and V), the heme cofactor was rapidly oxidized upon exposure to O_2 (see Fig. S3c). This has similarly been observed for *Ec*DOS Gβ Arg mutants (Tanaka *et al.*, 2007). Our data also indicate that W283 is critical for initiating conformational signaling from the PAS domain. This is perhaps not surprising given that the PAS Iβ strand connects directly to the C-terminal HAMP 4 domain, and W283 resides close to the PAS "DxT" motif, which has been proposed to be involved in conformational signaling (Airola *et al.*, 2013a, Moglich *et al.*, 2009b). None of the 15 W283 mutants in this study retained WT function

(Fig. 25a) and PAS-W283F was the only Trp mutant that preserved a WT O_2 affinity (Fig. 26b). The side chain of Phe is similar in size to the nitrogen-containing Trp pyrrole ring that is predicted to hydrogen-bond with heme-bound O_2. However, Phe lacks a hydrogen-bonding moiety. One possibility is that O_2 binding is supported by a solvent molecule in the distal pocket that acts as a hydrogen bond donor; this scenario was observed in a DevS mutant from *Mycobacterium tuberculosis* when the O_2-stabilizing Tyr residue was replaced with Phe (Yukl *et al.*, 2008). In this study, Aer2-W283F retained partial functionality (as a signal-on biased mutant), but Aer2 is clearly fine-tuned to use Trp for O_2 binding and signal initiation.

The hypothesis that the Hβ Leu, L264, moves out of the ligand-binding site when O_2 binds to heme [Fig 22c, (Airola *et al.*, 2013a)], was supported by the results of this study. Notably, the bulky Trp substitution, L264W, appeared to block O_2 binding, and L264K formed a hexa-coordinate heme that did not bind O_2. However, the Hβ Leu itself was not specifically required for function: Aer2-L264F and Aer2-L264Q retained some functionality, and L264 substitutions that occur in other Aer2 PAS-like homologs, Val and Ile (Fig. S2), resulted in Aer2 receptors that bound and responded to O_2 (Figs. 25 and 26). Interestingly, smaller hydrophobic replacements, L264A and L264G, resulted in non-responsive Aer2 receptors that did not bind O_2, and furthermore, were rapidly oxidized by it. This suggests that, i) the size of the amino acid at the Hβ Leu is important, and ii) Hβ Leu may be choreographed to move concomitantly with the Iβ Trp so that Trp can rotate into place and bond with O_2 (see Fig. 22c). Notably,

O_2 binding alone was not sufficient for PAS signaling. Aer2-M187A bound O_2 but was unable to respond to it. M187 resides on the Aβ strand, adjacent to W283 on Iβ, but it does not exhibit a significant conformational shift between the cyanomet and ferric PAS-heme structures. Still, the distortion caused by the Ala replacement at residue 187 could feasibly block PAS β-sheet signaling rearrangements that are required for downstream signaling.

Like Aer2-M187A, most of the mutants in this study were signal-off mutants that did not respond to O_2 or CO (Fig. 25a). The amino acid changes in these mutants most likely disengage PAS control of the downstream HAMP 4-5 unit so that HAMP 4-5 continues to inhibit the activity of the kinase control module. D285A specifically disrupts the conserved "DxT" motif that has a proposed role in conformational signaling between the PAS and C-terminal HAMP domains (Airola *et al.*, 2013a, Moglich *et al.*, 2009b). In Aer2-N199A, the Ala substitution could also disrupt interactions between the PAS N-terminal cap (N-cap, Aα′ helix, Fig. 22b) and the PAS core (Cα helix); these interactions are required for both structural stability (Fig. 24a, N199A was the least stable receptor in this study) and for N-cap reorientation during signaling (Key *et al.*, 2007, Airola *et al.*, 2013a).

All of the PAS peptides tested in this study (with the exception of PAS-L264K) bound CO with an affinity that was the same as the WT peptide or better (M187A and L264G bound CO in the nanomolar range, Fig. 26b). This is not surprising since heme-CO binding does not require amino acid stabilization due to its high inherent affinity for heme (Tsai *et al.*, 2012a). However, heme-CO

124

binding did not predict function. Mutants that responded to CO bound it with WT affinity (W283I and V, and L264F), but so did many of the mutants that did not respond to CO (Figs. 25 and 26). In these latter instances, CO binding apparently could not induce the conformational changes required for signal transduction.

These studies provide insight into the mechanisms used by the Aer2 PAS domain to regulate heme-binding, ligand-binding, and initiate conformational signaling. The results support the model based on differences between the cyanomet and ferric PAS-heme structures, corroborating the roles of W283 and L264 in O_2-stabilization and PAS signaling [Fig. 22, (Airola *et al.*, 2013a)]. When O_2 binds to Aer2-PAS, it generates a conformational signal that is transmitted via the PAS Iβ strand to modulate the activity of the C-terminal HAMP and kinase control domains. Future studies will test an expanded model whereby O_2-mediated signaling evokes a PAS dimer-to-monomer transition (Airola *et al.*, 2013a), resulting in the signal-off conformation of HAMP 4, the signal-on conformation of HAMP 5 (Airola *et al.*, 2013c), and de-inhibition of the kinase control module (Watts *et al.*, 2011b).

Materials and Methods

Bacterial Plasmids and Strains

Full-length *P. aeruginosa* PAO1 Aer2[1-679] (PA0176) was expressed from pLH1, a pProEX-derived plasmid that expresses Aer2 with an N-terminal His$_6$ tag (Watts *et al.*, 2011b). The Aer2 PAS domain, Aer2[173-289], was likewise expressed from pProEX with an N-terminal His$_6$ tag (Watts *et al.*,

2011b). Full-length Aer2 was expressed in chemoreceptorless *E. coli* strains

BT3388 [*tar*, *tsr*, *trg*, *tap*, *aer* (Yu *et al.*, 2002)] and UU2610 [*tar*, *tsr*, *trg*, *tap*, *aer*,

cheR, *cheB* (Zhou *et al.*, 2011)]. UU2610 also lacks the *E. coli* adaptation

enzymes CheR and CheB. Aer2 PAS peptides were expressed in *E. coli*

BL21(DE3).

Mutagenesis and Cloning

Site-directed mutagenesis was performed on pLH1 using site-specific

primers and *PfuUltra* II Fusion DNA polymerase (Agilent Technologies, Santa

Clara, CA). To replace native codons with Ala or Val codons, 30 amplification

cycles were performed with an annealing temperature of 55 °C. For site-directed

random mutagenesis, primers containing an equimolar mix of all four nucleotides

at the L264 or W283 codons were used; however, the amplification conditions

above consistently created DNA insertions following the primer site. To solve this

problem, we tested stepwise annealing temperatures from 55 °C to 68 °C and

analyzed the constructs created. The lowest proportion of DNA inserts occurred

when 68 °C was used as the annealing temperature and 20 amplification cycles

were performed. These conditions yielded no obvious bias for codon

replacements with one, two or three nucleotide changes and were subsequently

used to create most of the site-specific random mutants identified in this study.

Site-specific mutagenesis products were treated with DpnI (New England

Biolabs, Ipswich, MA) to remove template strands and then electroporated into *E.

coli*. Aer2 expression was induced with 600 μM IPTG and products of the correct

size were confirmed by Western blotting with HisProbe™-HRP (Thermo Scientific, Rockford, IL). All mutations were confirmed by sequencing the entire coding sequence of *aer2*.

To create Aer2-PAS peptides expressing specific amino acid changes in the PAS domain, the PAS coding region (residues 173-289) was PCR-amplified from pLH1-derived plasmids using *PfuUltra* II Fusion DNA polymerase. PCR products were ligated into the NcoI and SalI sites of pProEX. Peptide expression and DNA sequencing was performed as described above.

Steady-State Cellular Aer2 Levels

The steady-state cellular levels of the full-length Aer2 mutants were compared with that of WT Aer2 after inducing BT3388 cells with 50 μM IPTG. In contrast, the cellular levels of the PAS peptides were compared with that of WT Aer2[173-289] after inducing BL21(DE3) cells with 100 μM IPTG. Samples were electrophoresed in duplicate and experiments were repeated on two-four separate days. Bands were visualized on HisProbe Western blots and quantified on a BioSpectrum® digital imager (UVP, Upland, CA).

Behavioral Assays

BT3388 cells were grown at 30 °C in tryptone broth containing 0.5 μg ml^{-1} thiamine and induced with 200 μM IPTG. At this induction level, the number of Aer2 receptors in *E. coli* is comparable with the total number of chemoreceptors in WT *E. coli* cells (Watts *et al.*, 2011b). Cells were placed into a gas perfusion

chamber where the gas was toggled between air (20.9% O_2) and N_2, and cell behavior was analyzed (Rebbapragada *et al.*, 1997a, Taylor *et al.*, 2007). Mutants that were signal-off (smooth swimming in air and in N_2) were retested after induction with 1 mM IPTG to produce higher cellular levels of Aer2. Behavioral responses to O_2 were repeated two or more times on at least two separate days. To determine CO responses, BT3388 cells (induced with 200 µM IPTG) were perfused with N_2 for 30 sec prior to perfusing with CO gas (>99% purity, Sigma-Aldrich, St. Louis, MO), which was added through the open end of the chamber for 10 sec. For Aer2-W283I and Aer2-W283V, CO responses were also tested while air was being perfused.

Protein Purification

WT Aer2[173-289]/BL21(DE3) and relevant mutants were grown in LB broth, Lennox, containing 25 µg ml^{-1} 5-aminolevulinic acid (Sigma-Aldrich) to enhance heme synthesis and incorporation. After 3-5 hours of induction with 600 µM IPTG, cells were centrifuged at 10,000 x *g* for 15 minutes and resuspended to 1% of their original volume in lysis buffer (50 mM Tris, pH 7.5, 500 mM NaCl and 10 mM imidazole) containing 0.3 mg ml^{-1} lysozyme, 1 µg ml^{-1} DNase I and 100 µl of Protease Inhibitor Cocktail for His-tagged proteins (Sigma-Aldrich). The cells were lysed by freeze-thawing five times, followed by sonication. Soluble protein was acquired by removing cellular debris at low speed (10,000 x *g* for 20 min) and the membrane fraction at high speed (485,000 x *g* for 1 h). The high-speed supernatant was applied to a Ni-NTA agarose column (Qiagen, Valencia,

128

CA) and allowed to empty by gravity flow. The column was washed with 10 column volumes of wash buffer 1 (50 mM Tris, pH 7.5, 500 mM NaCl and 20 mM imidazole), followed by 8-10 column volumes of wash buffer 2 (50 mM Tris, pH 7.5, 500 mM NaCl and 50 mM imidazole). Aer2 peptides were eluted by adding 1 ml of elution buffer (50 mM Tris, pH 7.5, 500 mM NaCl and 250 mM imidazole) to the column, but only the red colored fraction was collected. For proteins with no obvious red color, two ~0.4 ml elution fractions were collected. Aer2 peptides were usually most concentrated in the second eluted fraction. The concentration of eluted protein was determined using a BCA™ Protein Assay (Thermo Scientific) and the quality of the sample was determined by staining SDS-PAGE gels with Coomassie Brilliant Blue.

Heme Binding

The proportion of heme bound to the WT Aer2[173-289] PAS domain was determined using a pyridine hemochrome assay [(Appleby & Bergersen, 1980), with modifications communicated by M. Gilles-Gonzalez]. Briefly, WT PAS peptide and hemin standards (10 to 50 μM) were added to an alkaline pyridine solution and scanned from 350 to 700 nm under both dithionite-reduced and ferricyanide-oxidized conditions. Heme concentrations were determined from the reduced minus oxidized spectra, using an extinction coefficient of 23.4 mM^{-1}cm^{-1} for the absorbance difference of $A_{556nm(red)}$ minus $A_{539nm(ox)}$. The heme content determined from the pyridine hemochrome assay was used to standardize PAS-heme concentrations used in ligand-binding assays.

To determine whether purified PAS peptides had heme-binding defects, 10 µM imidazole-bound PAS peptides were scanned from 300 nm to 700 nm in a BioMate™ 3S spectrophotometer (Thermo Scientific). Samples were overlaid by zeroing at 700 nm and the maximum absorbance of each soret peak was determined. Maximum soret absorbances were divided by the maximum soret absorbance of the WT PAS peptide. Peptide concentrations were determined by electrophoresing 2.5 µg of each purified protein in duplicate on SDS-PAGE as outlined above, staining gels with Coomassie Brilliant Blue and quantifying the density of each PAS peptide on a BioSpectrum® digital imager. The average density of each PAS peptide was divided by the average density of the WT PAS peptide (which itself was usually 85-90% pure). The heme-content/peptide ratio was then calculated for each mutant and averaged from multiple purifications. Ratios below 40% indicated a substantial heme-binding defect from which gas affinity constants were generally not determined.

Gas Binding Affinities

Deoxy-heme was created by adding 0.5 mM dithionite to 4-10 µM anaerobic PAS-heme in an anaerobic hood (Coy Laboratory Products, Grass Lake, MI). Deoxy-PAS was added to a quartz septum-sealed cuvette (Starna Cells, Atascadero, CA) and used directly for CO-binding. For O_2 affinities, sufficient O_2 was added to the cuvette to oxidize the dithionite (as determined spectrophotometrically). To create gas-saturated buffers, buffer (50 mM Tris, pH 8.0, 50 mM KCl and 5% v/v ethylene glycol) was perfused with either CO (Sigma-

Aldrich) or air. To create 50% CO-saturated buffer, a volume of N_2-saturated buffer was added to an equal volume of CO-saturated buffer in a Reacti-Vial™ (Thermo Scientific) and used immediately. Gas solutions were transferred to gas-tight Hamilton syringes (Hamilton, Reno, NV) and titrated into the deoxy protein solution. Stepwise spectra were recorded on a Beckman DU® 650 spectrophotometer (Beckman Coulter, Brea, CA) after each addition of buffer. The amount of bound gas was estimated from the UV/Vis spectrum by linear interpolation of the unliganded (Fe^{2+}) and liganded (Fe^{2+}-O_2, Fe^{2+}-CO) spectra. For WT PAS and most of the PAS mutants, the soret maxima occurred at 428-432 nm for deoxy heme, 414-416 nm for oxy heme, and 421-422 nm for carbonmonoxy heme. After O_2 titrations were complete, CO was perfused directly into the cuvette to differentiate O_2-bound protein from met-heme protein. O_2-bound or ferrous protein, but not ferric protein, showed CO-bound spectra after the addition of CO.

Met-Heme Absorption Spectra

To create met-heme, 50 µM purified PAS peptide was oxidized with 50 µM potassium ferricyanide at room temperature for 15 min. To evaluate met-heme spectra, samples were purified on a Micro Bio-Spin® column (Bio-Rad, Hercules, CA) and scanned spectrophotometrically.

Acknowledgements

References

Kato J, Kim HE, Takiguchi N, Kuroda A, Ohtake H. 2008. *Pseudomonas aeruginosa* as a model microorganism for investigation of chemotactic behaviors in ecosystem. J Biosci Bioeng 106:1-7.

Sampedro I, Parales RE, Krell T, Hill JE. 2014. Pseudomonas chemotaxis. FEMS Microbiol Rev.

Hong CS, Shitashiro M, Kuroda A, Ikeda T, Takiguchi N, Ohtake H, Kato J. 2004. Chemotaxis proteins and transducers for aerotaxis in *Pseudomonas aeruginosa*. FEMS Microbiol Lett 231:247-252.

Watts KJ, Taylor BL, Johnson MS. 2011. PAS/poly-HAMP signalling in Aer-2, a soluble haem-based sensor. Mol Microbiol 79:686-699.

Guvener ZT, Tifrea DF, Harwood CS. 2006. Two different *Pseudomonas aeruginosa* chemosensory signal transduction complexes localize to cell poles and form and remould in stationary phase. Mol Microbiol 61:106-118.

Biswas M, Dey S, Khamrui S, Sen U, Dasgupta J. 2013. Conformational barrier of CheY3 and inability of CheY4 to bind FliM control the flagellar motor action in Vibrio cholerae. PLoS One 8:e73923.

Hyakutake A, Homma M, Austin MJ, Boin MA, Hase CC, Kawagishi I. 2005. Only one of the five CheY homologs in *Vibrio cholerae* directly switches flagellar rotation. J Bacteriol 187:8403-8410.

Dasgupta J, Dattagupta JK. 2008. Structural determinants of *V. cholerae* CheYs that discriminate them in FliM binding: comparative modeling and MD simulation studies. J Biomol Struct Dyn 25:495-503.

Garvis S, Munder A, Ball G, de Bentzmann S, Wiehlmann L, Ewbank JJ, Tummler B, Filloux A. 2009. *Caenorhabditis elegans* semi-automated liquid screen reveals a specialized role for the chemotaxis gene cheB2 in *Pseudomonas aeruginosa* virulence. PLoS Pathog 5:e1000540.

Schuster M, Hawkins AC, Harwood CS, Greenberg EP. 2004. The *Pseudomonas aeruginosa* RpoS regulon and its relationship to quorum sensing. Mol Microbiol 51:973-985.

Garcia-Fontana C, Corral Lugo A, Krell T. 2014. Specificity of the CheR2 methyltransferase in *Pseudomonas aeruginosa* is directed by a C-terminal pentapeptide in the McpB chemoreceptor. Sci Signal 7:ra34.

Moglich A, Ayers RA, Moffat K. 2009. Structure and signaling mechanism of Per-ARNT-Sim domains. Structure 17:1282-1294.

Sawai H, Sugimoto H, Shiro Y, Ishikawa H, Mizutani Y, Aono S. 2012. Structural basis for oxygen sensing and signal transduction of the heme-based sensor protein Aer2 from *Pseudomonas aeruginosa*. Chem Commun (Camb) 48:6523-6525.

Airola MV, Huh D, Sukomon N, Widom J, Sircar R, Borbat PP, Freed JH, Watts KJ, Crane BR. 2013. Architecture of the soluble receptor Aer2 indicates an in-line mechanism for PAS and HAMP domain signaling. J Mol Biol 425:886-901.

Gilles-Gonzalez MA, Gonzalez G. 2005. Heme-based sensors: defining characteristics, recent developments, and regulatory hypotheses. J Inorg Biochem 99:1-22.

Dunin-Horkawicz S, Lupas AN. 2010. Comprehensive analysis of HAMP domains: Implications for transmembrane signal transduction. J Mol Biol 397:1156-1174.

Garcia D, Watts KJ, Johnson MS, Taylor BL. 2016. Delineating PAS-HAMP interaction surfaces and signalling-associated changes in the aerotaxis receptor Aer. Mol Microbiol 100:156-172.

Airola MV, Sukomon N, Samanta D, Borbat PP, Freed JH, Watts KJ, Crane BR. 2013. HAMP domain conformers that propagate opposite signals in bacterial chemoreceptors. PLoS Biology 11:e1001479.

Airola MV, Watts KJ, Bilwes AM, Crane BR. 2010. Structure of concatenated HAMP domains provides a mechanism for signal transduction. Structure 18:436-448.

Kerby RL, Youn H, Roberts GP. 2008. RcoM: a new single-component transcriptional regulator of CO metabolism in bacteria. J Bacteriol 190:3336-3343.

Podust LM, Ioanoviciu A, Ortiz de Montellano PR. 2008. 2.3 A X-ray structure of the heme-bound GAF domain of sensory histidine kinase DosT of *Mycobacterium tuberculosis*. Biochemistry 47:12523-12531.

Kloek AP, Yang J, Mathews FS, Frieden C, Goldberg DE. 1994. The tyrosine B10 hydroxyl is crucial for oxygen avidity of Ascaris hemoglobin. J Biol Chem 269:2377-2379.

Olson JS, Mathews AJ, Rohlfs RJ, Springer BA, Egeberg KD, Sligar SG, Tame J, Renaud JP, Nagai K. 1988. The role of the distal histidine in myoglobin and haemoglobin. Nature 336:265-266.

Worrall JA, van Roon AM, Ubbink M, Canters GW. 2005. The effect of replacing the axial methionine ligand with a lysine residue in cytochrome c-550 from *Paracoccus versutus* assessed by X-ray crystallography and unfolding. FEBS J 272:2441-2455.

Zhou Q, Ames P, Parkinson JS. 2011. Biphasic control logic of HAMP domain signalling in the *Escherichia coli* serine chemoreceptor. Mol Microbiol 80:596-611.

Tan E, Rao F, Pasunooti S, Pham TH, Soehano I, Turner MS, Liew CW, Lescar J, Pervushin K, Liang ZX. 2013. Solution structure of the PAS domain of a thermophilic YybT protein homolog reveals a potential ligand-binding site. J Biol Chem 288:11949-11959.

Rao F, Ji Q, Soehano I, Liang ZX. 2011. Unusual heme-binding PAS domain from YybT family proteins. J Bacteriol 193:1543-1551.

Dunham CM, Dioum EM, Tuckerman JR, Gonzalez G, Scott WG, Gilles-Gonzalez MA. 2003. A distal arginine in oxygen-sensing heme-PAS domains is essential to ligand binding, signal transduction, and structure. Biochemistry 42:7701-7708.

Gilles-Gonzalez MA, Gonzalez G, Sousa EH, Tuckerman J. 2008. Oxygen-sensing histidine-protein kinases: assays of ligand binding and turnover of response-regulator substrates. Methods Enzymol 437:173-189.

Tsai AL, Berka V, Martin E, Olson JS. 2012. A "sliding scale rule" for selectivity among NO, CO, and O(2) by heme protein sensors. Biochemistry 51:172-186.

Tsai AL, Martin E, Berka V, Olson JS. 2012. How do heme-protein sensors exclude oxygen? Lessons learned from cytochrome c', *Nostoc puntiforme* heme nitric oxide/oxygen-binding domain, and soluble guanylyl cyclase. Antioxid Redox Signal 17:1246-1263.

Delgado-Nixon VM, Gonzalez G, Gilles-Gonzalez MA. 2000. DOS, a heme-binding PAS protein from *Escherichia coli*, is a direct oxygen sensor. Biochemistry 39:2685-2691.

Tanaka A, Takahashi H, Shimizu T. 2007. Critical role of the heme axial ligand, Met95, in locking catalysis of the phosphodiesterase from *Escherichia coli* (Ec DOS) toward cyclic diGMP. J Biol Chem 282:21301-21307.

Karow DS, Pan D, Tran R, Pellicena P, Presley A, Mathies RA, Marletta MA. 2004. Spectroscopic characterization of the soluble guanylate cyclase-like heme domains from *Vibrio cholerae* and *Thermoanaerobacter tengcongensis*. Biochemistry 43:10203-10211.

Kosowicz JG, Boon EM. 2013. Insights into the distal heme pocket of H-NOX using fluoride as a probe for H-bonding interactions. J Inorg Biochem 126:91-95.

Jain R, Chan MK. 2003. Mechanisms of ligand discrimination by heme proteins. J Biol Inorg Chem 8:1-11.

Martinkova M, Kitanishi K, Shimizu T. 2013. Heme-based globin-coupled oxygen sensors: linking oxygen binding to functional regulation of diguanylate cyclase, histidine kinase, and methyl-accepting chemotaxis. J Biol Chem 288:27702-27711.

Yukl ET, Ioanoviciu A, Nakano MM, de Montellano PR, Moenne-Loccoz P. 2008. A distal tyrosine residue is required for ligand discrimination in DevS from *Mycobacterium tuberculosis*. Biochemistry 47:12532-12539.

Key J, Hefti M, Purcell EB, Moffat K. 2007. Structure of the redox sensor domain of *Azotobacter vinelandii* NifL at atomic resolution: signaling, dimerization, and mechanism. Biochemistry 46:3614-3623.

Yu HS, Saw JH, Hou S, Larsen RW, Watts KJ, Johnson MS, Zimmer MA, Ordal GW, Taylor BL, Alam M. 2002. Aerotactic responses in bacteria to photoreleased oxygen. FEMS Microbiol Lett 217:237-242.

Rebbapragada A, Johnson MS, Harding GP, Zuccarelli AJ, Fletcher HM, Zhulin IB, Taylor BL. 1997. The Aer protein and the serine chemoreceptor Tsr independently sense intracellular energy levels and transduce oxygen, redox, and energy signals for *Escherichia coli* behavior. Proc Natl Acad Sci U S A 94:10541-10546.

Taylor BL, Watts KJ, Johnson MS. 2007. Oxygen and redox sensing by two-component systems that regulate behavioral responses: behavioral assays and structural studies of Aer using in vivo disulfide cross-linking. Methods Enzymol 422:190-232.

Appleby CA, Bergersen FJ. 1980. Preparation and experimental use of leghaemoglobin. J. Wiley and Sons.

CHAPTER 4

ADDITIONAL FINDINGS

Investigating Aer PAS-HAMP and PAS-Proximal Signaling Domain

Interactions in Kinase-off and Kinase-on Signaling States

Early evidence for PAS-HAMP interactions in the *E. coli* Aer receptor included the requirement of the HAMP domain for proper PAS folding, stability, and FAD binding (Rebbapragada *et al.*, 1997a, Herrmann *et al.*, 2004, Buron-Barral *et al.*, 2006a). In Chapter 2 of this dissertation, residues that were solvent inaccessible overlapped with signal-on lesions in the PAS domain (Garcia *et al.*, 2016, Campbell *et al.*, 2010). Four PAS residues (N98C, V100C, M112C, and I114C) were located within the inaccessible region on the PAS β-scaffold, and these residues were able to crosslink with HAMP residues (Q284C and L251C) located on the inaccessible surface on HAMP-AS2 (Campbell *et al.*, 2010, Garcia *et al.*, 2016). These data confirmed that the PAS and HAMP domains are in close proximity and suggest that this PAS-HAMP interaction surface relays signals. In this chapter, I will present unpublished work wherein I investigated potential contacts between PAS-HAMP and PAS-Proximal signaling regions in each signaling state.

PAS-HAMP crosslinking was previously demonstrated using cysteine replacements at HAMP residues Gln248 and Leu251 (see Chapter 2). Additional crosslinking data were obtained using L251C in the HAMP domain, and D259C in the proximal signaling domain. PAS residues selected for cysteine replacement included Thr23, Val100, Val103, Met112, and Ill114. Val100 is

located on the PAS Hβ strand and Met112 and Ill114 are located on the PAS Iβ strand. The23 is located on the Aβ strand following the N-cap.

To simulate the activated state of Aer, N85S was engineered into the di-Cys mutants. PAS residue Asn85 is located on the Gβ strand and may be a link between the bound FAD and the β-scaffold (Campbell *et al.*, 2010). Replacing Asn85 with serine results in a kinase-on output (Campbell *et al.*, 2010). Aer di-Cys mutants were created from a pMB1 derivative that expressed either Aer-L251C or Aer-D259C. The N85S codon was then introduced into plasmids that contained the di-Cys mutants. Protein expression was determined after induction with 50 μM IPTG. However, expression was so low for di-Cys and N85S-di-Cys mutants containing D259C that Western blots had to be overexposed to detect protein bands. Moreover, increasing protein induction levels with 100 μM IPTG did not improve protein expression.

The di-Cys construct, Aer-V103C/L251C, was stable, but produced only 2% crosslinked dimers. This is in contrast to Aer-V100C/L251C, which produced 33% crosslinked dimers (Garcia *et al.*, 2016). This supports our interaction model, which predicts that Val103 is located further from Leu251 than is Val100. PAS-V103 begins a loop at the end of the Hβ strand, on which Val100 is located; the Hβ strand is proposed to be involved in PAS-HAMP signaling (Garcia *et al.*, 2016).

Residues in the proximal signaling domain change their accessibility as Aer alternates between kinase-on and kinase-off states (Garcia *et al.*, 2016). Aer-D259 lies within the proximal signaling domain, and was the only surface-

exposed residue in which a Cys-replacement both did not crosslink with itself in a dimer and was inaccessible to solvent in the kinase-on state of the receptor. Remarkably, the accessibility changed from 45% in the kinase-off state to only 3% in the kinase-on state. Thus, I investigated whether PAS residues might be contributing to this drop in accessibility by direct interactions. To simulate the kinase-on state, Aer-N85S was introduced into the Aer-D259C di-Cys mutants.

After crosslinking, Aer-V100C/D259C produced faint monomer and dimer bands, and 53% of the density was that of a crosslinked dimer, suggesting that these residues can collide. However, these results should be treated with caution, because faint banding usually indicates protein instability, and instability can be due to aberrant folding and a non-native conformation. The Aer-N85S/V100C/D259C protein was unstable. In addition, breakdown products were the only bands evident for the di-Cys N85S mutants Aer-T23C/N85S/D259C and Aer-N85S/M112C/D259C. Aer-N85S/I114C/D259C and Aer-N85S/V103C/D259C produced 41% and 60% crosslinked dimers respectively, but they were also highly unstable; breakdown products were detected for both mutants, with 47% breakdown product for Aer-N85S/I114C/D259C and 14% breakdown product for Aer-N85S/V103C/D259C. Notably, the previous work showed that both Aer-D259C and Aer-N85S/D259C were stable [Chapter 2, (Garcia *et al.*, 2016)], but as described here, the addition of another cysteine in the PAS domain leads to proteolysis. Thus, a definitive answer as to whether the PAS domain contributes to the drop in accessibility in the proximal signaling domain remains to be determined.

CHAPTER 5

GENERAL DISCUSSION

The purpose of this dissertation was to investigate PAS domain signaling mechanisms in the *E. coli* Aer and *P. aeruginosa* Aer2 receptors. Before the work presented in this dissertation, multiple studies had demonstrated that PAS domains have a conserved three-dimensional fold and are capable of accommodating diverse cofactors and ligands (Taylor *et al.*, 1999). Due to their structural similarities, a common signaling pathway among PAS domains had been proposed involving ligand induced structural changes on the PAS β-scaffold, the cofactor pocket, and in the N-terminus (Moglich *et al.*, 2009b). The findings described in Chapters 2, 3, and 4 support this hypothesis. More importantly, these data helped us to identify two distinct PAS signaling mechanisms in Aer and Aer2. We identified a lateral PAS-HAMP signaling mechanism in Aer, and obtained data supporting a linear PAS-HAMP signaling mechanism in Aer2. The signaling mechanisms in Aer and Aer2 provide two different signaling pathways that can be used as prototypes for membrane bound or cytoplasmic chemoreceptors that contain both PAS and HAMP domains.

Aer PAS Domain Study Conclusion

My studies on the Aer receptor have provided insight into a novel PAS signaling pathway. In Aer, the PAS signaling pathway involves the transmission of FAD redox changes from the PAS domain to the HAMP domain. It was hypothesized that FAD redox changes are transmitted to the HAMP domain via

an interaction between the PAS β-scaffold and the AS2 helix of the HAMP domain (Campbell *et al.*, 2010). This was based on a region of kinase-on lesions that were identified on the PAS β-scaffold (Campbell *et al.*, 2010). The work in Chapter 2 defined the interacting surfaces. After probing the Aer PAS surface with PEG-mal, the kinase-on lesions that were previously discovered overlapped with the region that was inaccessible to solvent. The inaccessible region on the β-scaffold of the PAS domain was not due to PAS-PAS interaction, suggesting the possibility that inaccessible residues were sequestered by the HAMP domain. Lesions with intermediate accessibility surrounded the inaccessible region on the β-scaffold. The N-cap was highly accessible suggesting that it is dynamic and does not interact with other domains. This conclusion agrees with previous findings that have shown that the N-cap collides with neighboring dimers (Watts *et al.*, 2006b).

Incorporating an N85S replacement renders Aer signal-on (Campbell *et al.*, 2010). This allowed us to compare accessibility changes in the HAMP domain when the receptor was kinase-off or kinase-on. In the kinase-off state (without PAS-N85S), residues on AS2 were inaccessible to solvent, suggesting that they were sequestered by the PAS domain. In the kinase-on state (with PAS-N85S), the same inaccessible region on AS2 became more accessible. In the kinase-on state, the proximal signaling domain had decreased accessibility while an increase in accessibility was seen at the end of the HAMP domain.

Overall, 25 separate PAS residues were tested for PAS-Q248C interaction. Seven of those 25 PAS residues (6 on the β-scaffold and 1 on the N-

cap) were able to form PAS-HAMP crosslinked dimers. Since protein crosslinking can occur during protein synthesis, chloramphenicol was added to PAS-HAMP di-Cys mutants to inhibit new protein synthesis. Only three PAS residues [N98C (Hβ), V100C (Hβ), and I114C (Iβ)] had an equivalent or increased proportion of PAS-Q248C crosslinked dimers. These results suggested that these PAS-HAMP residue combinations are in close proximity in the folded protein. To test for additional HAMP residues that could crosslink with PAS residues, HAMP-L251C was crosslinked with PAS-N98C, -V100C, -M112C, and -I114C. HAMP- L251C preferentially crosslinked with PAS-N98C, -M112C, and -I114C, while HAMP-Q248C showed greater crosslinking with either PAS-V100C and PAS-M112C than with L251C and these PAS residues. These results allowed us to adjust the previous Aer PAS-HAMP interaction model by rotating it ~180° (Campbell *et al*., 2010, Watts *et al*., 2008). Once the model was rotated, the inaccessible residues on the PAS and HAMP domains and the PAS-HAMP crosslinking data complimented each other. For example, HAMP-Q248C and HAMP-L251C are now located closer to the PAS residues that they preferentially crosslinked with. These results overwhelmingly demonstrate that PAS and HAMP are in close proximity and reveal the surface through which PAS controls HAMP signaling.

The surface accessibility study along with the crosslinking study revealed a novel lateral PAS-HAMP signal transmission mechanism. The results from Chapter 2 suggested that the proximity of the PAS domain controls the dynamics of the HAMP domain, which is in congruence with the biphasic static-dynamic signaling model. The biphasic static-dynamic signaling model states that the

signaling state of a receptor is dependent on the stability of the HAMP domain

(Zhou *et al.*, 2009). We propose that when PAS-FAD is oxidized, a close PAS-

HAMP interaction results in a static HAMP domain, a more dynamic proximal

signaling domain, a static kinase control module, and lower CheA kinase activity.

In contrast, when PAS-FAD is reduced, conformational changes in the PAS

domain decrease PAS-HAMP interactions. This results in a more dynamic HAMP

structure, resulting in a static proximal signaling domain, a more dynamic kinase

control module and increased CheA kinase activity. This model implies that

anything that alters the static-dynamic balance could produce a HAMP signal.

This would allow for lateral as well as linear signaling to the HAMP domain.

Aer2 PAS Domain Study Conclusion

Heme-based PAS domains are a unique subclass of signal sensors that

are capable of sensing O_2, CO, NO, and cellular redox state. They are involved

in the regulation of gene transcription, control of iron concentration via heme

uptake, and biofilm formation. The work presented in Chapter 3 focuses on the *b*-

type heme binding PAS domain of Aer2. Several *b*-type heme binding PAS

domains (e.g., FixL, DOS, RcoM, and PDEA-1) have a conserved proximal

coordinating Fα histidine residue (Kerby *et al.*, 2008, Gilles-Gonzalez *et al.*,

2005). Although the PAS domain of Aer2 also contains an Fα histidine residue,

the true proximal coordinating residue for Aer2 is actually the Eη histidine

residue, His234 (Garcia *et al.*, 2016, Sawai *et al.*, 2012, Airola *et al.*, 2013a). The

H234A substitution caused a substantial heme-binding defect (80% heme loss).

Alanine substitutions in residues located in the distal and proximal heme cleft (M187A, I195A, F220A, and F233A) also caused heme-binding defects.

I used alanine mutagenesis to study the importance of 16 conserved residues in the Aer2 PAS domain. Ten out of the 16 conserved residues did not bind or respond to O_2 or CO (this included the four heme pocket residues that were discussed above). Three alanine mutants (Aer2-A178V, Aer2-P237A, and Aer2-Q240A) had WT responses to both O_2 and CO. Aer2-D231A mediated WT behavior, but had a 30 second delayed smooth swimming response in anaerobic conditions. These mutants were located on the Eη and Fα helices. Aer2-D285 is located within the "DxT" motif that is proposed to transmit conformational changes from the PAS domain to HAMP 4 (Airola *et al.*, 2013a, Moglich *et al.*, 2009a). D285A caused the receptor to be signal-off, suggesting that the amino acid substitution disrupted the "DxT" motif and did not permit signal transmission. Leu264 and Thr287 are located on the PAS β-sheet. Substituting these residues with Ala resulted in locked signal-on receptors. The side chain of Aer2-L264 is suspended over the heme iron and is proposed to move out of the way to let O_2 bind to the heme iron. Aer2-T287 is located on the Iβ strand that is proposed to be involved in direct signal transmission to the HAMP 4 domain. Overall, many of the Aer2-PAS mutants had heme-binding defects and resulted in signal-off receptors. This suggests that in Aer2, conserved PAS residues are critical for stabilizing the heme cleft, which is also crucial for signal transmission.

A structural comparison between the unliganded (ferric) and ligand bound (cyanomet) structures of the Aer2 PAS domain revealed global conformational

changes (Sawai *et al.*, 2012, Airola *et al.*, 2013a). Leu264 on Hβ may move away from the heme-Fe center to allow O_2 binding and Trp283 on Iβ may rotate 90° to stabilize O_2 binding via its indole group.

In Aer2, smaller hydrophobic substitutions at Leu264 (L264A and L264G), resulted in a non-responsive receptors that did not bind O_2, and were rapidly oxidized. These results indicate the Leu264 is not only involved in PAS signaling but also plays a role in preventing heme iron oxidation. In addition, Trp283 is important for preventing dissociation of bound O_2, which also suggests that O_2 is the native ligand of the Aer2 PAS domain. The distal residues in myoglobin similarly play crucial roles in inhibition of heme iron autoxidation and also prevent dissociation and protonation of bound O_2 (Brantley *et al.*, 1993).

Although O_2 is thought to be the native ligand of Aer2, Aer2 can also bind other oxy-gases like CO (Watts *et al.*, 2011b). We analyzed Aer2 mutants that had WT, signal-off, or signal-off biased responses to O_2 for their response to CO. Most of the PAS mutants that bound CO could not signal. In addition, Aer2-L264K was found to be in an unusual hexa-coordinated state, which did not allow the binding of any gas. Overall, the work in Chapter 3 provides insight into the importance and function of conserved PAS residues in Aer2, and demonstrates the vital role of Leu264 and Trp283 in the ligand stabilization and PAS signaling. My data also supports the linear PAS-HAMP signaling mechanism that has been proposed from structural studies (Sawai *et al.*, 2012, Airola *et al.*, 2013a).

Future Directions

Aer PAS Domain

The Aer PAS domain study revealed lateral interaction surfaces between the PAS β-scaffold and the HAMP AS2 helix. However, questions remain as to exactly how the kinase-off and kinase-on states of the receptor affects PAS-HAMP interactions. Probing locked kinase-on and kinase-off Aer mutants with a spin label to identify PAS domain dynamics could reveal PAS domain movements between different signaling states. In addition, site-directed spin labeling can be used to specifically study the movement of residues on the Hβ and Iβ strands that have been shown to interact with HAMP residues, e.g., PAS residues Asn98, Val100, Met112 and I114. Performing these experiments will not only increase our understanding of the structural dynamics between different signaling states, but will also provide a detailed insight into the domain dynamics involved in lateral PAS-HAMP signaling that could be applied to other proteins.

Aer2 PAS Domain

The work performed on Aer2 showed that the majority of conserved amino acids in the Aer2 PAS domain are crucial for protein stability, heme-binding, ligand binding, and signaling. Many of the Aer2 mutants in the study were found to be locked in either signal-on or signal-off signaling state. Solving structures for locked signaling mutants should reveal PAS conformational changes between the two states of the receptor. In addition, the Aer2 mutants that were created can be studied in a biological system like that of *Caenorhabditis elegans*. By

doing so, PAS mutants can be used to evaluate the significance and role of Aer2 in *P. aeruginosa*. Work is currently underway in our laboratory to: i) show that the signal-off state favors PAS dimerization and that the signal-on state favors PAS monomerization, and ii) elucidate the role of Aer2 in *P. aeruginosa* virulence by investigating the interacting partners of CheY2.

Impact of this Work

The work presented in this dissertation is the first to reveal two variations of PAS-HAMP signaling mechanisms that can serve as models for other proteins containing PAS and HAMP domains. Studies on the Aer and Aer2 PAS domains revealed a common signaling pathway involving residues on the PAS β-scaffold, specifically the Hβ and Iβ strands. Understanding PAS domain signaling and sensing will potentially lead to targeting these domains for therapeutic and antimicrobial applications.

REFERENCES

Adler, J., (1966) Chemotaxis in bacteria. *Science* **153**: 708-716.

Airola, M.V., J. Du, J.H. Dawson & B.R. Crane, (2010a) Heme binding to the Mammalian circadian clock protein period 2 is nonspecific. *Biochemistry* **49**: 4327-4338.

Airola, M.V., D. Huh, N. Sukomon, J. Widom, R. Sircar, P.P. Borbat, J.H. Freed, K.J. Watts & B.R. Crane, (2013a) Architecture of the soluble receptor Aer2 indicates an in-line mechanism for PAS and HAMP domain signaling. *Journal of Molecular Biology* **425**: 886-901.

Airola, M.V., N. Sukomon, D. Samanta, P.P. Borbat, J.H. Freed, K.J. Watts & B.R. Crane, (2013b) HAMP domain conformers that propagate opposite signals in bacterial chemoreceptors. *PLOS Biology* **11**.

Airola, M.V., N. Sukomon, D. Samanta, P.P. Borbat, J.H. Freed, K.J. Watts & B.R. Crane, (2013c) HAMP domain conformers that propagate opposite signals in bacterial chemoreceptors. *PLOS Biology* **11**: e1001479.

Airola, M.V., K.J. Watts, A.M. Bilwes & B.R. Crane, (2010b) Structure of concatenated HAMP domains provides a mechanism for signal transduction. *Structure* **18**: 436-448.

Airola, M.V., K.J. Watts, A.M. Bilwes & B.R. Crane, (2010c) Structure of concatenated HAMP domains provides a mechanism for signal transduction. *Structure* *18*: 436-448.

Airola, M.V., K.J. Watts & B.R. Crane, (2010d) Identifying divergent HAMP domains and poly-HAMP chains. *The Journal of biological chemistry* **285**: le7; author reply 1e8.

Alexander, R.P. & I.B. Zhulin, (2007) Evolutionary genomics reveals conserved structural determinants of signaling and adaptation in microbial chemoreceptors. *Proceedings of the National Academy of Sciences of the United States of America* **104**: 2885-2890.

Alexandre, G. & I.B. Zhulin, (2001) More than one way to sense chemicals. *Journal of bacteriology* **183**: 4681-4686.

Ames, P. & J.S. Parkinson, (1994) Constitutively signaling fragments of Tsr, the Escherichia coli serine chemoreceptor. *Journal of bacteriology* **176**: 6340-6348.

Ames, P. & J.S. Parkinson, (2006) Conformational suppression of inter-receptor signaling defects. *Proceedings of the National Academy of Sciences of the United States of America* **103**: 9292-9297.

Ames, P., C.A. Studdert, R.H. Reiser & J.S. Parkinson, (2002) Collaborative signaling by mixed chemoreceptor teams in Escherichia coli. *Proceedings of the National Academy of Sciences of the United States of America* **99**: 7060-7065.

Ames, P., Q. Zhou & J.S. Parkinson, (2014) HAMP domain structural determinants for signalling and sensory adaptation in Tsr, the Escherichia coli serine chemoreceptor. *Mol Microbiol* **91**: 875-886.

Amin, D.N., B.L. Taylor & M.S. Johnson, (2006) Topology and boundaries of the aerotaxis receptor Aer in the membrane of Escherichia coli. *Journal of bacteriology* **188**: 894-901.

Appleby, C.A. & F.J. Bergersen, (1980) *Preparation and experimental use of leghaemoglobin.,* p. 315-335. J. Wiley and Sons.

Aravind, L. & C.P. Ponting, (1999) The cytoplasmic helical linker domain of receptor histidine kinase and methyl-accepting proteins is common to many prokaryotic signalling proteins. *FEMS Microbiol Lett* **176**: 111-116.

Armitage, J.P. & R. Schmitt, (1997) Bacterial chemotaxis: Rhodobacter sphaeroides and Sinorhizobium meliloti--variations on a theme? *Microbiology* **143 (Pt 12)**: 3671-3682.

Barnakov, A.N., L.A. Barnakova & G.L. Hazelbauer, (1999) Efficient adaptational demethylation of chemoreceptors requires the same enzyme-docking site as efficient methylation. *Proceedings of the National Academy of Sciences of the United States of America* **96**: 10667-10672.

Bass, R.B., S.L. Butler, S.A. Chervitz, S.L. Gloor & J.J. Falke, (2007) Use of site-directed cysteine and disulfide chemistry to probe protein structure and dynamics: applications to soluble and transmembrane receptors of bacterial chemotaxis. *Methods Enzymol* **423**: 25-51.

Berg, H.C., (2003) The rotary motor of bacterial flagella. *Annu Rev Biochem* **72**: 19-54.

Berg, H.C. & D.A. Brown, (1972) Chemotaxis in Escherichia coli analysed by three-dimensional tracking. *Nature* **239**: 500-504.

Berg, H.C. & P.M. Tedesco, (1975) Transient response to chemotactic stimuli in Escherichia coli. *Proceedings of the National Academy of Sciences of the United States of America* **72**: 3235-3239.

Bi, S. & L. Lai, (2015) Bacterial chemoreceptors and chemoeffectors. *Cellular and molecular life sciences : CMLS* **72**: 691-708.

Bibikov, S.I., L.A. Barnes, Y. Gitin & J.S. Parkinson, (2000) Domain organization and flavin adenine dinucleotide-binding determinants in the aerotaxis signal transducer Aer of *Escherichia coli*. *Proceedings of the National Academy of Sciences of the United States of America* **97**: 5830-5835.

Bibikov, S.I., R. Biran, K.E. Rudd & J.S. Parkinson, (1997a) A signal transducer for aerotaxis in *Escherichia coli*. *Journal of bacteriology* **179**: 4075-4079.

Bibikov, S.I., R. Biran, K.E. Rudd & J.S. Parkinson, (1997b) A signal transducer for aerotaxis in*Escherichia coli*. *J Bacteriol* **179**: 4075-4079.

Bibikov, S.I., A.C. Miller, K.K. Gosink & J.S. Parkinson, (2004) Methylation-independent aerotaxis mediated by the Escherichia coli Aer protein. *Journal of bacteriology* **186**: 3730-3737.

Bilwes, A.M., C.M. Quezada, L.R. Croal, B.R. Crane & M.I. Simon, (2001) Nucleotide binding by the histidine kinase CheA. *Nature structural biology* **8**: 353-360.

Biswas, M., S. Dey, S. Khamrui, U. Sen & J. Dasgupta, (2013) Conformational barrier of CheY3 and inability of CheY4 to bind FliM control the flagellar motor action in Vibrio cholerae. *PLoS One* **8**: e73923.

Borroni, P.F. & J. Atema, (1988) Adaptation in chemoreceptor cells. I. Self-adapting backgrounds determine threshold and cause parallel shift of response function. *Journal of comparative physiology. A, Sensory, neural, and behavioral physiology* **164**: 67-74.

Bourret, R.B., J. Davagnino & M.I. Simon, (1993) The carboxy-terminal portion of the CheA kinase mediates regulation of autophosphorylation by transducer and CheW. *Journal of bacteriology* **175**: 2097-2101.

Boyd, A. & M.I. Simon, (1980) Multiple electrophoretic forms of methyl-accepting chemotaxis proteins generated by stimulus-elicited methylation in Escherichia coli. *Journal of bacteriology* **143**: 809-815.

Brantley, R.E., Jr., S.J. Smerdon, A.J. Wilkinson, E.W. Singleton & J.S. Olson, (1993) The mechanism of autooxidation of myoglobin. *The Journal of biological chemistry* **268**: 6995-7010.

Briegel, A., M.S. Ladinsky, C. Oikonomou, C.W. Jones, M.J. Harris, D.J. Fowler, Y.W. Chang, L.K. Thompson, J.P. Armitage & G.J. Jensen, (2014) Structure of bacterial cytoplasmic chemoreceptor arrays and implications for chemotactic signaling. *Elife* **3**: e02151.

Briegel, A., D.R. Ortega, E.I. Tocheva, K. Wuichet, Z. Li, S. Chen, A. Muller, C.V. Iancu, G.E. Murphy, M.J. Dobro, I.B. Zhulin & G.J. Jensen, (2009) Universal architecture of bacterial chemoreceptor arrays. *Proceedings of*

the National Academy of Sciences of the United States of America **106**: 17181-17186.

Brown, J.H., C. Cohen & D.A. Parry, (1996) Heptad breaks in alpha-helical coiled coils: stutters and stammers. *Proteins* **26**: 134-145.

Brudler, R., T.E. Meyer, U.K. Genick, S. Devanathan, T.T. Woo, D.P. Millar, K. Gerwert, M.A. Cusanovich, G. Tollin & E.D. Getzoff, (2000) Coupling of hydrogen bonding to chromophore conformation and function in photoactive yellow protein. *Biochemistry* **39**: 13478-13486.

Buron-Barral, M.C., K.K. Gosink & J.S. Parkinson, (2006a) Loss- and gain-of-function mutations in the F1-HAMP region of the Escherichia coli aerotaxis transducer Aer. *Journal of bacteriology* **188**: 3477-3486.

Buron-Barral, M.D.C., K.K. Gosink & J.S. Parkinson, (2006b) Loss- and gain-of-function mutations in the F1-HAMP region of the Escherichia coli aerotaxis transducer Aer. *Journal of bacteriology* **188**: 3477-3486.

Butler, S.L. & J.J. Falke, (1998) Cysteine and disulfide scanning reveals two amphiphilic helices in the linker region of the aspartate chemoreceptor. *Biochemistry* **37**: 10746-10756.

Campbell, A.J., K.J. Watts, M.S. Johnson & B.L. Taylor, (2010) Gain-of-function mutations cluster in distinct regions associated with the signalling pathway in the PAS domain of the aerotaxis receptor, Aer. *Mol Microbiol* **77**: 575-586.

Campbell, A.J., K.J. Watts, M.S. Johnson & B.L. Taylor, (2011) Role of the F1 region in the Escherichia coli aerotaxis receptor Aer. *Journal of bacteriology* **193**: 358-366.

Chang, A.L., J.R. Tuckerman, G. Gonzalez, R. Mayer, H. Weinhouse, G. Volman, D. Amikam, M. Benziman & M.A. Gilles-Gonzalez, (2001) Phosphodiesterase A1, a regulator of cellulose synthesis in Acetobacter xylinum, is a heme-based sensor. *Biochemistry* **40**: 3420-3426.

Clarke, S. & D.E. Koshland, Jr., (1979) Membrane receptors for aspartate and serine in bacterial chemotaxis. *The Journal of biological chemistry* **254**: 9695-9702.

Collins, K.D., J. Lacal & K.M. Ottemann, (2014) Internal sense of direction: sensing and signaling from cytoplasmic chemoreceptors. *Microbiology and molecular biology reviews : MMBR* **78**: 672-684.

Crews, S.T., J.B. Thomas & C.S. Goodman, (1988) The Drosophila single-minded gene encodes a nuclear protein with sequence similarity to the per gene product. *Cell* **52**: 143-151.

Crooks, G.E., G. Hon, J.M. Chandonia & S.E. Brenner, (2004) WebLogo: a sequence logo generator. *Genome research* **14**: 1188-1190.

Crosson, S. & K. Moffat, (2001) Structure of a flavin-binding plant photoreceptor domain: insights into light-mediated signal transduction. *Proceedings of the National Academy of Sciences of the United States of America* **98**: 2995-3000.

Darzins, A., (1994) Characterization of a Pseudomonas aeruginosa gene cluster involved in pilus biosynthesis and twitching motility: sequence similarity to the chemotaxis proteins of enterics and the gliding bacterium Myxococcus xanthus. *Mol Microbiol* **11**: 137-153.

Dasgupta, J. & J.K. Dattagupta, (2008) Structural determinants of V. cholerae CheYs that discriminate them in FliM binding: comparative modeling and MD simulation studies. *Journal of biomolecular structure & dynamics* **25**: 495-503.

Delgado-Nixon, V.M., G. Gonzalez & M.A. Gilles-Gonzalez, (2000a) Dos, a heme-binding PAS protein from *Escherichia coli*, is a direct oxygen sensor. *Biochemistry* **39**: 2685-2691.

Delgado-Nixon, V.M., G. Gonzalez & M.A. Gilles-Gonzalez, (2000b) Dos, a heme-binding PAS protein from*Escherichia coli*, is a direct oxygen sensor. *Biochemistry* **39**: 2685-2691.

Dunham, C.M., E.M. Dioum, J.R. Tuckerman, G. Gonzalez, W.G. Scott & M.A. Gilles-Gonzalez, (2003) A distal arginine in oxygen-sensing heme-PAS domains is essential to ligand binding, signal transduction, and structure. *Biochemistry* **42**: 7701-7708.

Dunin-Horkawicz, S. & A.N. Lupas, (2010) Comprehensive analysis of HAMP domains: Implications for transmembrane signal transduction. *J Mol Biol* **397**: 1156-1174.

Edwards, J.C., M.S. Johnson & B.L. Taylor, (2006) Differentiation between electron transport sensing and proton motive force sensing by the Aer and Tsr receptors for aerotaxis. *Mol Microbiol* **62**: 823-837.

Etzkorn, M., H. Kneuper, P. Dunnwald, V. Vijayan, J. Kramer, C. Griesinger, S. Becker, G. Unden & M. Baldus, (2008) Plasticity of the PAS domain and a potential role for signal transduction in the histidine kinase DcuS. *Nat Struct Mol Biol* **15**: 1031-1039.

Falke, J.J. & G.L. Hazelbauer, (2001) Transmembrane signaling in bacterial chemoreceptors. *Trends in biochemical sciences* **26**: 257-265.

Falke, J.J. & K.N. Piasta, (2014) Architecture and signal transduction mechanism of the bacterial chemosensory array: progress, controversies, and challenges. *Curr Opin Struct Biol* **29**: 85-94.

Feng, X., J.W. Baumgartner & G.L. Hazelbauer, (1997) High- and low-abundance chemoreceptors in Escherichia coli: differential activities associated with closely related cytoplasmic domains. *Journal of bacteriology* **179**: 6714-6720.

Ferrandez, A., A.C. Hawkins, D.T. Summerfield & C.S. Harwood, (2002) Cluster II che genes from Pseudomonas aeruginosa are required for an optimal chemotactic response. *Journal of bacteriology* **184**: 4374-4383.

Ferris, H.U., S. Dunin-Horkawicz, L.G. Mondejar, M. Hulko, K. Hantke, J. Martin, J.E. Schultz, K. Zeth, A.N. Lupas & M. Coles, (2011) The mechanisms of HAMP-mediated signaling in transmembrane receptors. *Structure* **19**: 378-385.

Formaneck, M.S., L. Ma & Q. Cui, (2006) Reconciling the "old" and "new" views of protein allostery: a molecular simulation study of chemotaxis Y protein (CheY). *Proteins* **63**: 846-867.

Garcia, D., K.J. Watts, M.S. Johnson & B.L. Taylor, (2016) Delineating PAS-HAMP interaction surfaces and signalling-associated changes in the aerotaxis receptor Aer. *Mol Microbiol* **100**: 156-172.

Garcia-Fontana, C., A. Corral Lugo & T. Krell, (2014) Specificity of the CheR2 methyltransferase in Pseudomonas aeruginosa is directed by a C-terminal pentapeptide in the McpB chemoreceptor. *Sci Signal* **7**: ra34.

Garvis, S., A. Munder, G. Ball, S. de Bentzmann, L. Wiehlmann, J.J. Ewbank, B. Tummler & A. Filloux, (2009) Caenorhabditis elegans semi-automated liquid screen reveals a specialized role for the chemotaxis gene cheB2 in Pseudomonas aeruginosa virulence. *PLoS Pathog* **5**: e1000540.

Garzon, A. & J.S. Parkinson, (1996) Chemotactic signaling by the P1 phosphorylation domain liberated from the CheA histidine kinase of Escherichia coli. *Journal of bacteriology* **178**: 6752-6758.

Gennis, R.B. & V. Stewart, (1996) Respiration. In: *Escherichia coli* and *Salmonella*: Cellular and Molecular Biology. F.C. Neidhardt (ed). Washington, D.C.: ASM Press, pp. 217-261.

Gilles-Gonzalez, M.A. & G. Gonzalez, (2005) Heme-based sensors: defining characteristics, recent developments, and regulatory hypotheses. *J Inorg Biochem* **99**: 1-22.

Gilles-Gonzalez, M.A., G. Gonzalez, M.F. Perutz, L. Kiger, M.C. Marden & C. Poyart, (1994) Heme-based sensors, exemplified by the kinase FixL, are a new class of heme protein with distinctive ligand binding and autoxidation. *Biochemistry* **33**: 8067-8073.

Gilles-Gonzalez, M.A., G. Gonzalez, E.H. Sousa & J. Tuckerman, (2008) Oxygen-sensing histidine-protein kinases: assays of ligand binding and turnover of response-regulator substrates. *Methods Enzymol* **437**: 173-189.

Glekas, G.D., M.J. Plutz, H.E. Walukiewicz, G.M. Allen, C.V. Rao & G.W. Ordal, (2012) Elucidation of the multiple roles of CheD in Bacillus subtilis chemotaxis. *Mol Microbiol* **86**: 743-756.

Gong, W., B. Hao & M.K. Chan, (2000) New mechanistic insights from structural studies of the oxygen-sensing domain of Bradyrhizobium japonicum FixL. *Biochemistry* **39**: 3955-3962.

Gong, W., B. Hao, S.S. Mansy, G. Gonzalez, M.A. Gilles-Gonzalez & M.K. Chan, (1998) Structure of a biological oxygen sensor: a new mechanism for heme-driven signal transduction. *Proceedings of the National Academy of Sciences of the United States of America* **95**: 15177-15182.

Gonzalez, G., E.M. Dioum, C.M. Bertolucci, T. Tomita, M. Ikeda-Saito, M.R. Cheesman, N.J. Watmough & M.A. Gilles-Gonzalez, (2002) Nature of the displaceable heme-axial residue in the EcDos protein, a heme-based sensor from Escherichia coli. *Biochemistry* **41**: 8414-8421.

Gosink, K.K., M. del Carmen Buron-Barral & J.S. Parkinson, (2006) Signaling interactions between the aerotaxis transducer Aer and heterologous chemoreceptors in Escherichia coli. *Journal of bacteriology* **188**: 3487-3493.

Grebe, T.W. & J. Stock, (1998) Bacterial chemotaxis: the five sensors of a bacterium. *Curr Biol* **8**: R154-157.

Guvener, Z.T., D.F. Tifrea & C.S. Harwood, (2006) Two different Pseudomonas aeruginosa chemosensory signal transduction complexes localize to cell poles and form and remould in stationary phase. *Mol Microbiol* **61**: 106-118.

Hao, B., C. Isaza, J. Arndt, M. Soltis & M.K. Chan, (2002) Structure-based mechanism of O2 sensing and ligand discrimination by the FixL heme domain of Bradyrhizobium japonicum. *Biochemistry* **41**: 12952-12958.

Harper, S.M., L.C. Neil & K.H. Gardner, (2003) Structural basis of a phototropin light switch. *Science* **301**: 1541-1544.

Hazelbauer, G.L., J.J. Falke & J.S. Parkinson, (2008) Bacterial chemoreceptors: high-performance signaling in networked arrays. *Trends in biochemical sciences* **33**: 9-19.

Hazelbauer, G.L. & W.C. Lai, (2010) Bacterial chemoreceptors: providing enhanced features to two-component signaling. *Curr Opin Microbiol* **13**: 124-132.

He, Y.W., C. Boon, L. Zhou & L.H. Zhang, (2009) Co-regulation of Xanthomonas campestris virulence by quorum sensing and a novel two-component regulatory system RavS/RavR. *Mol Microbiol* **71**: 1464-1476.

Henry, J.T. & S. Crosson, (2011) Ligand-binding PAS domains in a genomic, cellular, and structural context. *Annual review of microbiology* **65**: 261-286.

Herrmann, S., Q. Ma, M.S. Johnson, A.V. Repik & B.L. Taylor, (2004) PAS domain of the Aer redox sensor requires C-terminal residues for native-fold formation and flavin adenine dinucleotide binding. *Journal of bacteriology* **186**: 6782-6791.

Hoffman, E.C., H. Reyes, F.F. Chu, F. Sander, L.H. Conley, B.A. Brooks & O. Hankinson, (1991) Cloning of a factor required for activity of the Ah (dioxin) receptor. *Science* **252**: 954-958.

Hong, C.S., A. Kuroda, T. Ikeda, N. Takiguchi, H. Ohtake & J. Kato, (2004a) The aerotaxis transducer gene aer, but not aer-2, is transcriptionally regulated by the anaerobic regulator ANR in Pseudomonas aeruginosa. *Journal of bioscience and bioengineering* **97**: 184-190.

Hong, C.S., A. Kuroda, N. Takiguchi, H. Ohtake & J. Kato, (2005) Expression of Pseudomonas aeruginosa aer-2, one of two aerotaxis transducer genes, is controlled by RpoS. *Journal of bacteriology* **187**: 1533-1535.

Hong, C.S., M. Shitashiro, A. Kuroda, T. Ikeda, N. Takiguchi, H. Ohtake & J. Kato, (2004b) Chemotaxis proteins and transducers for aerotaxis in Pseudomonas aeruginosa. *FEMS Microbiol Lett* **231**: 247-252.

Huang, S., J. Huang, A.P. Kloek, D.E. Goldberg & J.M. Friedman, (1996) Hydrogen bonding of tyrosine B10 to heme-bound oxygen in Ascaris hemoglobin. Direct evidence from UV resonance Raman spectroscopy. *The Journal of biological chemistry* **271**: 958-962.

Hughson, A.G. & G.L. Hazelbauer, (1996) Detecting the conformational change of transmembrane signaling in a bacterial chemoreceptor by measuring effects on disulfide cross-linking in vivo. *Proceedings of the National Academy of Sciences of the United States of America* **93**: 11546-11551.

Hulko, M., F. Berndt, M. Gruber, J.U. Linder, V. Truffault, A. Schultz, J. Martin, J.E. Schultz, A.N. Lupas & M. Coles, (2006) The HAMP domain structure implies helix rotation in transmembrane signaling. *Cell* **126**: 929-940.

Hyakutake, A., M. Homma, M.J. Austin, M.A. Boin, C.C. Hase & I. Kawagishi, (2005) Only one of the five CheY homologs in Vibrio cholerae directly switches flagellar rotation. *Journal of bacteriology* **187**: 8403-8410.

Jahreis, K., T.B. Morrison, A. Garzon & J.S. Parkinson, (2004) Chemotactic signaling by an Escherichia coli CheA mutant that lacks the binding domain for phosphoacceptor partners. *Journal of bacteriology* **186**: 2664-2672.

Jain, R. & M.K. Chan, (2003) Mechanisms of ligand discrimination by heme proteins. *Journal of biological inorganic chemistry : JBIC : a publication of the Society of Biological Inorganic Chemistry* **8**: 1-11.

Karow, D.S., D. Pan, R. Tran, P. Pellicena, A. Presley, R.A. Mathies & M.A. Marletta, (2004) Spectroscopic characterization of the soluble guanylate cyclase-like heme domains from Vibrio cholerae and Thermoanaerobacter tengcongensis. *Biochemistry* **43**: 10203-10211.

Kato, J., H.E. Kim, N. Takiguchi, A. Kuroda & H. Ohtake, (2008) Pseudomonas aeruginosa as a model microorganism for investigation of chemotactic behaviors in ecosystem. *Journal of bioscience and bioengineering* **106**: 1-7.

Kato, J., T. Nakamura, A. Kuroda & H. Ohtake, (1999) Cloning and characterization of chemotaxis genes in Pseudomonas aeruginosa. *Biosci Biotechnol Biochem* **63**: 155-161.

Ke, Y., M.J. Hunter, C.A. Ng, M.D. Perry & J.I. Vandenberg, (2014) Role of the cytoplasmic N-terminal Cap and Per-Arnt-Sim (PAS) domain in trafficking and stabilization of Kv11.1 channels. *The Journal of biological chemistry* **289**: 13782-13791.

Kearns, D.B., J. Robinson & L.J. Shimkets, (2001) Pseudomonas aeruginosa exhibits directed twitching motility up phosphatidylethanolamine gradients. *Journal of bacteriology* **183**: 763-767.

Kentner, D., S. Thiem, M. Hildenbeutel & V. Sourjik, (2006) Determinants of chemoreceptor cluster formation in Escherichia coli. *Mol Microbiol* **61**: 407-417.

Kerby, R.L., H. Youn & G.P. Roberts, (2008) RcoM: a new single-component transcriptional regulator of CO metabolism in bacteria. *Journal of bacteriology* **190**: 3336-3343.

Key, J., M. Hefti, E.B. Purcell & K. Moffat, (2007) Structure of the redox sensor domain of Azotobacter vinelandii NifL at atomic resolution: signaling, dimerization, and mechanism. *Biochemistry* **46**: 3614-3623.

Key, J. & K. Moffat, (2005) Crystal structures of deoxy and CO-bound bjFixLH reveal details of ligand recognition and signaling. *Biochemistry* **44**: 4627-4635.

Kloek, A.P., J. Yang, F.S. Mathews, C. Frieden & D.E. Goldberg, (1994) The tyrosine B10 hydroxyl is crucial for oxygen avidity of Ascaris hemoglobin. *J Biol Chem* **269**: 2377-2379.

Klose, D., N. Voskoboynikova, I. Orban-Glass, C. Rickert, M. Engelhard, J.P. Klare & H.J. Steinhoff, (2014) Light-induced switching of HAMP domain conformation and dynamics revealed by time-resolved EPR spectroscopy. *FEBS Lett* **588**: 3970-3976.

Kondoh, H., C.B. Ball & J. Adler, (1979) Identification of a methyl-accepting chemotaxis protein for the ribose and galactose chemoreceptors of Escherichia coli. *Proceedings of the National Academy of Sciences of the United States of America* **76**: 260-264.

Kosowicz, J.G. & E.M. Boon, (2013) Insights into the distal heme pocket of H-NOX using fluoride as a probe for H-bonding interactions. *J Inorg Biochem* **126**: 91-95.

Krell, T., J. Lacal, F. Munoz-Martinez, J.A. Reyes-Darias, B.H. Cadirci, C. Garcia-Fontana & J.L. Ramos, (2011) Diversity at its best: bacterial taxis. *Environmental microbiology* **13**: 1115-1124.

Krulwich, T.A., G. Sachs & E. Padan, (2011) Molecular aspects of bacterial pH sensing and homeostasis. *Nat Rev Microbiol* **9**: 330-343.

Lai, R.Z. & J.S. Parkinson, (2014) Functional suppression of HAMP domain signaling defects in the E. coli serine chemoreceptor. *J Mol Biol* **426**: 3642-3655.

Lai, W.C. & G.L. Hazelbauer, (2007) Analyzing transmembrane chemoreceptors using in vivo disulfide formation between introduced cysteines. *Methods Enzymol* **423**: 299-316.

Levin, M.D., T.S. Shimizu & D. Bray, (2002) Binding and diffusion of CheR molecules within a cluster of membrane receptors. *Biophys J* **82**: 1809-1817.

Li, M. & G.L. Hazelbauer, (2004) Cellular stoichiometry of the components of the chemotaxis signaling complex. *Journal of bacteriology* **186**: 3687-3694.

Li, M. & G.L. Hazelbauer, (2005) Adaptational assistance in clusters of bacterial chemoreceptors. *Mol Microbiol* **56**: 1617-1626.

Lindebro, M.C., L. Poellinger & M.L. Whitelaw, (1995) Protein-protein interaction via PAS domains: role of the PAS domain in positive and negative regulation of the bHLH/PAS dioxin receptor-Arnt transcription factor complex. *EMBO J* **14**: 3528-3539.

Little, R., P. Slavny & R. Dixon, (2012) Influence of PAS Domain Flanking Regions on Oligomerisation and Redox Signalling By NifL. *PloS one* **7**: e46651.

Lu, J. & C. Deutsch, (2001) Pegylation: a method for assessing topological accessibilities in Kv1.3. *Biochemistry* **40**: 13288-13301.

Ma, Q., M.S. Johnson & B.L. Taylor, (2005) Genetic analysis of the HAMP domain of the Aer aerotaxis sensor localizes flavin adenine dinucleotide-binding determinants to the AS-2 helix. *Journal of bacteriology* **187**: 193-201.

Ma, Q., F. Roy, S. Herrmann, B.L. Taylor & M.S. Johnson, (2004) The Aer protein of *Escherichia coli* forms a homodimer independent of the signaling domain and FAD binding. *Journal of bacteriology* **186**: 7456-7459.

Macnab, R.M. & D.E. Koshland, Jr., (1972) The gradient-sensing mechanism in bacterial chemotaxis. *Proceedings of the National Academy of Sciences of the United States of America* **69**: 2509-2512.

Maddock, J.R. & L. Shapiro, (1993) Polar location of the chemoreceptor complex in the *Escherichia coli* cell. *Science* **259**: 1717-1723.

Martinkova, M., K. Kitanishi & T. Shimizu, (2013) Heme-based globin-coupled oxygen sensors: linking oxygen binding to functional regulation of diguanylate cyclase, histidine kinase, and methyl-accepting chemotaxis. *The Journal of biological chemistry* **288**: 27702-27711.

Masduki, A., J. Nakamura, T. Ohga, R. Umezaki, J. Kato & H. Ohtake, (1995) Isolation and characterization of chemotaxis mutants and genes of Pseudomonas aeruginosa. *Journal of bacteriology* **177**: 948-952.

Matamouros, S., K.R. Hager & S.I. Miller, (2015) HAMP Domain Rotation and Tilting Movements Associated with Signal Transduction in the PhoQ Sensor Kinase. *MBio* **6**: e00616-00615.

McEvoy, M.M., D.R. Muhandiram, L.E. Kay & F.W. Dahlquist, (1996) Structure and dynamics of a CheY-binding domain of the chemotaxis kinase CheA

determined by nuclear magnetic resonance spectroscopy. *Biochemistry* **35**: 5633-5640.

Mechaly, A.E., N. Sassoon, J.M. Betton & P.M. Alzari, (2014) Segmental helical motions and dynamical asymmetry modulate histidine kinase autophosphorylation. *PLoS Biol* **12**: e1001776.

Meena, N., H. Kaur & A.K. Mondal, (2010) Interactions among HAMP domain repeats act as an osmosensing molecular switch in group III hybrid histidine kinases from fungi. *The Journal of biological chemistry* **285**: 12121-12132.

Miller, A.S., S.C. Kohout, K.A. Gilman & J.J. Falke, (2006) CheA Kinase of bacterial chemotaxis: chemical mapping of four essential docking sites. *Biochemistry* **45**: 8699-8711.

Miyatake, H., M. Mukai, S.Y. Park, S. Adachi, K. Tamura, H. Nakamura, K. Nakamura, T. Tsuchiya, T. Iizuka & Y. Shiro, (2000) Sensory mechanism of oxygen sensor FixL from *Rhizobium meliloti:* crystallographic, mutagenesis and resonance Raman spectroscopic studies. *J Mol Biol* **301**: 415-431.

Moglich, A., R.A. Ayers & K. Moffat, (2009a) Design and signaling mechanism of light-regulated histidine kinases. *Journal of molecular biology* **385**: 1433-1444.

Moglich, A., R.A. Ayers & K. Moffat, (2009b) Structure and signaling mechanism of Per-ARNT-Sim domains. *Structure* **17**: 1282-1294.

Mondejar, L.G., A. Lupas, A. Schultz & J.E. Schultz, (2012) HAMP domain-mediated signal transduction probed with a mycobacterial adenylyl cyclase as a reporter. *J Biol Chem* **287**: 1022-1031.

Morais Cabral, J.H., A. Lee, S.L. Cohen, B.T. Chait, M. Li & R. Mackinnon, (1998) Crystal structure and functional analysis of the HERG potassium channel N terminus: a eukaryotic PAS domain. *Cell* **95**: 649-655.

Morrison, T.B. & J.S. Parkinson, (1994) Liberation of an interaction domain from the phosphotransfer region of CheA, a signaling kinase of Escherichia coli. *Proceedings of the National Academy of Sciences of the United States of America* **91**: 5485-5489.

Nambu, J.R., J.O. Lewis, K.A. Wharton, Jr. & S.T. Crews, (1991) The *Drosophila single-minded* gene encodes a helix-loop-helix protein that acts as a master regulator of CNS midline development. *Cell* **67**: 1157-1167.

Natarajan, J., A. Schultz, U. Kurz & J.E. Schultz, (2014) Biochemical characterization of the tandem HAMP domain from Natronomonas

pharaonis as an intraprotein signal transducer. *The FEBS journal* **281**: 3218-3227.

Neiditch, M.B., M.J. Federle, A.J. Pompeani, R.C. Kelly, D.L. Swem, P.D. Jeffrey, B.L. Bassler & F.M. Hughson, (2006) Ligand-induced asymmetry in histidine sensor kinase complex regulates quorum sensing. *Cell* **126**: 1095-1108.

Ni, M., J.M. Tepperman & P.H. Quail, (1999) Binding of phytochrome B to its nuclear signalling partner PIF3 is reversibly induced by light. *Nature* **400**: 781-784.

Niwano, M. & B.L. Taylor, (1982) Novel sensory adaptation mechanism in bacterial chemotaxis to oxygen and phosphotransferase substrates. *Proceedings of the National Academy of Sciences of the United States of America* **79**: 11-15.

Oka, Y., T. Matsushita, N. Mochizuki, P.H. Quail & A. Nagatani, (2008) Mutant screen distinguishes between residues necessary for light-signal perception and signal transfer by phytochrome B. *PLoS genetics* **4**: e1000158.

Olson, J.S., A.J. Mathews, R.J. Rohlfs, B.A. Springer, K.D. Egeberg, S.G. Sligar, J. Tame, J.P. Renaud & K. Nagai, (1988) The role of the distal histidine in myoglobin and haemoglobin. *Nature* **336**: 265-266.

Park, S.Y., C.M. Quezada, A.M. Bilwes & B.R. Crane, (2004) Subunit exchange by CheA histidine kinases from the mesophile Escherichia coli and the thermophile Thermotoga maritima. *Biochemistry* **43**: 2228-2240.

Parkinson, J.S., (2010) Signaling Mechanisms of HAMP Domains in Chemoreceptors and Sensor Kinases. *Annu. Rev. Microbiol.* **64**: 101–122

Parkinson, J.S., G.L. Hazelbauer & J.J. Falke, (2015) Signaling and sensory adaptation in Escherichia coli chemoreceptors: 2015 update. *Trends in microbiology* **23**: 257-266.

Pellequer, J.L., K.A. Wager-Smith, S.A. Kay & E.D. Getzoff, (1998) Photoactive yellow protein: a structural prototype for the three-dimensional fold of the PAS domain superfamily. *Proceedings of the National Academy of Sciences of the United States of America* **95**: 5884-5890.

Petrova, O.E. & K. Sauer, (2012) PAS domain residues and prosthetic group involved in BdlA-dependent dispersion response by Pseudomonas aeruginosa biofilms. *Journal of bacteriology* **194**: 5817-5828.

Podust, L.M., A. Ioanoviciu & P.R. Ortiz de Montellano, (2008) 2.3 A X-ray structure of the heme-bound GAF domain of sensory histidine kinase DosT of Mycobacterium tuberculosis. *Biochemistry* **47**: 12523-12531.

Porter, S.L., G.H. Wadhams & J.P. Armitage, (2008) Rhodobacter sphaeroides: complexity in chemotactic signalling. *Trends in microbiology* **16**: 251-260.

Rajagopal, S. & K. Moffat, (2003) Crystal structure of a photoactive yellow protein from a sensor histidine kinase: conformational variability and signal transduction. *Proceedings of the National Academy of Sciences of the United States of America* **100**: 1649-1654.

Rao, F., Q. Ji, I. Soehano & Z.X. Liang, (2011) Unusual heme-binding PAS domain from YybT family proteins. *J Bacteriol* **193**: 1543-1551.

Rebbapragada, A., M.S. Johnson, G.P. Harding, A.J. Zuccarelli, H.M. Fletcher, I.B. Zhulin & B.L. Taylor, (1997a) The Aer protein and the serine chemoreceptor Tsr independently sense intracellular energy levels and transduce oxygen, redox, and energy signals for *Escherichia coli* behavior. *Proceedings of the National Academy of Sciences of the United States of America* **94**: 10541-10546.

Rebbapragada, A., M.S. Johnson, G.P. Harding, A.J. Zuccarelli, H.M. Fletcher, I.B. Zhulin & B.L. Taylor, (1997b) The Aer protein and the serine chemoreceptor Tsr independently sense intracellular energy levels and transduce oxygen, redox, and energy signals for*Escherichia coli*behavior. *Proc Natl Acad Sci U S A* **94**: 10541-10546.

Reinelt, S., E. Hofmann, T. Gerharz, M. Bott & D.R. Madden, (2003) The structure of the periplasmic ligand-binding domain of the sensor kinase CitA reveals the first extracellular PAS domain. *The Journal of biological chemistry* **278**: 39189-39196.

Repik, A., A. Rebbapragada, M.S. Johnson, J.O. Haznedar, I.B. Zhulin & B.L. Taylor, (2000a) PAS domain residues involved in signal transduction by the Aer redox sensor of *Escherichia coli*. *Mol Microbiol* **36**: 806-816.

Repik, A., A. Rebbapragada, M.S. Johnson, J.O. Haznedar, I.B. Zhulin & B.L. Taylor, (2000b) PAS domain residues involved in signal transduction by the Aer redox sensor of*Escherichia coli*. *Mol Microbiol* **36**: 806-816.

Samanta, D., J. Widom, P.P. Borbat, J.H. Freed & B.R. Crane, (2016) Bacterial Energy Sensor Aer Modulates the Activity of the Chemotaxis Kinase CheA Based on the Redox State of the Flavin Cofactor. *The Journal of biological chemistry* **291**: 25809-25814.

Sampedro, I., J. Kato & J.E. Hill, (2015) Elastin degradation product isodesmosine is a chemoattractant for Pseudomonas aeruginosa. *Microbiology* **161**: 1496-1503.

Sampedro, I., R.E. Parales, T. Krell & J.E. Hill, (2014) Pseudomonas chemotaxis. *FEMS microbiology reviews*.

Sawai, H., H. Sugimoto, Y. Shiro, H. Ishikawa, Y. Mizutani & S. Aono, (2012) Structural basis for oxygen sensing and signal transduction of the heme-based sensor protein Aer2 from Pseudomonas aeruginosa. *Chemical communications* **48**: 6523-6525.

Schultz, J.E. & J. Natarajan, (2013) Regulated unfolding: a basic principle of intraprotein signaling in modular proteins. *Trends Biochem Sci* **38**: 538-545.

Schuster, M., A.C. Hawkins, C.S. Harwood & E.P. Greenberg, (2004) The Pseudomonas aeruginosa RpoS regulon and its relationship to quorum sensing. *Mol Microbiol* **51**: 973-985.

Shimizu, T., (2013) The Heme-Based Oxygen-Sensor Phosphodiesterase Ec DOS (DosP): Structure-Function Relationships. *Biosensors (Basel)* **3**: 211-237.

Springer, W.R. & D.E. Koshland, Jr., (1977) Identification of a protein methyltransferase as the cheR gene product in the bacterial sensing system. *Proceedings of the National Academy of Sciences of the United States of America* **74**: 533-537.

Starrett, D.J. & J.J. Falke, (2005) Adaptation mechanism of the aspartate receptor: electrostatics of the adaptation subdomain play a key role in modulating kinase activity. *Biochemistry* **44**: 1550-1560.

Stewart, R.C., K. Jahreis & J.S. Parkinson, (2000) Rapid phosphotransfer to CheY from a CheA protein lacking the CheY-binding domain. *Biochemistry* **39**: 13157-13165.

Stock, A.M. & J. Guhaniyogi, (2006) A new perspective on response regulator activation. *Journal of bacteriology* **188**: 7328-7330.

Studdert, C.A. & J.S. Parkinson, (2005) Insights into the organization and dynamics of bacterial chemoreceptor clusters through in vivo crosslinking studies. *Proceedings of the National Academy of Sciences of the United States of America* **102**: 15623-15628.

Swain, K.E. & J.J. Falke, (2007) Structure of the conserved HAMP domain in an intact, membrane-bound chemoreceptor: a disulfide mapping study. *Biochemistry* **46**: 13684-13695.

Swain, K.E., M.A. Gonzalez & J.J. Falke, (2009) Engineered socket study of signaling through a four-helix bundle: evidence for a yin-yang mechanism in the kinase control module of the aspartate receptor. *Biochemistry* **48**: 9266-9277.

Swanson, R.V., S.C. Schuster & M.I. Simon, (1993) Expression of CheA fragments which define domains encoding kinase, phosphotransfer, and CheY binding activities. *Biochemistry* **32**: 7623-7629.

Tan, E., F. Rao, S. Pasunooti, T.H. Pham, I. Soehano, M.S. Turner, C.W. Liew, J. Lescar, K. Pervushin & Z.X. Liang, (2013) Solution structure of the PAS domain of a thermophilic YybT protein homolog reveals a potential ligand-binding site. *J Biol Chem* **288**: 11949-11959.

Tanaka, A., H. Takahashi & T. Shimizu, (2007) Critical role of the heme axial ligand, Met95, in locking catalysis of the phosphodiesterase from Escherichia coli (Ec DOS) toward Cyclic diGMP. *J Biol Chem* **282**: 21301-21307.

Taylor, B.L., (1983) Role of proton motive force in sensory transduction in bacteria. *Annu Rev Microbiol* **37**: 551-573.

Taylor, B.L., (2007) Aer on the inside looking out: paradigm for a PAS-HAMP role in sensing oxygen, redox and energy. *Mol Microbiol* **65**: 1415-1424.

Taylor, B.L. & D.E. Koshland, Jr., (1974) Reversal of flagellar rotation in monotrichous and peritrichous bacteria: generation of changes in direction. *Journal of bacteriology* **119**: 640-642.

Taylor, B.L., K.J. Watts & M.S. Johnson, (2007) Oxygen and redox sensing by two-component systems that regulate behavioral responses: behavioral assays and structural studies of aer using in vivo disulfide cross-linking. *Methods Enzymol* **422**: 190-232.

Taylor, B.L. & I.B. Zhulin, (1999) PAS domains: internal sensors of oxygen, redox potential, and light. *Microbiology and molecular biology reviews : MMBR* **63**: 479-506.

Terwilliger, T.C., E. Bogonez, E.A. Wang & D.E. Koshland, Jr., (1983) Sites of methyl esterification on the aspartate receptor involved in bacterial chemotaxis. *The Journal of biological chemistry* **258**: 9608-9611.

Terwilliger, T.C. & D.E. Koshland, Jr., (1984) Sites of methyl esterification and deamination on the aspartate receptor involved in chemotaxis. *The Journal of biological chemistry* **259**: 7719-7725.

Terwilliger, T.C., J.Y. Wang & D.E. Koshland, Jr., (1986) Surface structure recognized for covalent modification of the aspartate receptor in

chemotaxis. *Proceedings of the National Academy of Sciences of the United States of America* **83**: 6707-6710.

Tsai, A.L., V. Berka, E. Martin & J.S. Olson, (2012a) A "sliding scale rule" for selectivity among NO, CO, and O(2) by heme protein sensors. *Biochemistry* **51**: 172-186.

Tsai, A.L., E. Martin, V. Berka & J.S. Olson, (2012b) How do heme-protein sensors exclude oxygen? Lessons learned from cytochrome c', Nostoc puntiforme heme nitric oxide/oxygen-binding domain, and soluble guanylyl cyclase. *Antioxidants & redox signaling* **17**: 1246-1263.

Tuckerman, J.R., G. Gonzalez, E.H. Sousa, X. Wan, J.A. Saito, M. Alam & M.A. Gilles-Gonzalez, (2009) An oxygen-sensing diguanylate cyclase and phosphodiesterase couple for c-di-GMP control. *Biochemistry* **48**: 9764-9774.

Uchida, T., I. Sagami, T. Shimizu, K. Ishimori & T. Kitagawa, (2012) Effects of the bHLH domain on axial coordination of heme in the PAS-A domain of neuronal PAS domain protein 2 (NPAS2): conversion from His119/Cys170 coordination to His119/His171 coordination. *J Inorg Biochem* **108**: 188-195.

Ukaegbu, U.E. & A.C. Rosenzweig, (2009a) Structure of the redox sensor domain of Methylococcus capsulatus (Bath) MmoS. *Biochemistry* **48**: 2207-2215.

Ukaegbu, U.E. & A.C. Rosenzweig, (2009b) Structure of the Redox Sensor Domain of Methylococcus capsulatus (Bath) MmoS (dagger) (double dagger). *Biochemistry* **48**: 2207-2215.

Wang, C., J. Sang, J. Wang, M. Su, J.S. Downey, Q. Wu, S. Wang, Y. Cai, X. Xu, J. Wu, D.B. Senadheera, D.G. Cvitkovitch, L. Chen, S.D. Goodman & A. Han, (2013) Mechanistic insights revealed by the crystal structure of a histidine kinase with signal transducer and sensor domains. *PLoS Biol* **11**: e1001493.

Wang, J., J. Sasaki, A.L. Tsai & J.L. Spudich, (2012) HAMP domain signal relay mechanism in a sensory rhodopsin-transducer complex. *The Journal of biological chemistry* **287**: 21316-21325.

Watts, K.J., M.S. Johnson & B.L. Taylor, (2006a) Minimal requirements for oxygen sensing by the aerotaxis receptor Aer. *Mol Microbiol* **59**: 1317-1326.

Watts, K.J., M.S. Johnson & B.L. Taylor, (2008) Structure-function relationships in the HAMP and proximal signaling domains of the aerotaxis receptor Aer. *Journal of bacteriology* **190**: 2118-2127.

Watts, K.J., M.S. Johnson & B.L. Taylor, (2011a) Different Conformations of the Kinase-On and Kinase-Off Signaling States in the Aer HAMP Domain. *Journal of bacteriology* **193**: 4095-4103.

Watts, K.J., Q. Ma, M.S. Johnson & B.L. Taylor, (2004a) Interactions between the PAS and HAMP domains of the *Escherichia coli* aerotaxis receptor Aer. *Journal of bacteriology* **186**: 7440-7449.

Watts, K.J., Q. Ma, M.S. Johnson & B.L. Taylor, (2004b) Interactions between the PAS and HAMP domains of the*Escherichia coli*aerotaxis receptor Aer. *J Bacteriol* **186**: 7440-7449.

Watts, K.J., K. Sommer, S.L. Fry, M.S. Johnson & B.L. Taylor, (2006b) Function of the N-terminal cap of the PAS domain in signaling by the aerotaxis receptor Aer. *Journal of bacteriology* **188**: 2154-2162.

Watts, K.J., B.L. Taylor & M.S. Johnson, (2011b) PAS/poly-HAMP signalling in Aer-2, a soluble haem-based sensor. *Molecular microbiology* **79**: 686-699.

Weerasuriya, S., B.M. Schneider & M.D. Manson, (1998) Chimeric chemoreceptors in Escherichia coli: signaling properties of Tar-Tap and Tap-Tar hybrids. *Journal of bacteriology* **180**: 914-920.

Williams, S.B. & V. Stewart, (1999) Functional similarities among two-component sensors and methyl-accepting chemotaxis proteins suggest a role for linker region amphipathic helices in transmembrane signal transduction. *Mol Microbiol* **33**: 1093-1102.

Worrall, J.A., A.M. van Roon, M. Ubbink & G.W. Canters, (2005) The effect of replacing the axial methionine ligand with a lysine residue in cytochrome c-550 from Paracoccus versutus assessed by X-ray crystallography and unfolding. *The FEBS journal* **272**: 2441-2455.

Wu, J., J. Li, G. Li, D.G. Long & R.M. Weis, (1996) The receptor binding site for the methyltransferase of bacterial chemotaxis is distinct from the sites of methylation. *Biochemistry* **35**: 4984-4993.

Wuichet, K., R.P. Alexander & I.B. Zhulin, (2007) Comparative genomic and protein sequence analyses of a complex system controlling bacterial chemotaxis. *Methods in Enzymology* **422**: 1-31.

Wuichet, K. & I.B. Zhulin, (2010) Origins and diversification of a complex signal transduction system in prokaryotes. *Science signaling* **3**: ra50.

Xie, Z., L.E. Ulrich, I.B. Zhulin & G. Alexandre, (2010) PAS domain containing chemoreceptor couples dynamic changes in metabolism with chemotaxis. *Proceedings of the National Academy of Sciences of the United States of America* **107**: 2235-2240.

Yeh, S.R., M. Couture, Y. Ouellet, M. Guertin & D.L. Rousseau, (2000) A cooperative oxygen binding hemoglobin from Mycobacterium tuberculosis. Stabilization of heme ligands by a distal tyrosine residue. *The Journal of biological chemistry* **275**: 1679-1684.

Yu, H.S., J.H. Saw, S. Hou, R.W. Larsen, K.J. Watts, M.S. Johnson, M.A. Zimmer, G.W. Ordal, B.L. Taylor & M. Alam, (2002) Aerotactic responses in bacteria to photoreleased oxygen. *FEMS Microbiol Lett* **217**: 237-242.

Yukl, E.T., A. Ioanoviciu, M.M. Nakano, P.R. de Montellano & P. Moenne-Loccoz, (2008) A distal tyrosine residue is required for ligand discrimination in DevS from Mycobacterium tuberculosis. *Biochemistry* **47**: 12532-12539.

Zhao, J. & J.S. Parkinson, (2006a) Cysteine-scanning analysis of the chemoreceptor-coupling domain of the Escherichia coli chemotaxis signaling kinase CheA. *Journal of bacteriology* **188**: 4321-4330.

Zhao, J. & J.S. Parkinson, (2006b) Mutational analysis of the chemoreceptor-coupling domain of the Escherichia coli chemotaxis signaling kinase CheA. *Journal of bacteriology* **188**: 3299-3307.

Zhao, R., E.J. Collins, R.B. Bourret & R.E. Silversmith, (2002) Structure and catalytic mechanism of the E. coli chemotaxis phosphatase CheZ. *Nature structural biology* **9**: 570-575.

Zhou, Q., P. Ames & J.S. Parkinson, (2009) Mutational analyses of HAMP helices suggest a dynamic bundle model of input-output signalling in chemoreceptors. *Mol Microbiol* **73**: 801-814.

Zhou, Q., P. Ames & J.S. Parkinson, (2011) Biphasic control logic of HAMP domain signalling in the Escherichia coli serine chemoreceptor. *Molecular microbiology* **80**: 596-611.

Zhou, Y.F., B. Nan, J. Nan, Q. Ma, S. Panjikar, Y.H. Liang, Y. Wang & X.D. Su, (2008) C4-dicarboxylates sensing mechanism revealed by the crystal structures of DctB sensor domain. *J Mol Biol* **383**: 49-61.

Zhulin, I.B., (2001) The superfamily of chemotaxis transducers: from physiology to genomics and back. *Advances in microbial physiology* **45**: 157-198.

Zhulin, I.B. & B.L. Taylor, (1998) Correlation of PAS domains with electron transport-associated proteins in completely sequenced microbial genomes. *Mol Microbiol* **29**: 1522-1523.

Zhulin, I.B., B.L. Taylor & R. Dixon, (1997) PAS domain S-boxes in Archaea, Bacteria and sensors for oxygen and redox. *Trends in biochemical sciences* **22**: 331-333.

Zoltowski, B.D., C. Schwerdtfeger, J. Widom, J.J. Loros, A.M. Bilwes, J.C. Dunlap & B.R. Crane, (2007) Conformational switching in the fungal light sensor Vivid. *Science* **316**: 1054-1057.